Dissertation

Thiolate protected gold catalysts for oxidation reactions

Ausgeführt zum Zwecke der Erlangung des akademischen Grades eines Doktors der technischen Wissenschaften unter der Leitung von

Univ. Prof. Dr. rer.nat. Günther Rupprechter

und

Dr. Noelia Barrabes Rabanal

E165 Institut für Materialchemie

Eingereicht an der Technischen Universität Wien, Fakultät für Technische Chemie von

Msc. Clara Isabel Garcia Yago

Matrikelnummer: 01650795

Südtirolerplatz 9 / 24 – 1040 Wien

Wien, am 02.07.2020

Eidesstattliche Erklärung:

Ich erkläre hiermit, dass ich die vorliegende Dissertationsarbeit selbständig angefertigt habe und keine anderen Hilfsmittel verwendet worden sind, als die von mir als Quellen angegebenen. Wörtliche und sinngemäße Zitate sind entsprechend gekennzeichnet worden.

Wien, am 02.07.2020

Clara Isabel Garcia Yago

Acknowledgments

First, I would like to thank Dr. Noelia Barrabés for making this thesis possible and for all the help and support during the process. Also, I would like to thank Prof. Günther Rupprechter for his continuous support and for giving me the opportunity to carry out my work in his research group at the Institute for Material Chemistry, and to present the results of my work at various international conferences and workshops. I am grateful for funding by TU Wien Innovative Project, FWF SFB FOXSI and FWF DK+ Solids4Fun. I would also like to thank Prof. Ernst Pittenauer for agreeing to be on the examining committee. Next, I would like to thank Prof. Michael Stöger-Pollach from USTEM for teaching me scanning electron microscopy and for measuring challenging samples. Additionally, I would like to thank Pr. Christoph Rameshan for his XPS measurements, as well as for giving me such sterling recommendations and of course for the very enjoyable time we spent together. I would also like to express my gratitude to Dr. Peter Kregsamer from Atominstitute for facilitating the XRF measurements, information that was crucial to understanding the catalytic data.

I would like to especially thank my colleagues Vera Truttmann and Stephan Pollitt for all our experiences both in the lab and in the different synchrotron facilities where we had the chance to spend so much time. I would never have been able to survive the pressure without their help and I consider them more friends than colleagues as they were always there even in the most complicated circumstances. I am very grateful to all my colleagues at the Institute for their help using some very delicate equipment, particularly to Thomas Haunold, Dr. Klaus Dobrezberger, Dr. Nevzat Yigit and Lorenz Lindenthal.

I also really appreciate Pr. Karin Föttinger for teaching me so much about infrared and for the emotional support. I would like to mention Prof. Georg Madsen, Dr. Jesús Carrete and Dr. Bonny Dongre for the scientific discussions and for making DFT calculations look a little less scary.

And indeed everyone else who was willing to help, discuss a given topic, or just go out for a drink. I would also like to mention my co-worker Irene Lopez for her contribution in ALBA during our measurements in 2018 and 2019 and for her motivation, as can be seen in our common publications. I also enjoyed sharing a few evenings out with her in Vienna and in Barcelona.

Last but far from least I would like to honor the memory of my mother, Rosa Maria Yago Micó, who made me the person that I am today and who spent 22 years motivating me to study and to give my best. This work is fully dedicated to her. I am also blessed with family and friends from Spain, without whom I would never have been able to achieve so much. In particular, I would like to thank my godmother, Maite Asunción, for her unconditional support, my godfather Javier Llorens for his faith on my talent and also Isabel Santacatalina for teaching me how to deal with science and life. Thanks also to Markus Pasztorek, who is always there, he also knows the real price of this dissertation as we suffered and paid for it together. I thank him for his patience, and his understanding.

Abbreviations

AC	Activated carbon
ATR	Attenuated total reflection
$Au_n(SR)_m$	Thiolate protected gold clusters, n=number of gold atoms and n=number of thiol ligands
CNT	Carbon nanotubes
CO	Carbon monoxide
DFT	Density functional theory
DOS	Density of states
DRIFTS	Diffuse Reflectance Infrared Fourier Transform Spectroscopy
DRS	Diffuse reflectance spectroscopy
ESI	Electrospray ionization
EtOH	Ethanol
EXAFS	Extended x-ray absorption fine structure
FCC	Face-centered cubic
HAP	Hydroxyapatite
$HAuCl_4$	Gold (III) chloride trihydrate
HERFD-XAS	High-energy resolution fluorescence detected X-ray absorption spectroscopy
HAADF-STEM	High-angle annular dark-field scanning transmission electron microscopy
HOMO-LUMO	Highest occupied molecular orbital-lowest unoccupied molecular orbital
HR-TEM	High resolution transmission electron microscopy
IR	Infrared spectroscopy

MALDI	Matrix assisted laser desorption ionization
MS	Mass spectroscopy
2-PET	2-phenylethanethiol
SAM	Self-assembled monolayer
SC-XRD	Single-crystal x-ray diffraction
STEM	Scanning transmission electron microscopy
TGA	Thermogravimetric analysis
TOF	Turnover frequency
UV-Vis	Ultraviolet-visible spectroscopy
wt	Weight tare
XANES	X-ray absorption near edge structure
XAS	X-ray absorption spectroscopy

Contents

TU Bibliothek
WIEN Your knowledge hub

Abstract

Thiolate protected clusters supported on oxides have become increasingly relevant as model systems in heterogeneous catalysis. Their well-defined morphology and atomically defined structure are crucial to establish structure-reactivity correlations. In the present work, three main aspects of catalyst design are discussed: size, support and doping. The focus of this thesis is to evaluate how these aspects affect the stability and reactivity in oxidation reactions. Initially, the stability of Au_{25} and Au_{144} clusters, supported either on TiO_2 or SiO_2, is investigated upon pretreatment and upon liquid phase oxidation reaction. A size and support effect was revealed by XAS, DRS and STEM. Upon pretreatment, Au_{144} was more stable, which may be related to its specific cluster core structure and staple configuration. The catalytic properties in liquid phase cyclohexane oxidation were clearly size dependent, with Au_{144} being more active, in particular in the case of SiO_2 supported catalysts. However, with respect to selectivity, TiO_2 supported catalysts led to higher KA (KA: ketone-alcohol) production than SiO_2 supported ones. The different reaction pathway, as observed by *in-situ* ATR, can explain the different reactivity. HERFD-XAS measurements allowed to investigate the differences in the stability. A significant sintering during the reaction was revealed, especially significant for Au_{144}/TiO_2 catalysts.

In the second part of this work, the influence of doping the Au cluster structure with silver and palladium on the stability and the catalytic properties was investigated. Therefore, two different types of heterogeneous test reactions were employed: gas phase CO oxidation and liquid phase cyclohexane oxidation. In case of palladium, sintering was observed by means of XAFS during cyclohexane oxidation. Only titanium oxide supported clusters showed activity for catalytic CO oxidation. For this reaction, a significantly higher activity was observed with $PdAu_{24}$ compared to monometallic Au_{25} nanoclusters. After pretreatment and CO oxidation, CO adsorbed on Pd was detected by *in-situ* DRIFT spectroscopy, indicating a migration of the Pd dopant from the Au cluster core to the cluster surface. Increasing the number of Pd dopant atoms in the Au structure led to a preferential location of Pd in the clusters' staples. The combination

of oxidative and reductive thermal pretreatment resulted in the formation of isolated Pd surface sites within Au, as evidenced by *in-situ* DRIFTS, XAFS and *ex-situ* XPS.

Ag doping was investigated both in CO and cyclohexane oxidation. For CO oxidation, a decrease in the catalytic activity was observed, which could be correlated with the lower stability of bimetallic AgAu clusters as previously reported. The same decrease in the catalytic activity is also observed for cyclohexane oxidation, while a higher selectivity to the desired products is achieved. As the support material also plays a significant role in heterogenous catalysis, the materials employed in this part of the study were extended to silicate zeolites and aluminosilicate zeolites. Indeed, a dependence of the catalytic activity on the support could be confirmed, with the activity decreasing in the order TiO_2 > silicate zeolites > SiO_2 > aluminosilicate zeolites. This once more points out the importance of the support morphology and composition.

Overall, the work of this thesis demonstrates the crucial role of the Au nanocluster composition and of the support material in determining reactivity and stability of gold catalysts. These parameters are key elements for catalytic applications and tuning them enables the design of new catalysts.

Kurzfassung

Cluster mit Thiolatliganden auf Metalloxidträgern haben zunehmende Bedeutung als Modellsysteme für heterogene Katalyse erlangt, da deren definierte Morphologie und atomar definierte Struktur die Untersuchung von Struktur-Wirkungsbeziehungen ermöglicht. In der vorgelegten Arbeit werden drei Aspekte des Katalysatordesigns behandelt: Größe, Trägermaterial und Dotierung. Als zentrale Fragestellung widmet sich diese Dissertation dem Einfluss dieser Aspekte auf die Stabilität und Reaktivität von Nanoclustern in Oxidationsreaktionen. Zunächst wurde dabei die Stabilität von Au_{25} und Au_{144} Clustern immobilisiert auf TiO_2 bzw. SiO_2, die Vorbehandlungen und einer Oxidationsreaktion in flüssiger Phase ausgesetzt wurden, untersucht. Eine klare Abhängigkeit der Stabilität von Clustergröße und Trägermaterial konnte durch XAS, DRS und STEM nachgewiesen werden. Au_{144} wies größere Stabilität unter den Bedingungen der Vorbehandlung auf, was auf dessen spezifische Clusterstruktur, d.h. Clusterkern und Anordnung der schützenden Gold-Liganden-Gruppierungen darauf, zurückzuführen sein könnte. Die katalytische Aktivität in Cyclohexanoxidation in flüssiger Phase zeigte eine klare Abhängigkeit von der Clustergröße, wobei Au_{144} aktiver war, vor allem in Kombination mit SiO_2 als Trägermaterial. In Bezug auf die Selektivität konnten jedoch mit Clustern aufgebracht auf TiO_2 höhere KA-Werte (KA: Keton-Alkohol) erzielt werden. Dies kann auf die unterschiedlichen Reaktionsmechanismen bei Verwendung verschiedener Trägermaterialien zurückgeführt werden, welche auch mittels *in-situ* ATR beobachtet wurden. Die Unterschiede in der Stabilität wurden durch HERFD-XAS Messungen genauer untersucht. Zudem konnte auch eine deutliche Agglomeration der Nanocluster während der Reaktion festgestellt werden, insbesondere für das Au_{144}/TiO_2 System.

Im zweiten Teil der vorgelegten Arbeit wurde der Einfluss von Dotierungen mit Silber bzw. Palladium auf die Stabilität der Goldcluster und deren Eigenschaften als Katalysatoren untersucht. Dazu wurden zwei verschiedene Typen von heterogenen Testreaktionen herangezogen: CO Oxidation in der Gasphase und Cyclohexanoxidation in flüssiger Phase. Im Fall der Palladiumdotierung wurde Agglomeration der Nanocluster im Zuge der Oxidation von

Cyclohexan durch XAFS festgestellt. Für CO Oxidation zeigten nur die TiO$_2$ immobilisierten bimetallischen Cluster Aktivität, wobei mit PdAu$_{24}$ eine weitaus größere Aktivität als mit monometallischen Au$_{25}$ Clustern erreicht werden konnte. Nach Vorbehandlung und CO Oxidation konnte CO adsorbiert auf Pd mittels *in-situ* DRIFT-Spektroskopie detektiert werden, was auf eine Migration des dotierten Pd-Atoms vom Clusterkern zur Oberfläche hinweist. Bei Erhöhung des Pd Anteils in der Au-Nanoclusterstruktur waren die Pd-Atome hauptsächlich in den Metall-Thiolat-Gruppierungen lokalisiert, welche den Kern umgeben. Eine Kombination aus oxidativer und reduktiver thermischer Vorbehandlung führte zur Bildung von isolierten, oberflächlichen Pd-Atomen innerhalb der Goldclusterstruktur, was durch *in-situ* DRIFTS, XAFS und *ex-situ* XPS nachgewiesen werden konnte.

Der Einfluss einer Dotierung mit Silber wurde sowohl in CO- als auch in Cyclohexanoxidation untersucht. Im Fall der CO Oxidation wurde eine Verringerung der katalytischen Aktivität beobachtet, welche in der geringen Stabilität der bimetallischen AgAu Cluster, die bereits von anderen Gruppen publiziert wurde, begründet sein könnte. Eine ähnliche Reduktion der katalytischen Aktivität wurde auch im Fall der Cyclohexanoxidation festgestellt, allerdings konnte hierbei im Vergleich zu monometallischen Goldclustern eine höhere Selektivität für die gewünschten Produkte erreicht werden. Da auch das verwendete Trägermaterial in der heterogenen Katalyse eine entscheidende Rolle spielen kann, wurden die in dieser Studie verwendeten Materialien auf Zeolithe auf Silikat- bzw. Aluminosilikatbasis ausgeweitet. Tatsächlich konnte eine Abhängigkeit der katalytischen Aktivität vom verwendeten Trägermaterial festgestellt werden, wobei die Aktivität in folgender Reihenfolge abnahm: TiO$_2$ > Silikat Zeolith > SiO$_2$ > Aluminosilikat Zeolith. Diese Befunde belegen einmal mehr die Bedeutung der Morphologie und der Zusammensetzung des Trägermaterials.

Zusammenfassend zeigt die vorliegende Dissertation deutlich, dass die spezifische Zusammensetzung von Au-Nanoclustern, sowie das verwendete Trägermaterial die Reaktivität und Stabilität von Goldcluster-Katalysatoren maßgeblich beeinflussen können. Diese Parameter sind Schlüsselelemente für katalytische Anwendungen und gezielte Modifikation derselben unabdinglich für die Herstellung zukünftiger Katalysatoren.

Chapter 1

Introduction
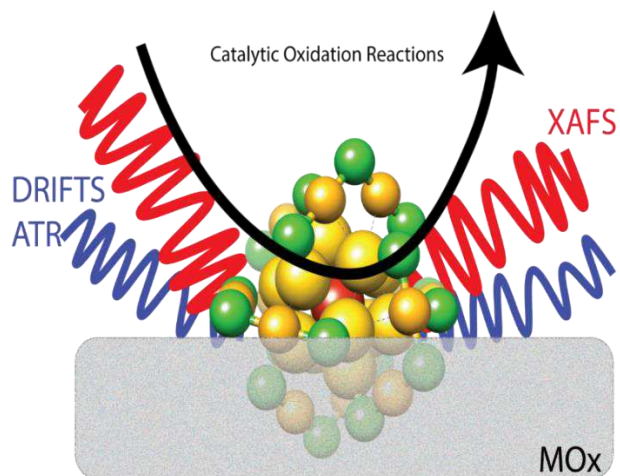
1. Catalysis: general concepts

Catalysis is used to convert raw materials into valuable chemicals, materials and fuels in an efficient and environmentally benign manner. Catalytic processes are therefore essential to industry and to the world economy. In addition to the production of commodity chemicals, materials and fuels, catalysis is also used in energy conversion (e.g. for H_2 production and fuel cells [3]), in pollution control (e.g. for flue-gas cleaning, water purification, automobile emission [4]) and in food production (e.g. enzymatic catalysis in baking processes) [5].

By formal definition, a catalyst is a substance that accelerates the rate of a chemical reaction without itself being consumed by the reaction. The catalyst increases the reaction rate by offering an alternative reaction pathway that requires less free energy to reach the transition state of the rate-limiting step [6]. For example, Figure 1-1 shows how the activation energy E_a for the oxidation of CO to CO_2 is decreased when the reaction occurs on the surface of a heterogeneous catalyst [7-10]. The catalyst does not change the Gibbs free energy — it only changes the kinetics of the reaction, not the thermodynamics. Catalysts are used because of their ability to enhance the rate of chemical reactions [11], often by many orders of magnitude.
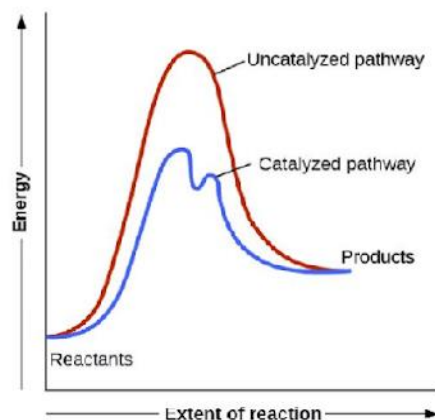
Figure 1-1 *This potential energy diagram shows the effect of a catalyst on the activation energy. The catalyst provides a different reaction path with a lower activation energy. As shown, the catalyzed pathway involves a two-step mechanism (note the presence of two transition states) and an intermediate species (represented by the valley between the two transitions states) [12].*

There are two types of catalytic processes: heterogeneous and homogeneous. In heterogeneous catalysis, the catalyst materials are solids which are applied in gas, liquid or gas/liquid phase reactions. The reaction then takes place on the solid catalyst surface. Specific interactions of the adsorbed reactants with the surface lead to certain reaction pathways which can be described by elementary steps involving lower activation energies when compared to uncatalyzed reactions. If several catalyzed reactions are possible, the difference in the respective activation barriers will determine the selectivity of the catalyst for the desired reaction. Certain structural features, e.g. defects or reconstructions, along with the specific chemical composition of the surface under reaction conditions, are important for catalyst performance. Characteristic descriptors useful for industrial catalysts are: activity (including stability), selectivity, pellet shape (resulting in pressure drop in a given reactor), regenerability and factors such as mechanical and chemical stability (against attrition and other phenomena causing loss of mechanical stability) and [13] [14].

In contrast to heterogeneous catalysis, a homogeneously catalyzed reaction is characterized by all the reaction components being in a single liquid phase where the catalyst is a molecular defined structure. The advantage of molecular catalysis is the ability to steer chemo-, regio- and stereo-selectivity via the molecular design of the catalyst, which in many cases cannot be achieved with multisite heterogeneous catalysts. One particular challenge — mostly relevant to technical applications — is the required separation of the catalyst from the homogeneous reaction solution. This separation can be achieved by a two phase system where the catalysis takes place in one phase and the products migrate to the second phase and are thus separated (known as 'multiphase catalysis'). The coating of a heterogeneous support with a homogeneous catalyst or the coating of a support with a liquid carrying the catalyst are two other, rather elegant, ways to separate reaction products efficiently from a molecular catalyst. [15]

1.1.   Nanocatalysis

Nanomaterials have attracted a lot of attention due to their properties being different from the bulk. Bulk materials can be described by the laws of classical physics, but in a metal particle the properties change with the reduction in size (where quantum size effects may occur) [16]. In bulk metals, the atomic orbital is combined with delocalized electrons forming continuous bands [17]. Each atom contributes with its atomic orbital, whose density increases slightly as more atoms are added to the structure. These bands are characterized by the density of states (DOS). However, when the number of atoms are significantly reduced, the continuous band is gradually replaced by discrete energy levels. In very small clusters, bands become delocalized molecular orbitals, and the band gaps are large enough to resemble the highest occupied molecular orbital - lowest unoccupied molecular orbital gap (HOMO-LUMO) (Figure 1-2). The change in electronic structure makes nanoparticles attractive for many applications such as optics, nanomedicine, and sensors.
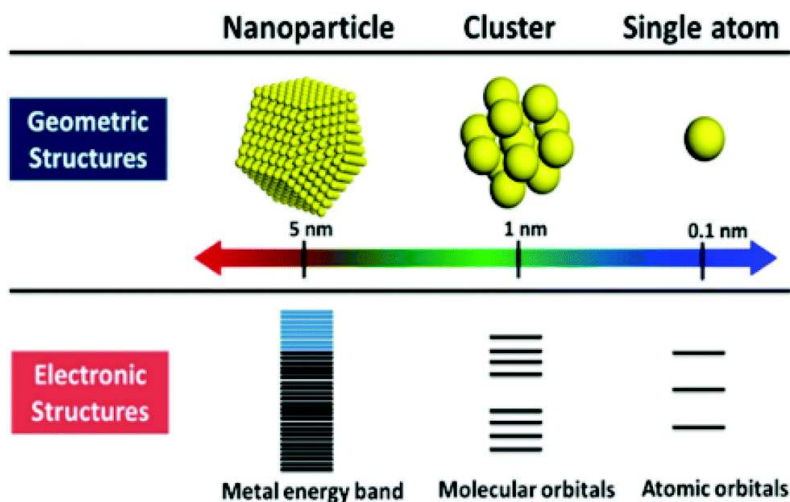
Figure 1-2 Geometric and electronic structures of single atom, clusters, and nanoparticles [18]

Another relevant property of nanomaterials is their high ratio of surface atoms that increase with decreasing particle size (Figure 1-2). The number of surface atoms is critical for catalysis, as they are known to be the active centers [19].

Full-shell clusters	Total number of atoms	Number of surface atoms	Surface atoms (%)
1 shell	13	12	92
2 shells	55	42	76
3 shells	147	92	63
4 shells	309	162	52
5 shells	561	252	45
6 shells	923	362	39

92 % 76 % 63 % 52 %

Decrease of surface to volume ratio for clusters of 13, 55, 147 to 309 atoms
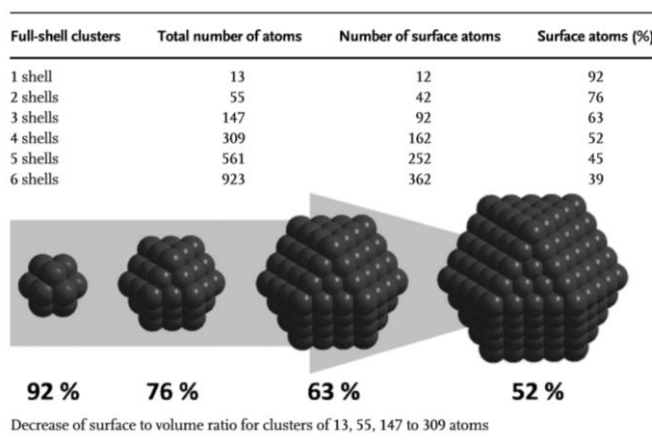
Figure 1-3 Number of surface atoms in relation to the total number of atoms in full shell clusters [19]

Numerous studies have already demonstrated that surface atoms at the edges or in the corners may be more active than those on planes, and that their number also increases with decreasing particle size [116-117]. As the amount of surface atoms present in nanoparticles will determine the catalytic reactivity, control of the size of nanoparticles is thus highly important [20-22].

For industrial processes, catalysts usually consist of metal particles supported on transition metal oxides such as ceria, alumina, silica or titania. The preparation methods include mechanical treatment, precipitation, thermal decomposition of metal–inorganic or metal-organic complexes, adsorption, ion exchange or impregnation. One drawback for all of the methods listed above is that a wide size distribution is generated and, as long as the larger particles are less active than the smaller ones, the catalytic activity can vary from one system to another. Moreover, in those systems it is difficult to establish a correlation between catalytic activity and morphology. These drawbacks have motivated the present research paper on clusters, as they are truly monodisperse systems with a maximal number of atoms exposed on the surface.

1.2.   Metal clusters

Metal clusters are located in the size range between single atoms and nanoparticles. They are composed of less than a few hundred atoms. Early research in this area looked at the finite-size effects on the physical properties of metal clusters in order to understand their microscopic origins [118][23]. With the development of advanced experimental and theoretical methods, it was possible to discover size-specific phenomena and physicochemical properties. For example, the development of new cluster production methods such as laser ablation coupled with mass spectrometry was crucial in discovering the most stable configurations due to the closure of electronic and/or geometric structures [24]. These observations — based on the Jellium model [25] and on superatoms [26] — helped establish concepts like electron shell closing.

Clusters containing a well-defined number of atoms offer an ideal platform for studying catalysis at the atomic level and can provide detailed and fundamental insight into catalytic processes that may be hampered by the complexity of catalysts prepared by more conventional methods. For this reason, a lot of research has been done on size-selected clusters. These are typically synthesized by employing physical methods in high vacuum systems where the clusters ions are generated using a gas-phase cluster ion source [27]. These well-defined systems are very attractive for theoretical studies but far from the real conditions that are involved in industrial catalysis.

Synthesis of metal clusters is usually achieved by using ligands as stabilizing agents [4]. Organic ligands such as thiols, acetylene, carbines, phosphines, and selenolates not only provide stability to the metal clusters but also modulate the electronic states of the clusters [28][29]. Here, we shall focus on different forms of thiolate-protected metal clusters. These are widely studied due to their strong sulphur–metal interactions which enable good stability in solution, straightforward synthetic procedures, and controlled cluster compositions, as well as the functionalization of stable clusters [30].

1.3. Thiolate protected gold clusters

As a noble metal, in general terms, gold had been thought to be inactive for catalysis since Haruta et al. [31] proved that dispersed Au nanoparticles on oxide supports can act as catalysts for low temperature CO oxidation reactions. Gold−thiol chemistry became significant in the 1980s owing to research on self-assembled monolayers (SAMs) of thiols on bulk gold surfaces [32]. Inspired by the SAM work, researchers started to exploit thiols for the synthesis and functionalization of gold nanoparticles in the 1990s. The most significant milestone was achieved by Brust et al. [33] in 1994 when they reported the synthesis of Au monolayer protected clusters via a two phase method using a phase transfer catalyst. These clusters were found to be highly monodisperse. Continuing with Brust et al.'s work, Whetten et al. reported solvent fractionation of polydisperse gold−thiolate nanoparticles, obtaining several distinct fractions in the 1.5−3.5-nm range [34]. Afterwards, even smaller particles were obtained with those species exhibited step-like optical absorption, indicating strong quantum size effects. Although Whetten et al. obtained several well-defined structures, the monodispersivity was still not fully achieved [35]. Further research was carried out with optimized reaction conditions. This involved using a large amount of thiol – e.g. thiol-to-gold ratios of 3:1 or higher – to convert Au(III) into Au(I)−SR polymers and using a large amount of the reducing agent (typically 10 equivalents of $NaBH_4$ per mole of gold) to reduce Au(I) to Au(0).
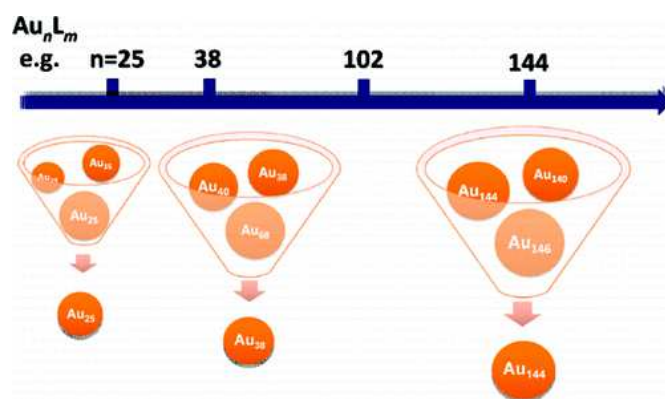
Figure 1-4 *Representative schema of stability of certain sized $Au_n(SR)_m$ nanoclusters. [36]*

After Tsukuda et al. reported the first glutathione (SG) protected cluster, Jin et al. pointed out that aqueous synthesis is often more complicated than that in the organic phase. Moreover the SG ligand system is not amenable to crystallization, nor to the use of selected phenylethanethiol (HSC_2H_4Ph) as a ligand, as had been used in the earlier synthesis of gold clusters [37]. By controlling the reaction temperature and aggregation conditions for the $[Au(I)-SR]_x$ polymeric intermediates, they achieved the formation of $Au_{25}(SC_2H_4Ph)_{18}$ clusters in high yield and high purity. Afterwards, the formula and synthetic procedures of many other cluster configurations, such as Au_{38}, Au_{144}, were reported and crystallization experiments combined with computational predictions were able to resolve each cluster´s structure and open the door to their use as a catalysis in many fields.

1.3.1. Structural and electronic properties

The material properties of gold thiolate clusters has encouraged a lot of research during the last few years. Advanced mass spectrometry [38] and X-ray crystallography [39] analysis reveal that when the particle size diameter is lower than 2 nm, the size dispersion of the nanoparticles becomes discrete, and only clusters of the formula $Au_m(SR)_n$ with particular values of (m, n) are thermodynamically stable products [40, 41]. Diverse authors have studied the origin of these so-called 'magic numbers' or preferential configurations. Initially – as Mingos et al. explained in their work about gold clusters stabilized by phosphines[42] – the inherent stability of thiolate protected clusters was explained in terms of the closing of electronic and/or geometric shells. However, more recently Negishi et al. [43] have pointed out that the high stability could be attributed to geometric rather than electronic factors.

Thiolate protected clusters possess a very specific geometry, i.e. a size dependent atomic packing symmetry, different from the face-center-cubic model characteristic of nanoparticles. Three representative examples of this size dependent structure are $Au_{25}(SR)_{18}$, $Au_{38}(SR)_{24}$ and $Au_{144}(SR)_{60}$:

- the crystal structure of $Au_{25}(SR)_{18}$ showing a center icosahedral Au_{13} kernel surrounded by an exterior gold shell composed of six long staples (-S-Au-S-Au-S-, denoted as $Au_2(SR)_3$ below)[44]. The entire particle adopts a quasi-D_{2h} symmetry and is protected by 18 thiolate ligands.

- $Au_{38}(SR)_{24}$ is composed of a face-fused bi-isocahedral Au_{23} core protected by six $Au_2(SR)_3$ extended motifs and three 'short' RS-Au-SR simple motifs. Among the motifs, the six $Au_2(SR)_3$ are evenly distributed on the two icosahedral Au_{13} subunits, while the three $Au(SR)_2$ motifs bridge the two icosahedral units.

- $Au_{144}(SR)_{60}$ cluster is composed of an icosahedral Au_{114} core with 30 short RS-Au-SR staples protecting the entire particle.

$Au_{25}(SR)_{18}$ $Au_{38}(SR)_{24}$ $Au_{144}(SR)_{68}$

Au(0)   S   Au(I)
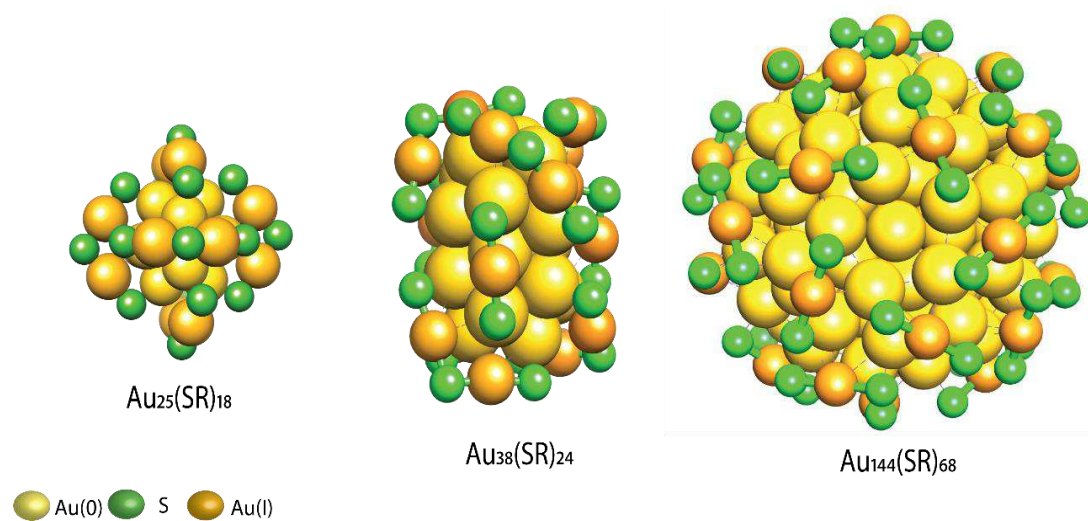
Figure 1-5 The crystal structures of $Au_{25}(SR)_{18}$ (left) and $Au_{38}(SR)_{24}$ (center) and $Au_{144}(SR)_{60}$ (right). Au is consider to be in the oxidation state 0 for the atoms in the core (yellow) and 1 for the atoms on the staple (orange)

The unique core/shell geometrical structure and electronic properties makes them particularly interesting; hence our desire to pursue their catalytic applications.

Another strategy to enhance certain properties is doping. This was often used in metallurgy, as designed alloys with a mixture of different metals usually outperform pure metals.

For instance, the hardness and corrosion resistance of copper can be immensely enhanced by mixing it with zinc and other metals, leading to the well-known alloy brass. This idea encouraged the cluster community to try to combine different metals inside gold nanoclusters. These materials became known as 'doped' clusters. Initially, the formation of doped clusters was confirmed using Matrix-Assisted Laser Desorption Ionization (MALDI) and Electrospray Ionization (ESI) Mass Spectrometry (MS) measurements [45]. Single-Crystal X-ray Diffraction (SC-XRD) measurements were also necessary to determine the exact positions of the foreign atoms in the parent cluster [46-47]. To date, only certain doped clusters have had their structures fully resolved, while the large majority remain unexplored.

Several studies pointed out that the introduction of dopant atoms can remarkably alter the cluster properties. This holds for their reactivity [48], stability [49], optical properties [50], and magnetism [51]. The changes in their properties can be related to an interplay between cluster geometry and electronic structure, both being affected by doping. In the case of gold, the dimension of the structure can be altered significantly by doping. For example, according to theoretical calculations a single Pd dopant atom will reduce the structure to its smallest possible size [52].

The electronic structure is also altered remarkably. This is particularly the case if the dopant atom has a different number of valence electrons, or when the dopant atom has a different electronegativity than the host element, inducing significant electron charge transfers [53]. The combination of these effects makes it difficult to predict the influence of doping on the stability or on the reactivity. In Chapters 4 and 5, we shall use HAADF-STEM to show how different types of doping affect the stability and how doping changes cluster performance under reaction conditions.

1.3.2. Thiolate protected clusters for catalytic applications

Ultrasmall (n<200) metal nanoclusters exhibit many unique properties such as luminescence [54-56], catalytic activity [57], chirality and magnetism [58, 59]. These properties make them attractive for a wide range of applications like thermal and photocatalysis [60], chemical sensing [61], biological labelling and biomedicine [62, 63]. This thesis will focus on their application in heterogeneous catalysis, as their small size provides several distinct features including a high specific surface area, a high fraction of low-coordinated atoms, quantum size effects, tuneable compositions, and unique surface structures (e.g. pocket-like sites) [57, 64].

Nanoclusters protected by thiol ligands often show somewhat lower activity — in certain reactions even largely inhibited reactivity [65-67]. Nonetheless, there are cases in which ligands are not as negative and, instead, can be utilized to exert beneficial effects on the catalytic reactions. In order to control product selectivity, for example [68]. However, in general terms it is necessary to induce partial or complete ligand removal to enhance contact between the surface metal atoms and the reactants, and in this way affect the catalytic activity. Common procedures include the immobilization of metal clusters onto support materials, followed by removal of ligands by means of a thermal treatment. The method of immobilization and of thermal pretreatment must be carefully chosen in order to avoid agglomeration or sintering. Available techniques to compare the sizes and distributions of clusters before and after ligand removal include High-Resolution Transmission Electron Microscopy (HRTEM) and X-ray Absorption Spectroscopy (XAS). A further step is to establish correlations between structure and catalytic activity, and for this purpose, special set-ups were developed.

In the following sections we shall discuss the main parameters that can affect catalytic activity, namely: the pretreatment effect, the size and support effect, the loading effect and the doping effect.

1.3.3. Pretreatment effect

There are many examples in the literature which reveal the importance of the pretreatment temperature and gas composition to activate the catalyst while keeping the structure. Initially Jin et al. examined the relative stability of Au–S binding modes in $Au_{25}(SG)_{18}$ clusters using NMR and optical spectroscopy[69]. They found that ligands directly attached to the Au core were more stable than the thiolate-gold bonds of the staple motifs. Some ligands were removed at temperatures of 160 °C, while the rest of the thiolates were stable until 180 °C. The same group also performed Thermogravimetric Analysis (TGA) of $Au_{25}(SR)_{18}$, $Au_{38}(SR)_{24}$ and $Au_{144}(SR)_{60}$ clusters[70]. They showed that mass loss begins at a temperature of around 200 °C with all ligands having been removed by ca. 250 °C. The calcined catalysts (200 °C for 2 h) showed a better catalytic activity for styrene epoxidation reactions due to the increased accessibility of the Au catalysts once the ligands had been partially removed.

Nie et al. examined the activation of phenylethanethiolate-stabilized $Au_{25}(SR)_{18}$ clusters on different oxide supports for CO oxidation and determined the highest values for ceria supports and activation at 150 °C under oxygen[71]. As the calcination time increased from 0.5 h to 1.5 h a drastic change in catalytic activity was observed (from 18.2% to 92.4%). However, catalytic activity did not show any improvement after a longer times.

Tsukuda et al. also examined the activation of $Au_{25}(SR)_{18}$ clusters on hydroxyapatite supports, and reported the highest activity for the selective oxidation for clusters without ligands. The total removal of ligands at 300°C was evidenced by the mass loss in the system [72].
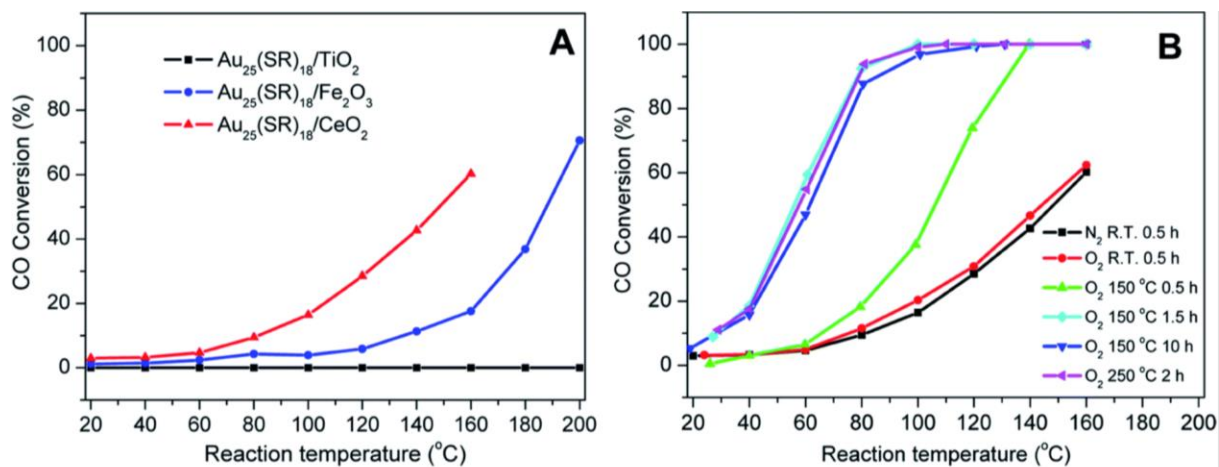
Figure 1-6 Activation of Au$_{25}$(SR)$_{18}$ clusters over different metal oxides for CO oxidation. (A) CO activity over different metal oxides as a function of temperature for unactivated clusters and (B) CO activity on ceria supports under different activation conditions [71].

Other studies employed X-ray Absorption Spectroscopy (XAS) as a valuable technique to explore cluster integrity upon calcination of supported-cluster materials. Gaur et al. looked into the activation of phenylethanethiolate- and hexanethiolate-stabilized Au$_{25}$(SR)$_{18}$ clusters on carbon supports [73]. They measured the Extended X-ray Absorption Fine Structure (EXAFS) after 1.5h in air at temperatures of 125 °C, 150 °C, 200 °C, and 250 °C and concluded that the thiolate ligands start being removed from the Au surface at 125 °C and are close to being completely removed by 250 °C. During the activation process, peaks due to Au–S species just below 2 Å slowly disappear. This indicates the removal of thiolate ligands. The growth in the first shell Au–Au peaks in the 2.5 to 3.0 Å region was attributed to sintering. The maximum activity for 4-nitrophenol reduction with NaBH$_4$ was seen for clusters activated at 250 °C.

Afterwards, Tsukuda et al. [66] also showed that some ligand removal was essential for liquid phase aerobic oxidation of benzyl alcohol on Au$_{25}$(SR)$_{18}$ clusters supported on carbon nano-sheet supports. They removed thiols by calcination under vacuum and found that ligands were increasingly removed at higher temperatures with little to no growth in cluster sizes. Interestingly, they found that the clusters without ligands had no activity, while those that still had some residual thiolates were selective catalysts for the oxidation of benzyl alcohol to benzaldehyde.

1.3.4. Support effect

A number of studies have also examined the role of the support in the resulting stability of Au clusters after activation. For example, Yan et al. looked at the activation of 6-mercaptohexanoic acid protected $Au_{25}(SR)_{18}$ clusters on various supports. No significant size growth of the clusters was seen on hydroxyapatite and Degussa P25 titanium supports, but significant sintering of the clusters was seen on activated carbon, graphene oxide, and silica supports. The suggestion is that the increased stability in the two systems is due to stronger interactions of the clusters with the supports [74].

In many cases, the support not only stabilizes the particles and prevents sintering, it also plays a significant role in the reaction [119]. Support materials for metal nanoparticles are described as being either reducible or 'active' (e.g. CeO_2 and TiO_2) or irreducible or 'inert' (e.g. SiO_2 Al_2O_3 and carbon) based on the nature of the interaction between the support and the nanoparticles. In general, reductive supports have stronger interaction nanocluster-support, while irreducible supports have a weaker one. For oxidations reactions, there is a common agreement that reducible supports such as TiO_2 or CeO_2 are more active than irreducible supports. For example, Schubert et al. [75] studied the support effect by means of isotopic scrambling experiments with labeled $^{36}O_2$ and concluded that gold catalysts supported on inert supports like SiO_2, Al_2O_3, and MgO are less active for CO oxidation than gold supported on reducible metal oxide such as Fe_2O_3. Computational simulations also support these results. For example, the first-principle simulations on Au_n (n≤20) clusters supported on MgO showed that the electron transfer between gold clusters and defects on the support (due to oxygen vacancy) play a significant role in activating Au nanoparticles for catalyzing CO oxidation [76].

The role of the support is also relevant in other types of reactions. For instance, Gao et al. performed a density functional theory study comparing two types of support: the 'inert' support of hexagonal boron nitride (h-BN) with the N and B vacancy defects and the 'active' support of rutile $TiO_2(110)$. They demonstrated that the rutile $TiO_2(110)$ support promotes H_2 dissociation due to the formation of the OH group near the supported gold cluster.[77]. Our work related to size and support effect is discussed in detail in Chapter 3. This work has already been published

in 2019 [78]. Consequently, the oxide material employed as support may have a strong influence on the stability of the supported cluster.

1.3.5. Loading effect

An additional relevant variable affecting the dispersion of the clusters on the surface is the relative weight % loading. Sintering can be reduced by ensuring optimum cluster loading onto supports during the impregnation step. Previous work by Xie et al. showed an optimum metal loading with 0.2%wt $Au_{25}(SC_{12}H_{25})_{18}$ clusters supported on carbon nanotubes (thermally activated at 300°C and 400°C), varying from 0.05–1.0 Au wt% [79], although in all the studied cases the size is lower than 2 nm. Lavenn et al. studied $Au_{25}(SPh\text{-}pNH_2)_{17}$ clusters supported on mesoporous silica SBA-15 (pretreated at 400 °C) varying the metal loading between 0.04 and 1.07 Au wt%. The analysis displayed similar average particle sizes: 1.9 ± 0.6 nm and 1.8 ± 0.5 nm for metal loadings of 0.04 but also in the case of 1.07 Au wt%. The preservation of average particle size at higher loading is likely due to the confinement of particles inside the silica mesoporous support [80]. From both studies, the main idea is that the loading should be controlled and keep into account during the catalyst preparation.

1.3.6. Doping effect

The exchange of 1 to n number of Au atoms with another metal, generally known as doping, has a strong effect both on the physical-chemical properties of the clusters and on their catalytic behavior.

Previous studies have already shown that doping can affect the catalytic properties of the nanoclusters [81]. The catalytic activity of $Pd_1Au_{24}(SR)_{18}$ supported on carbon nanotubes (CNT) was evaluated in the oxidation of benzyl alcohol [79]. The ligand-removed Pd_1Au_{24}/CNT catalyst was found to significantly enhance the catalytic activity (74% conversion of $PhCH_2OH$, compared

to 22% over undoped Au_{25}/CNT). The effect of the single Pd atom was ascribed to the change in the electronic structure of the cluster by electron transfer from Pd to Au. In the case of $Pt_1Au_{24}(SR)_{18}$ supported cluster on TiO_2, significantly higher activity was obtained in comparison to the undoped cluster.

In the selective oxidation of styrene reaction [82] a 90.8% conversion of styrene was obtained with the doped cluster catalyst compared to 58.9% of the undoped $Au_{25}(SR)_{18}$/TiO_2 catalyst. Moreover, the selectivity for benzaldehyde (89.9%) was higher than the $Au_{25}(SR)_{18}$/TiO_2 catalyst (54.0%). Pt doped clusters were also reported to be highly active in hydrogen production – even higher than Pt catalysts [83].

Pd- or Pt doped nanoclusters are more stable than pure gold nanoclusters, when contrasted with Ag or Cu doped ones. For Cu-doped nanoclusters, the lower stability has been attribute to the positions of the foreign atom in the cluster structure. However, diverse results have been observed, depending on the reaction type. Jin et al. explored the doping effects of bimetallic nanoclusters on styrene oxidation, reporting that Ag-doping increases the conversion of styrene and the benzaldehyde selectivity. In contrast, Cu showed no effect on the conversion but did increase the benzaldehyde selectivity [84].

Regarding silver doping, Zhu et al. studied the $[Ag_{46}Au_{24}(SR)_{32}](BPh_4)_2$ nanocluster structure-related catalytic properties. First, they compared the catalytic behavior of pure gold (Au_{25}/CNT) with pure silver (Ag_{44}/CNT) nanocluster catalysts in the styrene oxidation reaction. The results showed that gold clusters gave a higher conversion of styrene, whereas silver ones resulted in a higher selectivity to benzaldehyde. Afterwards, they compared these results with the bimetallic nanocluster ($Au_{24}Ag_{46}$/CNT) catalysts, observing a selectivity increase for epoxide (that is, >95%) along with better conversion [85].
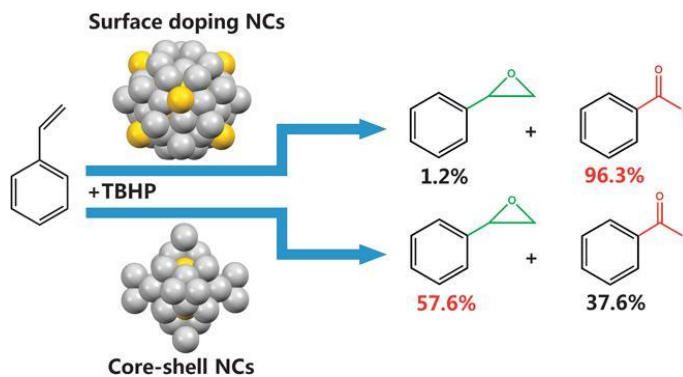
Figure 1-7 *Two different kinds of surface doped nanocluster catalysts in styrene oxidization [85].*

A recent study reported the catalytic effects of Cu, Ag, and Pt doped clusters supported on titanium for the carbon-carbon coupling reaction of *p*-iodoanisole and phenylacetylene. $Pt_1Au_{24}(SR)_{18}$ resulted in a drop in the catalytic activity keeping the selectivity to 1-methoxy-4-(2-phenylethynyl)benzene, while the $Ag_xAu_{25-x}(SR)_{18}$ nanoclusters gave an overall performance comparable to $Au_{25}(SR)_{18}$. Interestingly, $Cu_xAu_{25-x}(SR)_{18}$ nanoclusters increased the production of 4,4'-dimethoxy-1,1'-biphenyl, whereas the other three nanocluster catalysts did not. The conclusion is that the conversion is affected by the electronic effect and the selectivity is determined by the type of atoms on the M_xAu_{12-x} shell (M=Ag, Cu, and Au) in the nanocluster catalysts [86].

According to Deng et al., doping with other atoms like Cd, Hg or Ni is also possible with high activity being observed in cadmium doped clusters for benzyl alcohol oxidation [82]. Recently, even group XIV elements (Si, Ge, Sn, and Pb) have been investigated using Density Functional Theory (DFT) calculations [87]. Clearly, doping is still an expanding research topic. These new doping possibilities have opened the door for further research in the field of catalysis.

To conclude, catalytic activity is strongly affected by the nature of metal doping, i.e. the number of atoms exchanged and their position inside the core structure of the nanocluster. Our results on the effect of doping in different oxidation catalytic reactions can be found in Chapters 4 and 5.

1.4. Oxidation reactions

The catalytic activity of gold nanoparticles and clusters has been investigated in many liquid phase oxidations. First, Turner et al. have shown that gold can carry out selective oxidation reactions using only molecular oxygen, whereas previously additives such as hydrogen or a peroxide species were necessary as well. This behavior only emerges in nanoparticles smaller than 2 nm in diameter, a regime that can be accessed with the help of techniques from cluster chemistry [88].

As an example of O_2 activation, styrene oxidation has been systematically investigated. Firstly, Tsukuda et al. studied glutathione-protected Au_{25} clusters supported on hydroxyapatite (HAP). They observed the highest yield of styrene oxide for Au_{25}-HAP (92% at 12h) reported so far [57]. Following on from this work, Jin et al. investigated Au_{25}-HAP in more detail, revealing that HAP efficiently stabilizes the cluster, leading to a large increase in its catalytic activity compared to $Au_n(SR)_m/SiO_2$ [70]. In addition, Yuhan et al. investigated Au_{25} supported on CeO_2 nanorods and on CeO_2 nanoparticles, concluding that the support structure also plays a role in selectivity due to the charge distribution and the electron transfer of Au_{25} on CeO_2 [89]

Another interesting example of oxygen activation is the selective oxidation of sulfide to sulfoxide by iodosylbenzene. Sulfides can bind to the surface of gold nanoclusters via the interaction between the sulfur atom (–S–) and the gold surface, while sulfoxides only weakly bind to the gold surface. Jin et al. reported high catalytic activity (*e.g.* ~97% conv. of Ph–S–CH_3 and ~92% selectivity for Ph–S(=O)–CH_3 sulfoxide) for the TiO_2-supported $Au_{25}(SR)_{18}$ nanocluster catalysts.[90]. Afterwards, Gao et al. studied $Au_{144}(SCH_2Ph)_{60}/TiO_2$ and reported an excellent catalytic performance (92% conversion of methyl phenyl sulfide with 99% selectivity for sulfoxide) in the selective sulfoxidation, as well as size-dependence behavior ($Au_{144}(SCH_2Ph)_{60}$ > $Au_{99}(SPh)_{42}$ > $Au_{38}(SCH_2CH_2Ph)_{24}$ > $Au_{25}(SCH_2CH_2Ph)_{18}$) [91].

The aerobic oxidation of D-glucose into gluconic acid has also been investigated by Zhang et al. as a model reaction for different gold cluster sizes, including $Au_{25}(SR)_{18}$, $Au_{38}(SR)_{24}$, and $Au_{144}(SR)_{60}$ immobilized on activated carbon (AC). They observed a clear size dependence defined

as $Au_{144}(PET)_{60}/AC > Au_{38}(PET)_{24}/AC > Au_{25}(PET)_{18}/AC$. Moreover, the turnover frequency (TOF) for the $Au_{144}(PET)_{60}/AC$ catalyst was found to be 2.3 s^{-1}, which is much higher than those for the commercial Pd/AC and Pd-Bi/AC catalysts under identical reaction conditions [92].

All these examples point to the notion that the higher catalytic activity is mainly due to the distinctive frame structure and electronic properties of the gold nanoclusters and the protecting ligands. However, chemical processes involving harsh reaction conditions could lead to a decrease or even disappearance of catalytic activity due to the increasing size of formed particles. For this reason, in our work we have concentrated on two strategies to maintain the stability of gold nanoclusters under reaction conditions: the size and support effect (Chapter 3) and the doping effect (Chapters 4 and 5). As an example of catalytic application, we have looked at two types of oxidation reaction, one in liquid phase (cyclohexane oxidation) and another in gas phase (CO oxidation).

1.4.1 Cyclohexane oxidation
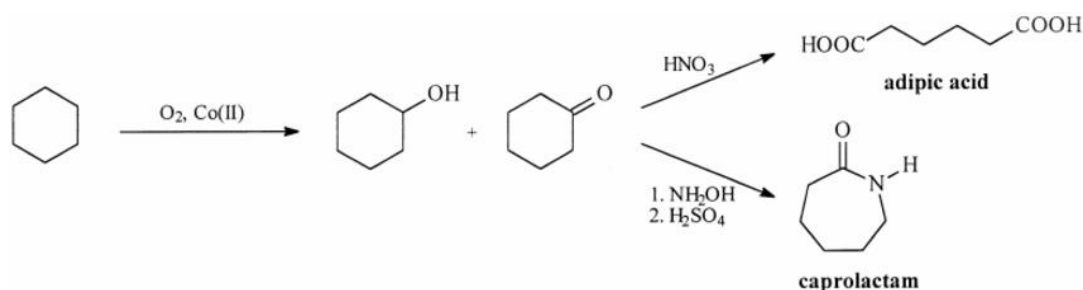
Figure 1.48 Conversion of cyclohexane to adipic acid or ε -caprolactam. [93]

Since pyridine was banned as a solvent in the chemical industry, many efforts have been made to develop new catalysts to oxidize cyclohexane under mild conditions. As it is shown in Figure 1-8, this reaction is relevant in industry in order to obtain nylon 6-6. Different strategies employing oxidation with hydrogen peroxide, tert-butyl hydroperoxide and molecular oxygen combined with metal particles supported on high surface oxides have been investigated. Cyclohexane oxidation with tert-butyl hydroperoxide gives much higher efficiencies in the presence of homogeneous or heterogeneous catalysts since this oxidant is more reactive.

However, its higher price makes it unattractive for industry. The ideal oxidant would be a combination of molecular oxygen with peroxide as it is cheaper and quite selective if temperatures not higher than 343 K are used [93]. The choice of appropriate catalyst is still a topic of discussion, however.

Thiolate protected gold clusters supported on oxides have been investigated in order to follow the effect of the presence of thiols, the size effect and metal composition effect. For example, Zhang et al. examined the activation of $Au_{38}(SR)_{24}$ clusters on alumina and ceria supports in air and inert atmospheres [94]. Activation pretreatment in an oxygen atmosphere was seen to be necessary and the best support was found to be cerium oxide. Interestingly, cyclohexanethiol was one of the by-products.

Zhao et al. studied Au clusters supported on mesoporous silica and ascribed their reactivity to the presence of low-coordinated Au (0) sites with high dispersion. They showed that Au clusters promote the activation of O_2 molecules and accelerate the formation of surface-active oxygen species [95].

Tsukuda et al. investigated the size effect on cyclohexane oxidation. Figure 1.4-9 shows the size dependence of the TOF of cyclohexane oxidation over Au_n/HAP. Volcano-like behaviour was observed, with the TOF peaking at Au_{39}. The size dependence in Figure 1.4-9 cannot be explained merely by geometrical factors such as surface area and the number of low-coordination sites.
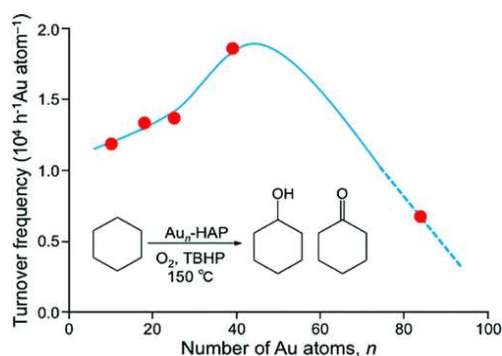
Figure 1.49 *Selective oxidation of cyclohexane to cyclohexanol and cyclohexanone with O_2 as the oxidant catalyzed by Au_n/HAP. Adapted with permission from [96]*

Beyond the studies cited however, a deeper understanding of the size and support effect on catalytic behavior of nanocluster catalysts and on the reaction mechanism has not yet been fully obtained. For this reason, cluster size and composition, as well as the support effect on the cyclohexane oxidation reaction using in-situ spectroscopy techniques was chosen as the topic of study for this thesis (Chapter 4).

1.4.2   CO oxidation

Carbon monoxide oxidation is one of the most studied reactions for gold catalysts and is often used as a reference. To date, hundreds of articles on CO oxidation have been published, but despite being a simple reaction, its mechanism has proven extremely difficult to establish. Different research groups have used different conditions and approaches — quite often without specifying important parameters. Nonetheless, it is generally agreed upon that catalytic activity in CO oxidation is associated with small gold particles (< 5 nm), rather than with large particles [97].

Further investigations have also corroborated the significance that the perimeter area of the metal–oxide interface plays in determining the catalytic performance for CO oxidation [98, 99]. With regards to the support effect, it has been shown that for CO oxidation Au supported on reducible supports such as TiO_2, Fe_2O_3, CeO_2, ZrO_2 etc. is much more active than non-reducible supports such as SiO_2 and Al_2O_3 [100]. The role of the ligands has been studied by Wu et al. They looked at the activation of $Au_{25}(SR)_{18}$ clusters on ceria rods for CO oxidation, noting that the thiolate ligands were a "double-edged sword" for CO oxidation as they blocked CO adsorption sites on Au while also being important in the retention of cluster integrity [101]. Detailed IR studies of CO adsorbed onto activated cluster surfaces have further shown that partially cationic (δ^+) Au sites at the Au/ceria interface are likely to be the major catalytic sites for CO oxidation, only appearing after calcination of the $Au_{25}(SR)_{18}$ clusters on ceria at temperatures of 150 °C and beyond. Interestingly, the Mars van Krevelen mechanism takes the dominant role in converting CO, which firstly reacts with the lattice oxygen of CeO_2, the gas-phase O_2 then refilling the

consumed oxygen, while the Langmuir-Hinshelwood mechanism of CO and O_2 activated by exposed Au sites takes the rest.

The negative role of the ligands has also been studied by Jin et al. [102], who corroborated the steric hindrance of ligands at the interface between the thiolate and CeO_2 inhibits CO adsorption onto Au sites thereby adversely affecting CO oxidation.

Using titania as a support, Wang et al. have studied CO oxidation catalyzed by supported Au nanocatalysts via molecular dynamics simulations. They followed the Au—CO species that migrates from the Au-cluster to react with a surface oxygen atom. The oxygen seems to be provided by the TiO_2 support via a Mars van Krevelen mechanism. [103].

Regarding size effect, Li et al. have performed a comprehensive study of catalytic activities of subnanometer Au clusters supported on $TiO_2(110)$ surface (Au_n/TiO_2, n = 1–4, 7, 16–20) by means of DFT calculations. They found that catalytic activities of the Au_n/TiO_2 systems increase with the size n up to Au_{18}, for which the hollow-cage Au_{18} isomer exhibits the highest activity for CO oxidation, with a reaction rate ~30 times higher than that of Au_7/TiO_2 system [104].

The doping effect has also been shown to affect the catalytic activity, although a general conclusion has not been achieved due to the complexity of these studies. Li et al. reported that it would be preferable for the adsorption of CO on the clusters to occur in the order $Cu_2Au_{23}(SCH_3)_{15}>Au_{25}(SCH_3)_{15}>Ag_2Au_{23}(SCH_3)_{15}$. They deemed the metal atoms thus exposed (Au, Ag, and Cu) to be the catalytic active sites (See Figure 1.4-10) [105].
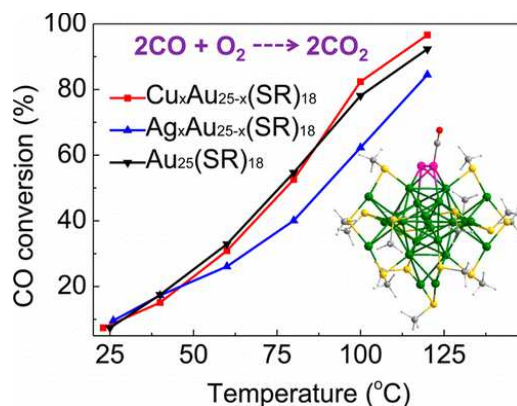
Figure 1-10 *Catalytic activity in the CO Oxidation Using Bimetallic M_xAu_{25-x} Clusters [105]*

In Chapters 5 and 6, we shall compare palladium doped clusters and silver doped clusters with their pure gold counterpart and the differences in catalytic activity will be investigated with different spectroscopic techniques such as IR and XAS.

1.5. X-ray Spectroscopic Studies of thiolate gold nanoclusters

Structural characterization of nanomaterials is challenging due to their small size. Many of the classical tools, such as powder X-ray diffraction measurements are challenging for samples in subnanometer range, since those are usually not perfectly crystalline. X-ray spectroscopy (including both absorption and photoemission spectroscopies) has emerged as a powerful tool to investigate the structure and electronic properties of nanomaterials. Particularly, X-ray absorption can provide average information regarding the oxidation state, chemical environment and structure (bond length). In particular, when these in-situ or ex-situ tools are combined with catalytic measurements they can provide deep insight into the structure and bonding of nanomaterials under reaction conditions [106].

Generally speaking, XAS can simply be treated as a cousin of the widely used UV−vis absorption spectroscopy. The major difference between these two absorption spectroscopy techniques is that XAS involves core-level electronic transitions, whereas the UV−vis absorption only involves valence-orbital related transitions. A typical XAS spectrum consists of two spectral

regions (Figure 1-11): X-ray Absorption Near Edge Structure (XANES) and Extended X-ray Absorption Fine Structure (EXAFS).
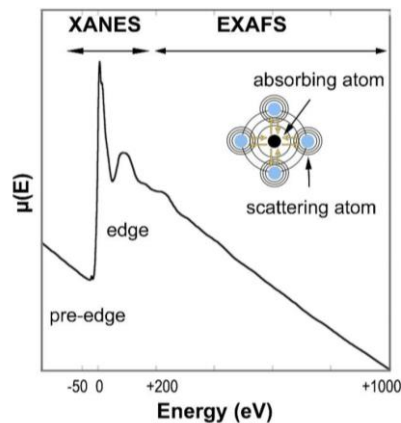
Figure 1-11 *Schematic representation of an XAS spectrum showing the two main regions. Adapted with permission from R. Ortega, A. Carmona, I. Llorens, P.L. Solari, X-ray absorption spectroscopy of biological samples. A tutorial, J. Anal. At. Spectrom. 27 (2012) 2054-2065*

XAS measures the way in which an X-ray beam is absorbed while passing through a material. As a result, a sharp attenuation of the X-ray beam – typically called an absorption edge — occurs when the incident photon energy is equivalent to the core level binding energy of the atom. The way in which the sample attenuates the X-ray beam provides information about the geometric and electronic environment around the nuclei under study. The quantity which describes this attenuation is called the X-ray absorption coefficient, μ, and is related to the X-ray beam intensity being measured by the equation:

Equation 1-1 X-ray absorption coefficient formula

$$\mu(E) = log(I/Io)$$

whereby I_o and I represent the intensity of the X-ray beam before and after transmission through the sample [107].

XAS is based on the analysis of the changes of μ, or on the oscillations of an X-ray absorption spectrum. Any element with core level electrons could be studied using XAS and it is applicable

to materials in any physical state (e.g. amorphous, liquid, etc...). However, in order to conduct an XAS experiment, a source of X-rays is needed that is both extremely bright and tunable across a wide energy range. For this reason, a synchrotron X-ray source is required.

1.5.1   Extended X-ray Absorption Fine Structure

EXAFS represents the quantitative structural portion of an XAS experiment. In an EXAFS experiment one can observe the attenuation of X-rays in the region far past the absorption edge. This attenuation originates from the absorption of an X-ray photon, which generates a photo-electron wave. The mechanism of EXAFS can be conceptually understood through several key steps:

(a) absorption of an X-ray photon;

(b) creation of a photoelectron wave and

(c) scattering of the photo-electron wave at neighboring atoms.

The way in which the outgoing and (back)scattered photoelectron waves interfere causes the attenuation of X-rays observed in the EXAFS region of an XAS experiment.
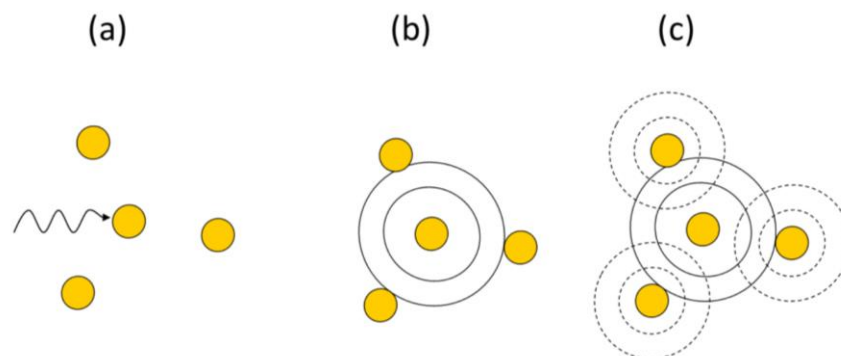
Figure 1-12 *Schematic representation of the main mechanism behind the modulation of μ in the EXAFS region and the wave off of neighboring atoms. The way in which the outgoing and backscattered photoelectron waves interfere causes the attenuation of X-rays observed in the EXAFS region of an XAS experiment [1].*

The photoelectron wave generated by X-ray absorption first travels through the material, eventually reaching a neighboring atom. This wave then interacts with the neighboring atom's

electron density, which in turn causes the photoelectron wave to be scattered back towards the original absorbing atom. The resulting phase and amplitude of this backscattered photoelectron depend on the incident photon energy and the atomic number of the neighboring atoms. Finally, this backscattered wave will add constructively or destructively to the original photoelectron wave. There are two possibilities:

- The backscattered wave is in phase with the original photoelectron wave. Then the absorption of X-rays by the sample— and thus μ — will increase.

- If the backscattering is out of phase there will be a decrease in μ.

By subtracting a background function to represent μ_0 and dividing by the 'edge jump' or $\Delta\mu_0$, the resulting fine structure, χ, is obtained, as shown in Equation 1-2.

***Equation 1-2** EXAFS fine structure*

$$\chi(E) = \frac{\mu(E) - \mu o(E)}{\Delta\mu o(E)}$$

Typically, χ is displayed as a function of the photoelectron wave vector, $\chi(k)$, rather than energy, whereby:

***Equation 1-3** K definition*

$$k = \sqrt{\frac{2m(E - Eo)}{\hbar^2}}$$

and m is the electron mass, E the energy of the incoming photon, E_o the binding energy of the core level electron, and $\hbar$ the reduced Planck constant. The fine structure, $\chi(k)$ (often referred to as k-space), represents a superposition of all the scattering paths around the absorbing nuclei. Due to the dependence of the backscattering amplitude on both energy and atomic number, it is common to weight $\chi(k)$ by kn, with n equal to 0, 1, 2 or 3, in order to make the amplitude of the spectrum more uniform. The $\chi(k)$ can then be treated by Fourier analysis, and the components

of $\chi(k)$ can be separated out based on distance from the absorbing atom, R, providing a radial bond distribution about the absorbing atom (Figure 1-13).
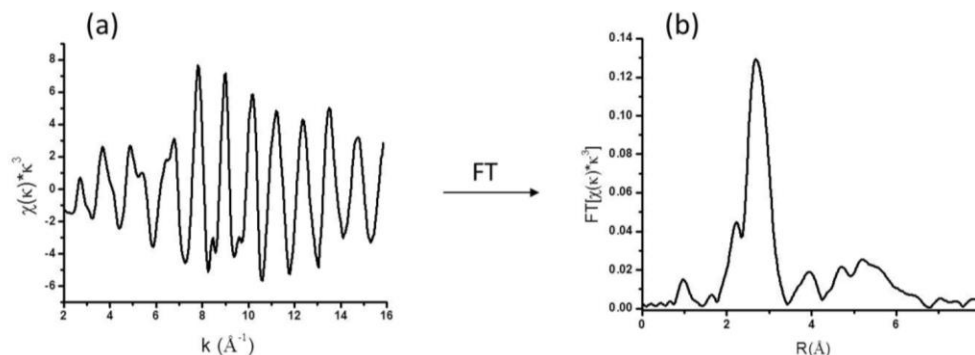
Figure 1-13 *The (a) $\chi(k)*k^3$ and (b) $FT[\chi(k)*k^3]$ obtained from XAS at the Au LIII-edge. By weighting the $\chi(k)$ by a factor of k^3 the oscillation amplitude is made more uniform across all values of k before Fourier transformation. The peaks in part (b) represent the radial bond distribution around the absorbing Au atom in Au foil, with the large peak at ~2.7Å representing the first Au-Au coordination shell.*

The Fourier transformation of the $\chi(k)$ can then be refined to a structural model of the material which will provide structural information about the local bonding environment. In order to refine an EXAFS spectrum and extract structural information about the scattering amplitude, the phase shift for the neighboring atoms must be determined. Traditionally this was achieved by collecting the EXAFS spectrum of a well-understood sample with a similar structure (e.g. foil, bulk material) and extracting the amplitude and phase from the experimental data. These days, however, these refinement standards are more commonly reproduced by simulations of structural models using the FEFF program code. This produces high quality EXAFS fitting files, which can then be refined to fit the experimental data.

1.5.2 X-ray Absorption Near-Edge Structure

Typically, the XANES region of an XAS spectrum extends to approximately 40 eV past the absorption edge (core level binding energy). Within this region 'near the edge' one can observe electronic transitions and multiple scattering photoelectric effects that can provide details about

the structure (lattice symmetry, coordinate environment) and electronic properties (oxidation state, band occupation) of the element being studied [108]. Specifically, transitions observed closest to absorption represent transitions from occupied core states to unoccupied valence states (Figure 1-14).
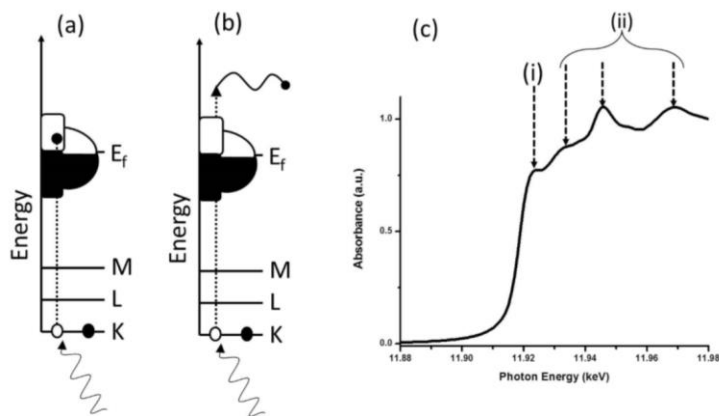
Figure 1-14 *Schematic representing (a) the transition of a core electron into an unoccupied energy state and (b) emission of a photoelectron following X-ray absorption. The Fermi level is marked by EF while the core levels are marked using XAS nomenclature. (c) represents the XANES region of an XAS scan of Au foil at the LIII-edge.*

These transitions can sometimes be lower in energy than the normal binding energy of the core electron, in which case they are called pre-edge features due to their occurrence before the normal absorption edge. Other features in a XANES spectra are associated with complex multiple scattering events that occur. XANES spectra can be process employing lineal combination of different references to get insights into the stability and evolution of a given system during a chemical reaction and to find out the oxidation states of said reaction. An example is described in detail in Chapter 3.

1.5.3   XAS for thiolate protected clusters

Uncovering the crystal structure of atomically precise gold nanoclusters can provide important insights into the electronic structure, stability, and unique coordination environments of Au. The main obstacles for finding the exact structure of the many different configurations are:

a) the lack of a repeating gold lattice

b) the challenge of growing single crystals

c) electron microscopy techniques for obtaining crystal packing information about the Au core

d) the organic ligand-Au interface is undetectable with such techniques.

A promising experimental approach in recent years has been to use X-ray absorption spectroscopy (XAS). There are several advantages for using XAS including: the measurement of subnanometer particle sizes (or seemingly amorphous materials), variable experimental conditions, e.g. solution-phase, temperature, in-situ redox, the ability to prove multiple absorption edges for different elements (Au, S, Se, etc.), and the fact that data analysis can reveal both metal-metal and metal-ligand structural environments [109].

The first XAS study of thiolate protected gold clusters was conducted on Au_{144} by MacDonald et al. [110]. They were able to determine the atomic structure of $Au_{144}(SR)_{60}$ with EXAFS by comparing the spectra differences depending on the nanocluster sizes at the Au L_3-edge and S K-edge. Figure 1-15 shows how the intensity of the S-Au pre-edge feature increases with the particle size. The white line intensity increase in the order of bulk $\rightarrow Au_{144} \rightarrow Au_{38} \rightarrow Au_{25}$, indicates a d-electron depletion as the size decreases [110].
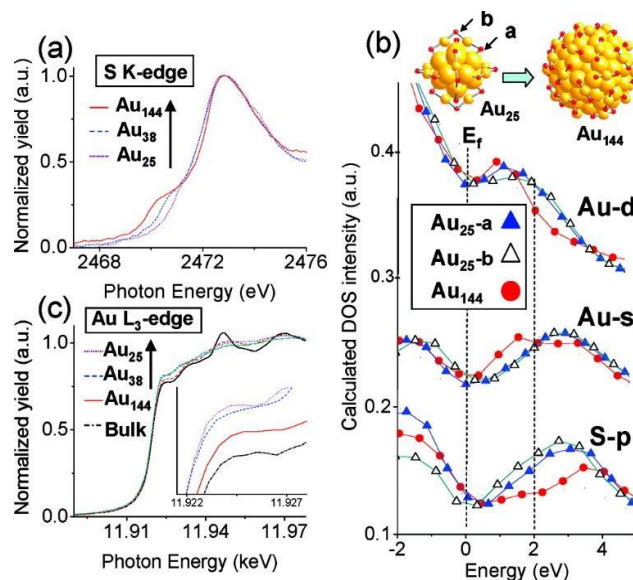
Figure 1-15 *XAFS analysis of different cluster sizes [110]*

Au$_{144}$, Au$_{38}$ and Au$_{25}$ have been extensively studied by XAFS, due to their resolved structures and the well established synthetic procedures. Figure 1-16 shows the results obtained by Tsukuda and Yamazoe within the detailed study of the structure using XAFS compared to X-ray crystallography data [110]. The CN (coordination number) and r (distance) values for the Au–S, Au–Au(S) and Au–Au(L) bonds obtained by EXAFS are in agreement with those determined by single crystal XRD data, demonstrating the efficiency of EXAFS measurements.
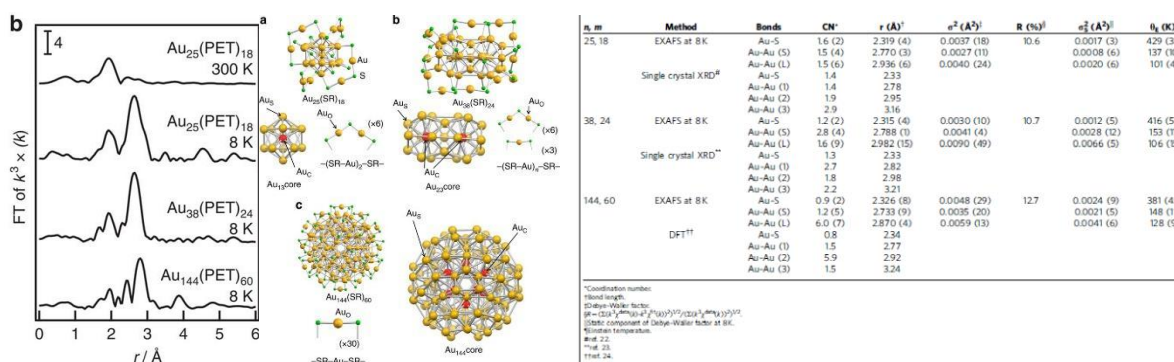
Figure 1-16 *Yamazoe, S., Takano, S., Kurashige, W. et al. Hierarchy of bond stiffnesses within icosahedral-based gold clusters protected by thiolates. Nat Commun 7, 10414 (2016)*

However, these studies were performed with nanoclusters in solution, and the structure can be affected once they are immobilized on oxide supports. In order to understand the catalytic

active site of Au nanoclusters, EXAFS spectra are measured at Au L_3-edge to understand the cluster surface local structure change after thermal pretreatment. Specifically, Au-Au and Au-S coordination numbers and Au-Au bond length can be related to ligand removal (Figure 1-16 Yamazoe, S., Takano, S., Kurashige, W. *et al.* Hierarchy of bond stiffnesses within icosahedral-based gold clusters protected by thiolates. *Nat Commun* 7, 10414 (2016)

Using EXAFS, Spivey et al. explored the stability of clusters during the thermal activation of Au_{38}/TiO_2 [73]. After reductive treatment at 400°C, the CN values of Au_{38}/TiO_2 increased, denoting an increase in the particle size. Liu et al. compared Au_{25} nanoclusters supported on SiO_2 as support before and after calcination [111]. Au L_3-edge EXAFS indicated the thiolate ligands were mostly removed by 200°C in air and by 300°C under He gas.

Using EXAFS to monitor the structure of $Au_n(SR)_m$ in-situ or ex-situ can help detect small changes on the Au nanocluster surface or in the core. In Chapter 4, XANES is used to investigate the size, the support and the pretreatment effect.

In the case of doping, the preferred location of the metal dopant and its effect on the structure can also be resolved using XAS measurements. Conveniently, XAS experiments can probe both the Au L_3-edge and the L_3- or K-edge of a 3d, 4d, or 5d heteroatom to provide complimentary data, identifying the location of the dopant site (center, surface, or staple). The dopant location and electronic properties of monopalladium-doped Au_{25} cluster is investigated using Pd K-edge XAS, and [112] Au Mossbauer spectroscopy for complementary data of the Au local structure. It was clear that Pd was located in the center position with a high Pd-Au CN of 10.7. More recently, Scott el al. have investigated AuPd bimetallic clusters supported on Al_2O_3 and subjected to thermal and $LiBH_4$ treatments. EXAFS analysis shows that depending on the thermal treatments bimetallic nanoparticles can expose isolated atomic Pd-surface sites on the $AuPd/Al_2O_3$ [113].

In a similar way, Ji et al. were able to identify the location of the Pt dopant in the center of the icosahedron Au_{13} core. A comparison of $Au_{24}Pt$ with the structure of Au_{25} using gold L_3-edge EXAFS clearly shows contraction of both metal–thiolate and metal–metal bond distances, caused by Pt doping [114].

Doping with other atoms has also been studied, most recently Au_{25} NCs doped with Cu or Ag atoms using XAS in conjunction with DFT calculations [115]. $Au_{23.8}Ag_{1.2}(SR)_{18}$ and $Au_{23.6}Cu_{1.4}(SR)_{18}$ NCs were synthesized (protected by phenylethanethiol), having compositions very close to single atom-doped Au_{25} NCs. First, DFT-optimized structures were determined for each system ($Au_{24}M(SR)_{18}$, where M is Ag or Cu) and for each possible dopant site location (center, surface, and staple). From these models, Ag K-edge and Cu K-edge EXAFS spectra were simulated to compare with the experimental data. For the monosilver system, EXAFS fitting results suggested Ag prefers the surface of Au_{25} from agreeable Ag-Au and Ag-S CN values. For the monocopper system, from the Cu K-edge perspective both EXAFS and XANES results show that the Cu atom occupies the staple site in Au_{25} NCs instead of the surface or core. The next step is to employ XANES and EXAFS to investigate complex systems (clusters on supports, with the presence of heteroatoms) under reaction conditions (temperature, gases). Our investigations into these type of systems are discussed along this work.

References

[1] J. Yano, V.K. Yachandra, X-ray absorption spectroscopy, Photosynth Res, 102 (2009) 241-254.

[2] Heterogeneous Catalysis and Solid Catalysts, Ullmann's Encyclopedia of Industrial Chemistry.

[3] S. Licht, B. Wang, S. Mukerji, T. Soga, M. Umeno, H. Tributsch, Efficient solar water splitting, exemplified by RuO2-catalyzed AlGaAs/Si photoelectrolysis, J Phys Chem B, 104 (2000) 8920-8924.

[4] J.T. Kummer, Catalysts for automobile emission control, Progress in Energy and Combustion Science, 6 (1980) 177-199.

[5] S. Singh, Enzyme Catalysis and Its Role in Food Processing Industries, 2018, pp. 143-165.

[6] K.L. Mercer, Activation Energy, J Am Water Works Ass, 111 (2019) 2-2.

[7] G.A. Fuentes, B.H. Davis, Impact of Physical-Chemistry in Developing Catalysis as a Science, Abstr Pap Am Chem S, 193 (1987) 4-Hist.

[8] Z.A. Piskulich, O.O. Mesele, W.H. Thompson, Activation Energies and Beyond, J Phys Chem A, 123 (2019) 7185-7194.

[9] G.A. Somorjai, S.M. Davis, The Surface Science of Heterogeneous Catalysis, Chemtech, 13 (1983) 502-511.

[10] A.F. Benton, Adsorption and catalysis in carbon monoxide oxidation, J Am Chem Soc, 45 (1923) 900-907.

[11] The Basics of Catalysis, Catalysis, pp. 39-75.

[12] Heterogeneous Catalysis, Catalysis, pp. 127-187.

[13] M. Beller, A. Renken, R.A. Santen, Catalysis from principles to applications, Wiley-VCH-Verl., Weinheim, 2012.

[14] R. Schlögl, Heterogeneous Catalysis, Angewandte Chemie International Edition, 54 (2015) 3465-3520.

[15] P.S. Pregosin, Applied Homogeneous Catalysis. By Arno Behr and Peter Neubert, Angewandte Chemie International Edition, 52 (2013) 1627-1627.

[16] Y. Volokitin, J. Sinzig, L.J. de Jongh, G. Schmid, M.N. Vargaftik, I.I. Moiseevi, Quantum-size effects in the thermodynamic properties of metallic nanoparticles, Nature, 384 (1996) 621-623.

[17] B. Hammer, J.K. Nørskov, Theoretical surface science and catalysis—calculations and concepts, Advances in Catalysis, Academic Press2000, pp. 71-129.

[18] L. Liu, A. Corma, Metal Catalysts for Heterogeneous Catalysis: From Single Atoms to Nanoclusters and Nanoparticles, Chem Rev, 118 (2018) 4981-5079.

[19] Concepts in Nanocatalysis, Nanomaterials in Catalysis, pp. 1-54.

[20] G.A. Somorjai, J. Carrazza, Structure sensitivity of catalytic reactions, Industrial & Engineering Chemistry Fundamentals, 25 (1986) 63-69.

[21] B. Ni, X. Wang, Face the Edges: Catalytic Active Sites of Nanomaterials, Adv Sci (Weinh), 2 (2015) 1500085-1500085.

[22] B. Gates, L. Guczi, H. Knözinger, Studies in Surface Science and Catalysis: Preface, Studies in Surface Science and Catalysis, 29 (1986).

[23] T. Tsukuda, H. Häkkinen, Chapter 1 - Introduction, in: T. Tsukuda, H. Häkkinen (Eds.) Frontiers of Nanoscience, Elsevier2015, pp. 1-7.

[24] T.P. Martin, T. Bergmann, H. Goehlich, T. Lange, Shell structure of clusters, The Journal of Physical Chemistry, 95 (1991) 6421-6429.

[25] M.L. Cohen, M.Y. Chou, W.D. Knight, W.A. De Heer, Physics of metal clusters, The Journal of Physical Chemistry, 91 (1987) 3141-3149.

[26] A.W. Castleman, S.N. Khanna, Clusters, Superatoms, and Building Blocks of New Materials, The Journal of Physical Chemistry C, 113 (2009) 2664-2675.

[27] A. Halder, L.A. Curtiss, A. Fortunelli, S. Vajda, Perspective: Size selected clusters for catalysis and electrochemistry, The Journal of Chemical Physics, 148 (2018) 110901.

[28] J. Yan, B.K. Teo, N. Zheng, Surface Chemistry of Atomically Precise Coinage–Metal Nanoclusters: From Structural Control to Surface Reactivity and Catalysis, Accounts Chem Res, 51 (2018) 3084-3093.

[29] V. Sudheeshkumar, K.O. Sulaiman, R.W.J. Scott, Activation of atom-precise clusters for catalysis, Nanoscale Advances, 2 (2020) 55-69.

[30] M.S. Bootharaju, C.P. Joshi, M.R. Parida, O.F. Mohammed, O.M. Bakr, Templated Atom-Precise Galvanic Synthesis and Structure Elucidation of a [Ag24Au(SR)18]– Nanocluster, Angewandte Chemie International Edition, 55 (2016) 922-926.

[31] M. Haruta, T. Kobayashi, H. Sano, N. Yamada, Novel Gold Catalysts for the Oxidation of Carbon-Monoxide at a Temperature Far Below 0-Degrees-C, Chem Lett, (1987) 405-408.

[32] C.D. Bain, E.B. Troughton, Y.T. Tao, J. Evall, G.M. Whitesides, R.G. Nuzzo, Formation of monolayer films by the spontaneous assembly of organic thiols from solution onto gold, J Am Chem Soc, 111 (1989) 321-335.

[33] M. Brust, M. Walker, D. Bethell, D.J. Schiffrin, R. Whyman, Synthesis of Thiol-Derivatized Gold Nanoparticles in a 2-Phase Liquid-Liquid System, J Chem Soc Chem Comm, (1994) 801-802.

[34] R.L. Whetten, J.T. Khoury, M.M. Alvarez, S. Murthy, I. Vezmar, Z.L. Wang, P.W. Stephens, C.L. Cleveland, W.D. Luedtke, U. Landman, Nanocrystal gold molecules, Adv Mater, 8 (1996) 428-433.

[35] T.G. Schaaff, M.N. Shafigullin, J.T. Khoury, I. Vezmar, R.L. Whetten, W.G. Cullen, P.N. First, C. Gutiérrez-Wing, J. Ascensio, M.J. Jose-Yacamán, Isolation of Smaller Nanocrystal Au Molecules: Robust Quantum Effects in Optical Spectra, The Journal of Physical Chemistry B, 101 (1997) 7885-7891.

[36] R. Jin, H. Qian, Z. Wu, Y. Zhu, M. Zhu, A. Mohanty, N. Garg, Size Focusing: A Methodology for Synthesizing Atomically Precise Gold Nanoclusters, The Journal of Physical Chemistry Letters, 1 (2010) 2903-2910.

[37] R.L. Donkers, D. Lee, R.W. Murray, Synthesis and Isolation of the Molecule-like Cluster Au38(PhCH2CH2S)24, Langmuir, 20 (2004) 1945-1952.

[38] K.M. Harkness, D.E. Cliffel, J.A. McLean, Characterization of thiolate-protected gold nanoparticles by mass spectrometry, Analyst, 135 (2010) 868-874.

[39] Y. Pei, X.C. Zeng, Investigating the structural evolution of thiolate protected gold clusters from first-principles, Nanoscale, 4 (2012) 4054-4072.

[40] Y. Negishi, Y. Takasugi, S. Sato, H. Yao, K. Kimura, T. Tsukuda, Magic-Numbered Aun Clusters Protected by Glutathione Monolayers (n = 18, 21, 25, 28, 32, 39): Isolation and Spectroscopic Characterization, J Am Chem Soc, 126 (2004) 6518-6519.

[41] M.M. Alvarez, J.T. Khoury, T.G. Schaaff, M.N. Shafigullin, I. Vezmar, R.L. Whetten, Optical Absorption Spectra of Nanocrystal Gold Molecules, The Journal of Physical Chemistry B, 101 (1997) 3706-3712.

[42] D.M.P. Mingos, Bonding in molecular clusters and their relationship to bulk metals, Chemical Society Reviews, 15 (1986) 31-61.

[43] Y. Negishi, N.K. Chaki, Y. Shichibu, R.L. Whetten, T. Tsukuda, Origin of Magic Stability of Thiolated Gold Clusters: A Case Study on Au25(SC6H13)18, J Am Chem Soc, 129 (2007) 11322-11323.

[44] M. Zhu, C.M. Aikens, F.J. Hollander, G.C. Schatz, R. Jin, Correlating the Crystal Structure of A Thiol-Protected Au25 Cluster and Optical Properties, J Am Chem Soc, 130 (2008) 5883-5885.

[45] R. Jin, C. Zeng, M. Zhou, Y. Chen, Atomically Precise Colloidal Metal Nanoclusters and Nanoparticles: Fundamentals and Opportunities, Chem Rev, 116 (2016) 10346-10413.

[46] H. Yang, Y. Wang, H. Huang, L. Gell, L. Lehtovaara, S. Malola, H. Häkkinen, N. Zheng, All-thiol-stabilized Ag44 and Au12Ag32 nanoparticles with single-crystal structures, Nat Commun, 4 (2013) 2422.

[47] J. Yan, H. Su, H. Yang, S. Malola, S. Lin, H. Häkkinen, N. Zheng, Total Structure and Electronic Structure Analysis of Doped Thiolated Silver [MAg24(SR)18]2– (M = Pd, Pt) Clusters, J Am Chem Soc, 137 (2015) 11880-11883.

[48] P. Ferrari, J. Vanbuel, E. Janssens, P. Lievens, Tuning the Reactivity of Small Metal Clusters by Heteroatom Doping, Accounts Chem Res, 51 (2018) 3174-3182.

[49] Y. Negishi, K. Munakata, W. Ohgake, K. Nobusada, Effect of Copper Doping on Electronic Structure, Geometric Structure, and Stability of Thiolate-Protected Au25 Nanoclusters, The Journal of Physical Chemistry Letters, 3 (2012) 2209-2214.

[50] S. Liu, Single-atom doping on thiolate-protected gold nanoclusters: a TDDFT study on the excited states, Materials Research Express, 6 (2019) 1150g1153.

[51] D.-e. Jiang, R. Whetten, Magnetic doping of a thiolated-gold superatom, (2009).

[52] P. Ferrari, H.A. Hussein, C.J. Heard, J. Vanbuel, R.L. Johnston, P. Lievens, E. Janssens, Effect of palladium doping on the stability and fragmentation patterns of cationic gold clusters, Phys Rev A, 97 (2018) 052508.

[53] A. Ghosh, O.F. Mohammed, O.M. Bakr, Atomic-Level Doping of Metal Clusters, Accounts Chem Res, 51 (2018) 3094-3103.

[54] Y. Yong, C. Li, X. Li, T. Li, H. Cui, S. Lv, Ag7Au6 Cluster as a Potential Gas Sensor for CO, HCN, and NO Detection, The Journal of Physical Chemistry C, 119 (2015) 7534-7540.

[55] R. Tian, S. Zhang, M. Li, Y. Zhou, B. Lu, D. Yan, M. Wei, D.G. Evans, X. Duan, Localization of Au Nanoclusters on Layered Double Hydroxides Nanosheets: Confinement-Induced Emission Enhancement and Temperature-Responsive Luminescence, Adv Funct Mater, 25 (2015) 5006-5015.

[56] J. Zheng, C. Zhou, M. Yu, J. Liu, Different sized luminescent gold nanoparticles, Nanoscale, 4 (2012) 4073-4083.

[57] G. Li, R. Jin, Atomically Precise Gold Nanoclusters as New Model Catalysts, Accounts of Chemical Research, 46 (2013) 1749-1758.

[58] S. Knoppe, T. Bürgi, Chirality in Thiolate-Protected Gold Clusters, Accounts Chem Res, 47 (2014) 1318-1326.

[59] M. Zhu, C.M. Aikens, M.P. Hendrich, R. Gupta, H. Qian, G.C. Schatz, R. Jin, Reversible Switching of Magnetism in Thiolate-Protected Au25 Superatoms, J Am Chem Soc, 131 (2009) 2490-2492.
[60] A. Kogo, N. Sakai, T. Tatsuma, Photocatalysis of Au25-modified TiO2 under visible and near infrared light, Electrochem Commun, 12 (2010) 996-999.
[61] G. Guan, Y. Cai, S. Liu, H. Yu, S. Bai, Y. Cheng, T. Tang, M.S. Bharathi, Y.-W. Zhang, M.-Y. Han, High-Level Incorporation of Silver in Gold Nanoclusters: Fluorescence Redshift upon Interaction with Hydrogen Peroxide and Fluorescence Enhancement with Herbicide, Chemistry – A European Journal, 22 (2016) 1675-1681.
[62] M.A.H. Muhammed, P.K. Verma, S.K. Pal, R.C.A. Kumar, S. Paul, R.V. Omkumar, T. Pradeep, Bright, NIR-Emitting Au23 from Au25: Characterization and Applications Including Biolabeling, Chemistry – A European Journal, 15 (2009) 10110-10120.
[63] M. Yu, J. Zheng, Clearance Pathways and Tumor Targeting of Imaging Nanoparticles, Acs Nano, 9 (2015) 6655-6674.
[64] S. Yamazoe, K. Koyasu, T. Tsukuda, Nonscalable Oxidation Catalysis of Gold Clusters, Accounts Chem Res, 47 (2014) 816-824.
[65] B. Panthi, A. Mukhopadhyay, L. Tibbitts, J. Saavedra, C.J. Pursell, R.M. Rioux, B.D. Chandler, Using Thiol Adsorption on Supported Au Nanoparticle Catalysts To Evaluate Au Dispersion and the Number of Active Sites for Benzyl Alcohol Oxidation, Acs Catal, 5 (2015) 2232-2241.
[66] T. Yoskamtorn, S. Yamazoe, R. Takahata, J.-i. Nishigaki, A. Thivasasith, J. Limtrakul, T. Tsukuda, Thiolate-Mediated Selectivity Control in Aerobic Alcohol Oxidation by Porous Carbon-Supported Au25 Clusters, Acs Catal, 4 (2014) 3696-3700.
[67] A. Shivhare, L. Wang, R.W.J. Scott, Isolation of Carboxylic Acid-Protected Au25 Clusters Using a Borohydride Purification Strategy, Langmuir, 31 (2015) 1835-1841.
[68] T. Mitsudome, M. Yamamoto, Z. Maeno, T. Mizugaki, K. Jitsukawa, K. Kaneda, One-step Synthesis of Core-Gold/Shell-Ceria Nanomaterial and Its Catalysis for Highly Selective Semihydrogenation of Alkynes, J Am Chem Soc, 137 (2015) 13452-13455.
[69] Z. Wu, R. Jin, Stability of the Two Au–S Binding Modes in Au25(SG)18 Nanoclusters Probed by NMR and Optical Spectroscopy, Acs Nano, 3 (2009) 2036-2042.
[70] Y. Zhu, H. Qian, R. Jin, An Atomic-Level Strategy for Unraveling Gold Nanocatalysis from the Perspective of Aun(SR)m Nanoclusters, Chemistry – A European Journal, 16 (2010) 11455-11462.
[71] X. Nie, H. Qian, Q. Ge, H. Xu, R. Jin, CO Oxidation Catalyzed by Oxide-Supported Au25(SR)18 Nanoclusters and Identification of Perimeter Sites as Active Centers, Acs Nano, 6 (2012) 6014-6022.
[72] Y. Liu, H. Tsunoyama, T. Akita, T. Tsukuda, Efficient and selective epoxidation of styrene with TBHP catalyzed by Au25 clusters on hydroxyapatite, Chem Commun, 46 (2010) 550-552.
[73] S. Gaur, J.T. Miller, D. Stellwagen, A. Sanampudi, C.S.S.R. Kumar, J.J. Spivey, Synthesis, characterization, and testing of supported Au catalysts prepared from atomically-tailored Au38(SC12H25)24 clusters, Phys Chem Chem Phys, 14 (2012) 1627-1634.
[74] J. Fang, J. Li, B. Zhang, X. Yuan, H. Asakura, T. Tanaka, K. Teramura, J. Xie, N. Yan, The support effect on the size and catalytic activity of thiolated Au25 nanoclusters as precatalysts, Nanoscale, 7 (2015) 6325-6333.

[75] M.M. Schubert, S. Hackenberg, A.C. van Veen, M. Muhler, V. Plzak, R.J. Behm, CO Oxidation over Supported Gold Catalysts—"Inert" and "Active" Support Materials and Their Role for the Oxygen Supply during Reaction, J Catal, 197 (2001) 113-122.

[76] A. Sanchez, S. Abbet, U. Heiz, W.D. Schneider, H. Häkkinen, R.N. Barnett, U. Landman, When Gold Is Not Noble: Nanoscale Gold Catalysts, The Journal of Physical Chemistry A, 103 (1999) 9573-9578.

[77] M. Gao, A. Lyalin, T. Taketsugu, Role of the Support Effects on the Catalytic Activity of Gold Clusters: A Density Functional Theory Study, Catalysts, 1 (2011) 18-39.

[78] C. García, S. Pollitt, M. van der Linden, V. Truttmann, C. Rameshan, R. Rameshan, E. Pittenauer, G. Allmaier, P. Kregsamer, M. Stöger-Pollach, N. Barrabés, G. Rupprechter, Support effect on the reactivity and stability of Au25(SR)18 and Au144(SR)60 nanoclusters in liquid phase cyclohexane oxidation, Catal Today, 336 (2019) 174-185.

[79] S. Xie, H. Tsunoyama, W. Kurashige, Y. Negishi, T. Tsukuda, Enhancement in Aerobic Alcohol Oxidation Catalysis of Au25 Clusters by Single Pd Atom Doping, Acs Catal, 2 (2012) 1519-1523.

[80] C. Lavenn, A. Demessence, A. Tuel, Au25(SPh-pNH2)17 nanoclusters deposited on SBA-15 as catalysts for aerobic benzyl alcohol oxidation, J Catal, 322 (2015) 130-138.

[81] A. Ghosh, O. Mohammed, O. Bakr, Atomic-Level Doping of Metal Clusters, Accounts Chem Res, 51 (2018).

[82] H. Qian, D.-e. Jiang, G. Li, C. Gayathri, A. Das, R.R. Gil, R. Jin, Monoplatinum Doping of Gold Nanoclusters and Catalytic Application, J Am Chem Soc, 134 (2012) 16159-16162.

[83] K. Kwak, W. Choi, Q. Tang, M. Kim, Y. Lee, D.-e. Jiang, D. Lee, A molecule-like PtAu24(SC6H13)18 nanocluster as an electrocatalyst for hydrogen production, Nat Commun, 8 (2017) 14723.

[84] G. Li, R. Jin, Atomic level tuning of the catalytic properties: Doping effects of 25-atom bimetallic nanoclusters on styrene oxidation, Catal Today, 278 (2016) 187-191.

[85] S. Wang, S. Jin, S. Yang, S. Chen, Y. Song, J. Zhang, M. Zhu, Total structure determination of surface doping [Ag$_{46}$Au$_{24}$(SR)$_{32}$](BPh$_4$)$_2$ nanocluster and its structure-related catalytic property, Science Advances, 1 (2015) e1500441.

[86] Z. Li, X. Yang, C. Liu, J. Wang, G. Li, Effects of doping in 25-atom bimetallic nanocluster catalysts for carbon–carbon coupling reaction of iodoanisole and phenylacetylene, Progress in Natural Science: Materials International, 26 (2016) 477-482.

[87] J. Camacho Gonzalez, A. Muñoz-Castro, Doping the Superatom with p-Elements: The Role of p-Block Endohedral Atoms in Bonding and Optical Properties of E@Au24(SR)18 (E = Si, Ge, Sn, and Pb) from Relativistic DFT Calculations, The Journal of Physical Chemistry C, 120 (2016) 27019-27026.

[88] M. Turner, V.B. Golovko, O.P.H. Vaughan, P. Abdulkin, A. Berenguer-Murcia, M.S. Tikhov, B.F.G. Johnson, R.M. Lambert, Selective oxidation with dioxygen by gold nanoparticle catalysts derived from 55-atom clusters, Nature, 454 (2008) 981-983.

[89] P. Huang, G. Chen, Z. Jiang, R. Jin, Y. Zhu, Y. Sun, Atomically precise Au25 superatoms immobilized on CeO2 nanorods for styrene oxidation, Nanoscale, 5 (2013) 3668-3672.

[90] G. Li, H. Qian, R. Jin, Gold nanocluster-catalyzed selective oxidation of sulfide to sulfoxide, Nanoscale, 4 (2012) 6714-6717.

[91] C. Liu, C. Yan, J. Lin, C. Yu, J. Huang, G. Li, One-pot synthesis of Au144(SCH2Ph)60 nanoclusters and their catalytic application, J Mater Chem A, 3 (2015) 20167-20173.

[92] J. Zhang, Z. Li, J. Huang, C. Liu, F. Hong, K. Zheng, G. Li, Size dependence of gold clusters with precise numbers of atoms in aerobic oxidation of d-glucose, Nanoscale, 9 (2017) 16879-16886.

[93] U. Schuchardt, D. Cardoso, R. Sercheli, R. Pereira, R. Da Cruz, M. Guerreiro, D. Mandelli, E. Spinacé, E. Pires, Cyclohexane Oxidation Continues to be a Challenge, Applied Catalysis A: General, 211 (2001) 1-17.

[94] B. Zhang, S. Kaziz, H. Li, M.G. Hevia, D. Wodka, C. Mazet, T. Bürgi, N. Barrabés, Modulation of Active Sites in Supported Au38(SC2H4Ph)24 Cluster Catalysts: Effect of Atmosphere and Support Material, The Journal of Physical Chemistry C, 119 (2015) 11193-11199.

[95] P. Wu, P. Bai, Z. Yan, G.X.S. Zhao, Gold nanoparticles supported on mesoporous silica: origin of high activity and role of Au NPs in selective oxidation of cyclohexane, Sci Rep-Uk, 6 (2016) 18817.

[96] Y. Liu, H. Tsunoyama, T. Akita, S. Xie, T. Tsukuda, Aerobic Oxidation of Cyclohexane Catalyzed by Size-Controlled Au Clusters on Hydroxyapatite: Size Effect in the Sub-2 nm Regime, Acs Catal, 1 (2011) 2-6.

[97] T.V.W. Janssens, B.S. Clausen, B. Hvolbæk, H. Falsig, C.H. Christensen, T. Bligaard, J.K. Nørskov, Insights into the reactivity of supported Au nanoparticles: combining theory and experiments, Top Catal, 44 (2007) 15.

[98] S.W. Lee, J.T. Song, J. Kim, J. Oh, J.Y. Park, Enhanced catalytic activity for CO oxidation by the metal–oxide perimeter of TiO2/nanostructured Au inverse catalysts, Nanoscale, 10 (2018) 3911-3917.

[99] X. Kang, H. Chong, M. Zhu, Au25(SR)18: The captain of the great nanocluster ship, Nanoscale, 10 (2018).

[100] S.D. Lin, M. Bollinger, M.A. Vannice, Low temperature CO oxidation over Au/TiO2 and Au/SiO2 catalysts, Catal Lett, 17 (1993) 245-262.

[101] Z. Wu, D.-e. Jiang, A.K.P. Mann, D.R. Mullins, Z.-A. Qiao, L.F. Allard, C. Zeng, R. Jin, S.H. Overbury, Thiolate Ligands as a Double-Edged Sword for CO Oxidation on CeO2 Supported Au25(SCH2CH2Ph)18 Nanoclusters, J Am Chem Soc, 136 (2014) 6111-6122.

[102] Y. Li, Y. Chen, S.D. House, S. Zhao, Z. Wahab, J.C. Yang, R. Jin, Interface Engineering of Gold Nanoclusters for CO Oxidation Catalysis, Acs Appl Mater Inter, 10 (2018) 29425-29434.

[103] Y.-G. Wang, D.C. Cantu, M.-S. Lee, J. Li, V.-A. Glezakou, R. Rousseau, CO Oxidation on Au/TiO2: Condition-Dependent Active Sites and Mechanistic Pathways, J Am Chem Soc, 138 (2016) 10467-10476.

[104] L. Li, Y. Gao, H. Li, Y. Zhao, Y. Pei, Z. Chen, X.C. Zeng, CO Oxidation on TiO2 (110) Supported Subnanometer Gold Clusters: Size and Shape Effects, J Am Chem Soc, 135 (2013) 19336-19346.

[105] W. Li, C. Liu, H. Abroshan, Q. Ge, X. Yang, H. Xu, G. Li, Catalytic CO Oxidation Using Bimetallic M x Au 25-x Clusters: A Combined Experimental and Computational Study on Doping Effects, The Journal of Physical Chemistry C, 120 (2016).

[106] D.C. Koningsberger, X-ray absorption: principles, applications, techniques of EXAFS, SEXAFS, and XANES, John Wiley and Sons, United States, 1988.

[107] H. Chen, M.M. Rogalski, J.N. Anker, Advances in functional X-ray imaging techniques and contrast agents, Physical chemistry chemical physics : PCCP, 14 (2012) 13469-13486.

[108] T.K. Sham, L-edge x-ray-absorption systematics of the noble metals Rh, Pd, and Ag and the main-group metals In and Sn: A study of the unoccupied density of states in 4d elements, Phys Rev B, 31 (1985) 1888-1902.

[109] S. Yamazoe, T. Tsukuda, X-ray Absorption Spectroscopy on Atomically Precise Metal Clusters, B Chem Soc Jpn, 92 (2019) 193-204.

[110] M.A. MacDonald, P. Zhang, H. Qian, R. Jin, Site-Specific and Size-Dependent Bonding of Compositionally Precise Gold–Thiolate Nanoparticles from X-ray Spectroscopy, The Journal of Physical Chemistry Letters, 1 (2010) 1821-1825.

[111] J. Liu, K.S. Krishna, Y.B. Losovyj, S. Chattopadhyay, N. Lozova, J.T. Miller, J.J. Spivey, C.S.S.R. Kumar, Ligand-Stabilized and Atomically Precise Gold Nanocluster Catalysis: A Case Study for Correlating Fundamental Electronic Properties with Catalysis, Chemistry – A European Journal, 19 (2013) 10201-10208.

[112] Y. Negishi, W. Kurashige, Y. Kobayashi, S. Yamazoe, N. Kojima, M. Seto, T. Tsukuda, Formation of a Pd@Au12 Superatomic Core in Au24Pd1(SC12H25)18 Probed by 197Au Mössbauer and Pd K-Edge EXAFS Spectroscopy, The Journal of Physical Chemistry Letters, 4 (2013) 3579-3583.

[113] A. Shivhare, R.W.J. Scott, Au25 clusters as precursors for the synthesis of AuPd bimetallic nanoparticles with isolated atomic Pd-surface sites, Mol Catal, 457 (2018) 33-40.

[114] S.L. Christensen, M.A. MacDonald, A. Chatt, P. Zhang, H. Qian, R. Jin, Dopant Location, Local Structure, and Electronic Properties of Au24Pt(SR)18 Nanoclusters, The Journal of Physical Chemistry C, 116 (2012) 26932-26937.

[115] S. Yamazoe, W. Kurashige, K. Nobusada, Y. Negishi, T. Tsukuda, Preferential Location of Coinage Metal Dopants (M = Ag or Cu) in [Au25–xMx(SC2H4Ph)18]− (x ~ 1) As Determined by Extended X-ray Absorption Fine Structure and Density Functional Theory Calculations, The Journal of Physical Chemistry C, 118 (2014) 25284-25290.

[116] G. Rupprechter, Sum Frequency Generation and Polarization–Modulation Infrared Reflection Absorption Spectroscopy of Functioning Model Catalysts from Ultrahigh Vacuum to Ambient Pressure, in: B.C. Gates, H. Knözinger (Eds.) Advances in Catalysis, Academic Press2007, pp. 133-263.

[117] J. Silvestre-Albero, G. Rupprechter, H.-J. Freund, From Pd nanoparticles to single crystals: 1,3-butadiene hydrogenation on well-defined model catalysts, Chemical Communications, (2006) 80-82.

[118] G. Schmid, The relevance of shape and size of Au55 clusters, Chemical Society Reviews, 37 (2008) 1909-1930.

[119] V. Sudheeshkumar, K.O. Sulaiman, R.W.J. Scott, Activation of atom-precise clusters for catalysis, Nanoscale Advances, 2 (2020) 55-69.

[120] Y. Suchorski, S.M. Kozlov, I. Bespalov, M. Datler, D. Vogel, Z. Budinska, K.M. Neyman, G. Rupprechter, The role of metal/oxide interfaces for long-range metal particle activation during CO oxidation, Nature Materials, 17 (2018) 519-522.

Chapter 2

Motivation

Heterogeneous catalysis by metal nanoparticles supported on oxides, can be limited in activity/selectivity due to variations in metal particle size, surface structure and bonding to the support. This poly-dispersity poses a serious challenge when seeking to establish definitive structure-activity relationships — which is of key importance for the development of new catalysts for specific reactions. In contrast, metal nanoclusters can be synthesized with a precise atomic number (<100 atoms) and, when deposited on a support, comprise truly monodisperse catalysts. Various studies which focus on Au show that once the clusters are supported on metal oxides, they exhibit excellent catalytic activity in oxidation and hydrogenation reactions. However, their stability under pretreatment and reaction conditions is very much related to the nature of the support material, as well as cluster size and composition. Therefore, an understanding of the effect of the cluster structure and of the nature of the oxide support materials is required in order to get insights into the structure-catalytic activity mechanism for future nanocluster catalyst design.

Our interest focuses on: (a) cluster size; (b) oxide material and (c) the heteroatom doping effect on the stability and catalytic properties in oxidation reactions. Catalytic activity is closely linked to the structure of the active site and its evolution under pretreatments and reaction conditions. Thus, the key questions which we have sought to address in order to understand the catalytic behavior of nanocluster catalysts are:

- How does cluster structure affect catalytic performance?

- Is there any change in the structure depending on the support or pretreatment?

- How does the nature of the oxide support material influence stability and the catalytic properties?

- What effect does heteroatom doping have on reactivity and stability?

- Are there any differences between the catalytic performance of the nanocluster catalysts in liquid phase oxidation reactions and in gas phase reactions?

In Chapter 4 two different cluster sizes ($Au_{25}(SC_2H_4Ph)_{18}$ and $Au_{144}(SC_2H_4Ph)_{60}$) on two different supports (TiO_2 and SiO_2) are examined. These clusters represent extremes of common cluster size studies and exhibit different core and staple configurations. Thus, special emphasis is put on the structure evolution of clusters upon deposition on the oxide materials, upon thermal pretreatment (ligand removal) and during liquid phase cyclohexane oxidation.

First, the pretreatment effect was investigated using DRS, HAADF-STEM and XAFS. The objective of the pretreatment study is to establish the conditions that allow the removal of ligands while avoiding sintering. Afterwards, the differences in the reaction mechanism were also analyzed using ATR. Differences in stability are also investigated using HERFD-XAS. See Chapter 4 for a discussion of these results.

The properties of these atomically designed nanoclusters can be fine-tuned by heteroatom doping. We look at the effect of palladium and silver doping of Au_{25} on the catalytic activity and stability in Chapters 4 and 5, respectively. In both chapters the work includes two types of oxidation reaction: the cyclohexane oxidation reaction (liquid phase) and the CO oxidation reaction (gas phase). In Chapter 4 differences in the adsorption and desorption of CO were followed using DRIFTS. XAFS measurements allow further understanding of the structure evolution under reaction conditions. In Chapter 5, the catalytic properties of silver-doped clusters are discussed looking at both types of reactions.

The application of supported thiolate protected gold clusters for catalysis is an emerging field. The current work hopes to contribute to the understanding of cluster dynamics under reaction conditions and to the further development of catalysis by thiolate metal nanoclusters.

Chapter 3

Materials and methods

1. Synthetic procedures

1.1 $Au_{25}(SC_2H_4Ph)_{18}$

$Au_{25}(SC_2H_4Ph)_{18}$ was synthesized according to the methods reported by Brust et al. [6-8]. Briefly, $Au_{25}(SC_2H_4Ph)_{18}$ clusters were prepared following the method of Shivhare et al. [6]: 50 ml of THF and 500 mg of $HAuCl_4$ $3H_2O$ were mixed with 1,2 eq. of TOAB and stirred for 10 minutes. Then, 0,85 ml of phenylethanethiol was added to the solution and stirred until it became transparent. 480 mg of $NaBH_4$ in 10 ml of ice cold water were added at once, leading to a dark brown reaction mixture. The solution was stirred for four days under ambient conditions, before the solvent evaporated. The precipitate was then washed several times with methanol.

1.2 $Au_{144}(SC_2H_4Ph)_{60}$

$Au_{144}(SC_2H_4Ph)_{60}$ was prepared following the method of Huifeng et al.[7] : 118 mg of $HAuCl_4 \bullet 3H_2O$ were mixed with 190 mg of TOAB in 15 ml of methanol and stirred for 15 minutes. Then, 0,213 ml of phenylethanethiol were added to the solution and stirred for another 15 minutes. 113 mg of $NaBH_4$ in 12 ml of ice cold water were added at once leading to a dark brown reaction mixture. The solution was stirred for five hours at ambient conditions. After this, the solvent evaporated and the precipitate was washed several times with methanol. Further purification of the clusters was done by size exclusion chromatography (SEC) as confirmed by UV-Vis spectroscopy and matrix-assisted laser desorption/ionization (MALDI) mass spectrometry [9, 10]

1.3 $Pd_1Au_{24}(SC_2H_4Ph)_{18}$

$PdAu_{24}(SC_2H_4Ph)_{18}$ was synthesized following a modified protocol from Negishi et al.[11]: Briefly, 0,1121g Na_2PdCl_4 (0,450mmol; 294,19 g/mol) and 373,3 mg $HAuCl_4$ $3H_2O$ (0,948 mmol; 393,83 g/mol) were both dissolved in 50 mL THF. The solution showed an orange colour. 0,539 g phenylethyl mercaptan (3,9mmol; 138,23g/mol) were added as a solution, the mixture was then stirred for 30 minutes at room temperature. Afterwards 0,5669g $NaBH_4$ (15mmol; 37,83g/mol)

were quickly mixed with cooled nanopure water and added to the mixture. The mixture (now a dirty brown colour) was then stirred for four hours while being cooled with ice (around 0°C). Afterwards, the organic phase evaporated and washed with methanol several times. The last step was an extraction with acetonitrile in order to separate $PdAu_{24}(SC_2H4Ph)_{18}$ (soluble in acetonitrile) from the undoped cluster[12]. However, as Bürgi et al[8] have already corroborated, this synthetic procedure leads to a mix of doped and undoped clusters (Au_{25}), so a further oxidation step is required to increase the doped cluster's purity.

1.4 $Pd_xAu_y(SC_2H_4Ph)_z$

$Pd_xAu_y(SC_2H_4Ph)_z$ was synthesized following the same protocol from Negishi *et al.*[13] as for the $PdAu_{24}(SC_2H_4Ph)_{18}$ clusters, but with further modifications. Briefly, 112.1 mg Na_2PdCl_4 and 373.3 mg $HAuCl_4 \cdot 3H_2O$ were dissolved in 50 mL THF. The solution showed an orange color. 0.539 g phenylethyl mercaptan were added as a solution, the mixture was then stirred at room temperature until it turned colorless. Afterwards, 0.5669 g $NaBH_4$ were quickly mixed with cooled nanopure water and added. The mixture (now a brown color) was not cooled to 0 °C for this synthesis, but stirred at RT. In addition, the stirring was reduced from 4 hours to 2-2.5 hours. Subsequently, the THF solvent was removed by rotary evaporation. The same purification procedure as for $PdAu_{24}(SC_2H_4Ph)_{18}$ was applied.

1.5 $Ag_xAu_{25-x}(SC_2H_4Ph)_{18}$

The synthesis was carried out similar to the one by Gottlieb et al. [14] 0,240 g $HAuCl_4$ 3 H_2O (0,609 mmol) were dissolved in 50 mL Milli-Q® of water. Afterwards, 0,0278 g of CF_3COOAg (0,126 mmol) were added. 0,465 g of TOABr (Tetraoctylammonium bromide; 0,859 mmol) was employed as a phase transfer agent and 45 mL THF (tetrahydrofuran) as a solvent. The resulting red solution was stirred for 15 minutes. Then, 0,500 mL of PET (phenylethanethiol; 3,73 mmol) ligand were added, which lead to a slow change of colour towards yellow. The solution was then

stirred again for 15 minutes.As a reducing agent 0,279 g of NaBH4 (7,38 mmol) was quickly dissolved in 15 ml of ice cold Milli-Q® water and immediately added to the yellow solution, which then suddenly became dark brown and produced bubbles for some seconds. The mixture was stirred for seven hours under nitrogen atmosphere.

2. Isolation method (SEC)

The separation of pure $Au_n(SR)_m$ from possible synthesis side products and from the excess of thiols is crucial for further characterization and precise catalyst research. Undesired cluster configurations or cluster fragments may induce changes in the catalytic performance or in selectivity. Therefore, different methods have been studied and optimized, such as size exclusion chromatography and high performance liquid chromatography (HPLC). For this study only SEC has been applied, as HPLC usually concerns analytical scale quantities (~10 µL). Size exclusion chromatography permits a rather large mass (~ 20 mg) of polydisperse clusters to be separated into distinct sizes. Gautier et al. developed a separation method on ligand protected particles using a porous stationary phase: SX1 bio-beads (Biorad, particle sizes 40 - 80 µm)[15]. Here the stationary phase contains multiple pore sizes. Small clusters are able to enter a higher amount of pores compared to larger particles. As a result, smaller sized clusters have a longer residence time in the pores while clusters with the largest hydrodynamic radius do not have the ability to enter into the pores of the beads. This allows clusters with largest hydrodynamic volumes to elute first, followed by intermediate size clusters and finally the smallest sizes of clusters (see Figure. 3-17) Preparation of a SEC column is executed by swelling the beads for several hours in the chosen solvent. Several eluting agents such as THF and DCM can be used, however toluene is most common for isolation of $Au_{25}(SR)_{18}$ clusters. After stabilization of the swollen beads on the column, a minimal volume of cluster is added and with the eluting solvent, the batch of clusters is separated. Afterwards several fractions corresponding to different sizes of clusters can be isolated and analyzed by UV-vis for identification.
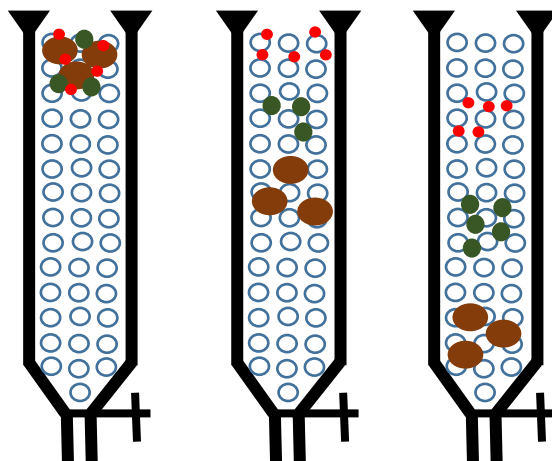
Figure 3-17 *Schematic representation of size expulsion chromatography columns with a polydisperse sample*

3. Catalyst preparation

To produce catalysts with a theoretical 1%wt Au loading, the corresponding amounts of clusters were dissolved in toluene and stirred with the oxide support material (TiO_2 or SiO_2) for 24 hours. Then the catalysts were separated from the solvent by centrifugation and decantation. The remains of the toluene were removed at 80 °C in a drying cabinet (1 h). The %wt Au of the catalysts was determined by Total Reflection X-ray Fluorescence (TXRF).

Catalysts were pretreated (activated) in air at 150 or 250 °C for one hour (previous ramp of 5 °C/min) except those used without pretreatment.

In Chapter 5, the pretreatment study was the following: Different gas phase compositions during pretreatment were evaluated to find the optimal conditions for activation of the $PdAu_{24}/TiO_2$ catalyst. All other parameters were kept constant (250 °C maximum temperature, 10 °C/min ramp for heating up, 40 min holding time at 250 °C, 50 ml/min total gas flow): 1) argon pretreatment (2x40 min; pretAr); 2) oxidative pretreatment with 5% O_2 in argon, cool down to RT under argon (pretO$_2$), argon pretreatment; 3) reductive pretreatment with 5% H_2 in argon, cool down to RT under H_2, argon pretreatment (pretH$_2$) and 4) oxidative pretreatment with 5% O_2 in argon, cool down to RT under argon, reductive pretreatment with 5% H_2 in argon, cool down to RT under H_2 (pretO$_2$-H$_2$). The pretO$_2$ and pretH$_2$ pretreatment are followed by an argon

pretreatment at the same temperature in order to discard the effect of different pretreatment durations, which was found to have a significant effect on the catalyst activation by Lie *et al.*[16]

4. Characterization Techniques

UV-Vis spectra of nanoclusters dissolved in CH_2Cl_2 were recorded on a Perkin Elmer Lambda 750 UV-Vis spectrometer. For Diffuse Reflectance Spectra (DRS) of catalysts, the same instrument was employed coupled to a 60 mm integration sphere.

All **matrix-assisted laser desorption ionization (MALDI)** mass spectrometric measurements were performed using a reflectron (RTOF) mass spectrometer (Shimadzu). For analytical experiments, 2,4,6-trihydroxyacetophenone (Sigma-Aldrich) was selected as the MALDI-MS matrix. MALDI RTOF mass spectra were acquired near threshold laser irradiance to obtain mass spectra of sufficient mass spectrometric resolution [3000–5000 at full width half-maximum (fwhm)]. All displayed mass spectra were based on averaging 300–600 single and unselected laser pulses (λ = 337 nm at 50 Hz).

An STA 409 PC from Netzsch was employed for **thermogravimetic analysis**. The gases were controlled with a 647°C multigas controller and with MKS mass-flow controllers. Samples were heated from 25 °C to 400 °C with a rate of 10 °C/min under inert atmosphere (N_2).

High-angle annular dark-field scanning transmission electron microscopy (HAADF-STEM) imaging was performed using a 200 kV FEI Tecnai F20 S-TWIN analytical (scanning) transmission electron microscopy [(S)TEM] instrument equipped with a Gatan GIF Tridiem filter. The energy resolution was $\leq$1 eV, the semi-convergence angle ~8 mrad, the semi-collection angle ~15 mrad, and the spatial resolution of the order of 0.5 nm. Supported clusters were directly impregnated on carbon-coated copper grids and plasma cleaning was used to remove possible hydrocarbons and adsorbed water.

X-ray photoelectron spectroscopy (XPS) measurements were performed using a photoelectron spectrometer (SPECS Surface Nano Analysis GmbH, Germany) equipped with a

PHOIBOS-100-MCD-5 hemispherical energy analyser and an XR50 X-ray source with a double Al/Mg anode (using Al-Kα irradiation here;hv = 1486.6 eV; 200 W). The catalyst powder samples were placed on transferrable sample holders using UHV-compatible conductive carbon tape. Unsupported, pure clusters were dropcast as a dichloromethane solution on highly oriented pyrolytic graphite (HOPG) for measurement. Spectra were measured at room temperature using Al-Kα radiation (1486.61 eV) and an electron emission angle of 0°, with the analyzer operated in "large area" transmission mode.

The binding energy (BE) scale was calibrated by Au4f$_{7/2}$ (BE = 84.0 eV) core levels and C1s peaks at 284.5 eV for the studies from Chapter 4. The data analysis and peak fitting were performed with CasaXPS software. For quantitative analysis, the integral intensities of the spectra were corrected by their respective atomic sensitivity factors [17]. In the case of the studies in Chapter 5, (using CasaXPS) all spectra were referenced to the C 1s signal (C-C, 284.6 eV). Subsequently, peaks were fitted after Shirley background subtraction utilizing Gauss-Lorentz sum functions and consistent values of full width half maxima (FWHM). Peak positions (Au 4d$_{5/2}$: 333-335 eV and Pd 3d$_{5/2}$: 335-339 eV), doublet separation (Au 4d: 18.1 eV, Au 4f: 3.7 eV, Pd 3d: 5.3 eV) and peak area ratios (d$_{5/2}$:d$_{3/2}$ = 3:2 and f$_{7/2}$:f$_{5/2}$ = 4:3) were constraint, according to the NIST XPS data base.

Chemical analysis with Total Reflection X-ray Fluorescence (TXRF) was performed with the supported clusters samples to determine the %wt using an ATOMIKA 8030C X-ray fluorescence analyser. This spectrometer employs total reflection geometry with an energy-dispersive Si(Li)-detector (energy resolution 160eV). The measurements were taken with the monochromatised Mo-Kα excitation mode (17.48 keV) at ~70% of the critical angle for total reflection of X-rays (1.2 mrad, angle of incidence), for 100 s live time, at 50 kV and 47 mA. Samples were applied to the total reflecting supports — namely quartz reflectors for TiO$_2$ matrix and Plexiglas reflectors for SiO$_2$ matrix — by taking 1mg of the sample mixed with 5μl of 1% poly vinyl alcohol solution (for fixation). Blank measurements of the unloaded reflectors were taken prior to each specimen measurement in order to avoid cross contamination of specimens. Results for Au were obtained scaled to 100% mass of Ti and Si respectively. Detection limits for the quantified elements under consideration Si, Ti and Au are in the range of 10-100 μg/g.

5. Catalytic Activity Studies: Cyclohexane oxidation reaction

Figure 3-18 *Cyclohexane oxidation reaction set-up*

The selective oxidation of cyclohexane was performed (solvent free) as reported previously [18] [19]: 100 mg of the catalyst (2%wt Au), 10 ml of cyclohexane and 80 µl of tert-butyl hydroperoxide (initiator) were added to a quartz beaker and exposed to a 2.5 ml/min O_2 flow. The batch reaction was carried out at 75 °C. Reactants and products identified by GC-MS, with samples taken at one hour intervals. The GC method was optimized to improve product separation (with symmetrical peaks without fronting or tailing). A fused silica capillary column J&W DBWAX 30N 0,15µ with 30 m x 0,257 m dimensions was employed (80 KPa pressure, 130°C for the first seven minutes with a heating rate of 15 °C/min till 180 °C). The retention times and sensitivities were determined by external standards.

6. Catalytic activity studies: CO oxidation reaction

CO oxidation in gas phase was performed in a flow reactor coupled to a Micro GC. Gases were regulated with Bronkhorst mass flow controllers, reaction temperature was regulated by a cylindrical oven with temperature sensor placed inside the catalyst and a PID controller (see Figure 3-19 and 3-20).
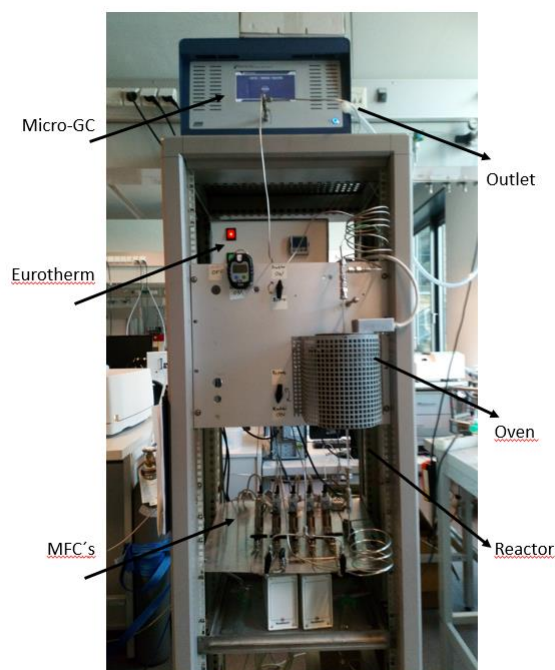
Figure 3-19 Full gas phase reactor image

The catalyst was placed inside a quartz glass tube attached to quartz wool to avoid movements. The total gas flow was 50 ml/min for all the experiments. The outlet gas was analysed by online micro-GC (INFICON Micro GC fusion^{TM}) equipped with two columns, a 3-meter Rt-Q-Bond precolumn with divinylbenzene as stationary phase for the alkanes' separation and a main column type Molsieve coated with Zeolites was used for the separation of lighter and faster gases, as CO, O_2, and CO. A schematic representation is shown in Figure 3-20.
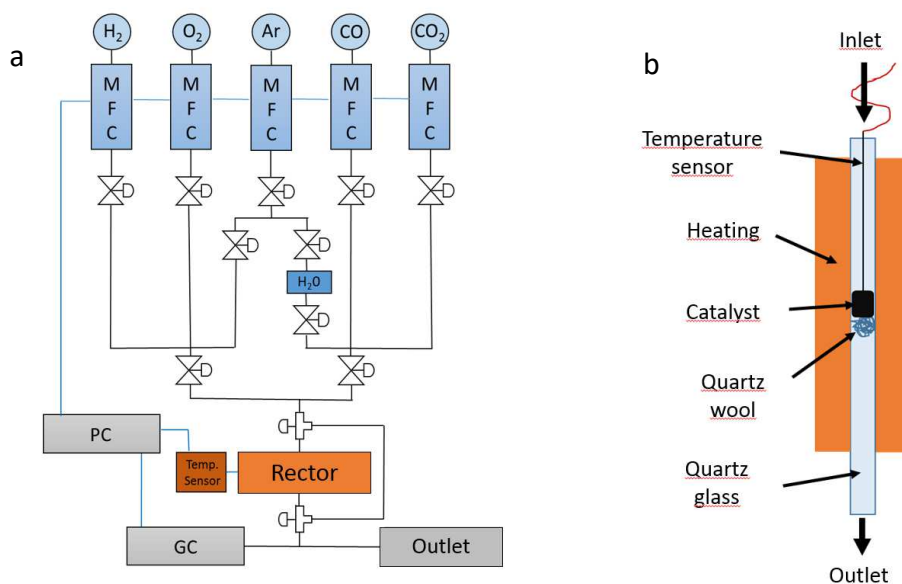
Figure 3-20 a) Schematic representation of the gas-phase reactor set-up: the blue lines represent the electric connections. The black lines represent the tube connections with the 2-way and 3-way valves b) Schematic representation of the reactor: the catalyst is in the middle of the glass tube, supported by glass wool, with the temperature sensor placed inside the catalyst. The oven surrounds the glass tube.

Pretreatments were performed as described in the previous section. For the optimal pretreatment (pretO$_2$-H$_2$), 40 min oxidation (5% O$_2$ in argon) at 250 °C (10 °C/min rate), followed (after cooling down) by 40 min reduction (5% H$_2$ in argon) with the same temperature and rate as the previous oxidation was employed. Once the catalyst was pretreated, CO oxidation was performed with 1:2 CO:O$_2$ in argon. The reaction was conducted with temperature steps (150 °C, 175°C, 200 °C, 225 °C, 250 °C), and each temperature was held for 30 min to reach the steady state. For all the experiments, 15 mg of catalyst were employed.

The measured areas of the products and the by-products of the cyclohexane oxidation were used to determine the cyclohexane conversion and the selectivity for the products as follows:

$$X(xh) = \frac{Area\ cyclohexane(0h) - Area\ cyclohexane(xh)}{Area\ cyclohexane(xh)}$$

Equation 3-4 Conversion of cyclohexane after x hours of reaction time

$$S_p(xh) = \frac{Area\ of\ x\ product(xh)}{Area\ of\ all\ products(xh)}$$

Equation 3-5 *Selectivity for product after x hours of reaction time*

7. X-ray Absorption Spectroscopy Studies

For the pretreatment study in Chapter 4, spectra were recorded at the SuperXAS beamline at the Swiss Light Source (SLS) synchrotron. The intensity of the X-ray beam was provided by a Super Bend magnet (2.9 T) with ~ 6 x 10^{11} photons per second. The spectra were measured at Au L3-edge (11.919 keV) using a Si(111) channel-cut monochromator. A collimating mirror coated with silicon and a toroidal mirror coated with rhodium — both installed at 2.8 mrad — were used for focusing and for the elimination of higher harmonics. The incident X-rays had a spot size of 0.3 x 0.3 mm. The collection of the fluorescence signal was achieved by a five-element SDD detector (SGX). The liquid samples were dropcasted on kapton tape (polyimide) and the powder catalysts were pressed into pellets. While the measurements were being taken, the samples were cooled to liquid N_2 temperature with a cryo-gun. The Ifeffit software was used for data treatment.

For the stability study in Chapter 5, catalyst measurements were recorded at beamline ID26 at the European Synchrotron Research Facility. High Energy Resolution Fluorescence Detected (HERFD) XAS were recorded at Au L_3-edge (11.919 keV). The incident beam was selected using the (311) reflection from a double Si crystal monochromator. The spectrometer was equipped with a set of four Ge(555) analyser crystals (R = 1000 mm, r = 50 mm). A mask with a radius of 25 mm was placed in front of each analyser crystal in order to improve the energy resolution further. The overall bandwidth was 0.57 eV (FWHM), which is below the core hole lifetime (5.54eV) [20]. The Lα_1 fluorescence channel was monitored (9.71 keV). Samples were pressed as pellets and were measured in a cryostat (KONTI, CryoVac) cooled with liquid He. The typical operating temperature was 40 K. To test for self-absorption, pellets of a reference compound (sodium aurothiomalate) were measured with different concentrations. Gold in bulk form (Au foil), in cationic form (Au_2O_3), Au(I)- thiolate compounds (Sodium Aurothiomalate (hydrate)) and pure $Au_{25}(SC_2H_4Ph)_{18}$ and $Au_{144}(SC_2H_4Ph)_{60}$ were also measured as references.

X-ray Absorption Spectroscopy (XAS) measurements from Chapter 5 were performed at the CLAESS Beamline at Alba Synchrotron in fluorescence mode (Pd K-edge and Au-L$_3$ edge) in the beamline's solid-gas reactor multipurpose cell. The catalysts were pressed into pellets. The samples were pretreated inside the multipurpose cell at 250 °C for 40 min under oxygen flow (pretO$_2$; 5% O$_2$ in He, total flow: 45 ml/min; cool down 40 ml/min He) followed by a reductive pretreatment under hydrogen (pretH$_2$; 5% H$_2$ in He, total flow: 45 ml/min) at the same conditions. After cooling down (5% H$_2$ in He, total flow: 45 ml/min), the gas mix was changed to reaction conditions (reaction: 1.7% CO, 3.3% O$_2$ in He, total flow: 45 ml/min). The samples were heated up to 250 °C in 5 °C/min steps. The maximum temperature was held for 60 min, and then the reaction chamber was cooled down to rt (45 ml/min He). Extended X-ray Absorption Fine Structure (EXAFS) spectra were taken at 40 °C in He at the beginning, after pretreatment and after reaction for each sample, without opening the reaction chamber in between. The Artemis package[21] that uses the FEFF8 code[22] was applied for EXAFS data treatment.

8. In situ Infrared Spectroscopy Studies

8.1 ATR-FTIR

Attenuated Total Reflection (ATR) infrared spectroscopy was performed with a Vertex 70 (Bruker Optics) spectrometer equipped with a liquid-nitrogen-cooled mercury cadmium telluride (MCT) detector and a commercial mirror unit (SN 854). The Ge crystal (IRE 52(48) mm x 20 mm x 2 mm) was coated with a powder film of a freshly prepared catalyst and was placed into the vertical commercial reactor-cell (Specac). The background was recorded with the catalyst but in absence of liquid phase. After mounting the cell, cyclohexane was flown through the whole system in reflux configuration (batch) and the system was heated to 60 °C (the temperature closest to the catalytic measurements but avoiding evaporation). The reaction was started by flowing 2,5 ml/min O$_2$ and adding tert-butyl hydroperoxide. A series of consecutive (operando) spectra (200 scans per spectrum; resolution 4 cm^{-1}) was collected (20 s/spectra) for two hours, with the reactants/products being monitored by IR.
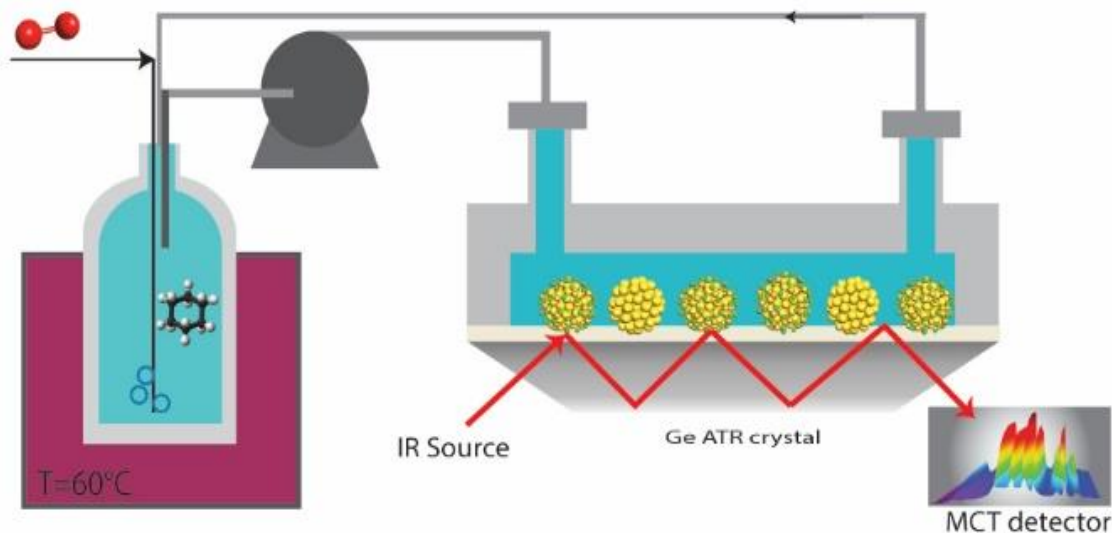
Figure 3-21 *Schematic set-up for ATR-FTIR measurements*

8.2 DRIFTS

Diffuse Reflectance Infrared Fourier Transform Spectroscopy (DRIFTS) studies were carried out on a Bruker Vertex 70 spectrometer with a liquid N_2-cooled MCT detector and with 4 cm^{-1} resolution. The stainless-steel flow cell (Pike) has a CaF_2 window and an oven. The inlet of the cell was connected to a gas manifold system with calibrated mass flow controllers to adjust the gas mixtures the outlet was connected to a mass spectrometer. Each sample was placed into a small ceramic cup and the exact weight was taken for normalization (~30 mg). After the pretreatment (see Chapter 5), the gases were changed to reaction conditions (1% CO, 2% O_2 in He, total flow: 50ml/min) without removing the sample in between. The reaction temperature was increased by 1 °C/min steps and kept at the maximum temperature of 250 °C (reached after 125 min) for 2 h. Afterwards, sample was cooled down to room temperature (under reaction gas mixture or inert gas flow, depending the experiment). To study the surface configuration of the used catalysts, 1% CO in He was flown through the cell until no further changes in the IR signal were observed. Afterwards, the cell was purged with inert gas to remove the CO. DRIFTS spectra were

taken over the course of the whole experiment by averaging 256 scans to achieve good signal to noise ratio. For background removal, the initial spectra of the catalysts were used.

References

[1] J.H. Scofield, Hartree-Slater Subshell Photoionization Cross-Sections at 1254 and 1487ev, J Electron Spectrosc, 8 (1976) 129-137.

[2] Y.M. Liu, H. Tsunoyama, T. Akita, S.H. Xie, T. Tsukuda, Aerobic Oxidation of Cyclohexane Catalyzed by Size-Controlled Au Clusters on Hydroxyapatite: Size Effect in the Sub-2 nm Regime, Acs Catal, 1 (2011) 2-6.

[3] L.X. Xu, C.H. He, M.Q. Zhu, S. Fang, A highly active Au/Al2O3 catalyst for cyclohexane oxidation using molecular oxygen, Catal Lett, 114 (2007) 202-205.

[4] J.L. Campbell, T. Papp, WIDTHS OF THE ATOMIC K–N7 LEVELS, Atomic Data and Nuclear Data Tables, 77 (2001) 1-56.

[5] A. Shivhare, S.J. Ambrose, H.X. Zhang, R.W. Purves, R.W.J. Scott, Stable and recyclable Au-25 clusters for the reduction of 4-nitrophenol, Chem Commun, 49 (2013) 276-278.

[6] H.F. Qian, R.C. Jin, Ambient Synthesis of Au-144(SR)(60) Nanoclusters in Methanol, Chem Mater, 23 (2011) 2209-2217.

[7] M. Brust, M. Walker, D. Bethell, D.J. Schiffrin, R. Whyman, Synthesis of Thiol-Derivatized Gold Nanoparticles in a 2-Phase Liquid-Liquid System, J Chem Soc Chem Comm, (1994) 801-802.

[8] A. Sels, N. Barrabes, S. Knoppe, T. Burgi, Isolation of atomically precise mixed ligand shell PdAu24 clusters, Nanoscale, 8 (2016) 11130-11135.

[9] A. Sels, G. Salassa, S. Pollitt, C. Guglieri, G. Rupprechter, N. Barrabés, T. Bürgi, Structural Investigation of the Ligand Exchange Reaction with Rigid Dithiol on Doped (Pt, Pd) Au25 Clusters, The Journal of Physical Chemistry C, 121 (2017) 10919-10926.

[10] The Basics of Catalysis, Catalysis, pp. 39-75.

[11] N. Barrabés, B. Zhang, T. Bürgi, Racemization of Chiral Pd2Au36(SC2H4Ph)24: Doping Increases the Flexibility of the Cluster Surface, J Am Chem Soc, 136 (2014) 14361-14364.

[12] E. Gottlieb, H. Qian, R. Jin, Atomic-Level Alloying and De-alloying in Doped Gold Nanoparticles, Chem. Eur. J., 19 (2013) 4238 - 4243.

Chapter 4

Support effect on the reactivity and stability of Au$_{25}$(SR)$_{18}$ and Au$_{144}$(SR)$_{60}$ nanoclusters in liquid phase cyclohexane oxidation
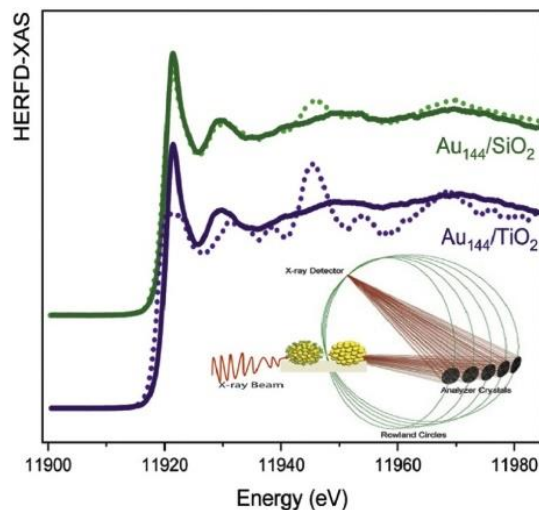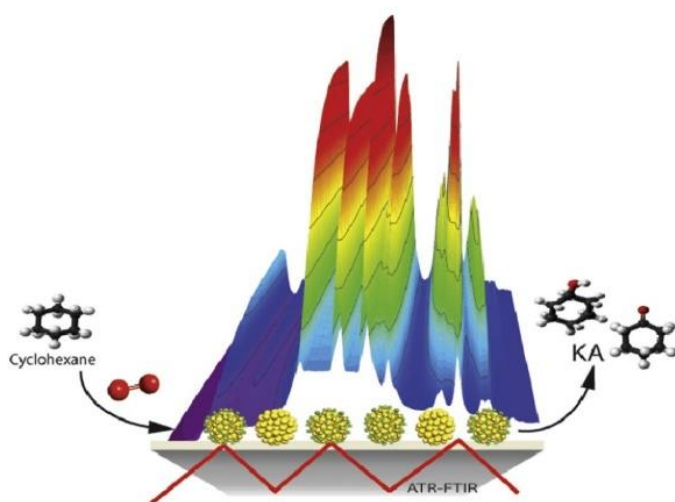
This chapter is based on the following publication: Clara García et al. Catalysis Today (2019) 336(1), 174-185 (https://doi.org/10.1016/j.cattod.2018.12.013)

1. Abstract

In this chapter, the stability of Au_{25} and Au_{144} clusters, supported either on TiO_2 or SiO_2, was examined upon thermal air pretreatment and, for the first time, upon liquid phase oxidation reaction. A pronounced influence of the support (TiO_2 vs. SiO_2) and cluster size (Au_{25} vs. Au_{144}) was revealed by XAS, DRS and STEM. Upon pretreatment, Au_{144} was more stable which may be related to its specific cluster core structure and staple configuration. The catalytic properties in liquid phase cyclohexane oxidation were clearly size dependent, with Au_{144} yielding higher TOF values, particularly in the case of SiO_2 supported catalysts. However, with respect to selectivity, TiO_2 supported catalysts led to higher KA production than SiO_2 supported ones. This can be explained by the different reaction pathways, as observed by *in situ* ATR. HERFD-XAS measurements of Au_{144}/TiO_2 catalysts revealed a pronounced cluster structure modification towards bulk gold during the reaction, in contrast to a high stability of Au_{144}/SiO_2. This study demonstrates the important role the support material has on the reactivity and stability of gold nanoclusters, which is key for their catalytic function.

2. Introduction

Gold catalysts were generally considered to be inactive until the 1980s, when Haruta [23] reported a high activity of Au particles smaller than 5 nm supported on 3d transition metal oxides. Following this, gold catalysis boomed and since then numerous synthetic methods have been explored aiming to control the size and shape of small gold particles. Recently, a step forward was achieved by the atomically controlled synthesis of nanoparticles with less than 100 atoms, which are referred to as nanoclusters [24-28]. Related to the small size of the nanoclusters (< 2 nm), gold exhibits unique properties, different from bulk gold and directly linked to the number of atoms and the cluster atomic structure. $Au_n(SR)_m$ nanoclusters tend to adopt highly symmetric core structures, such as icosahedral or tetrahedral geometry, different from the face-centered-cubic (fcc) structure of common gold nanoparticles [24, 29]. In addition, the small number of

atoms / minimal size induce strong electron energy quantization, different from the metallic band structure of larger gold nanoparticles or bulk gold.[30]

The outstanding size control during cluster synthesis opens up new opportunities for accurate studies of size-dependent properties, atomic structure effects and reaction mechanism in catalysis. Catalysis research of atomically precise gold nanoclusters is an emerging field with applications in many chemical processes [25, 31-33].

Previous studies revealed the strong dependence of the catalytic properties on the particle size and stability of gold nanoclusters in oxidation reactions. Valden and Goodman reported the structure sensitivity of CO oxidation on Au/TiO_2, with cluster sizes between 1 and 6 nm, related to quantum size effects associated with the supported Au clusters[34]. Theoretical studies showed the relation of the catalytic activity in CO oxidation with the adsorption capability depending on cluster size and structure, related to their HOMO-LUMO energy gaps [34, 35]. Recently, Y.Zhang et al. [36] show that size dependence differences in electronic structure influenced the adsorption behaviors of the substrate and product molecules on the cluster. In this case Aun(MPA)x (n=15,18 and 25) (MPA = 3-mercaptopropionic acid) clusters on a quartz slide surface were studied on fluorogenic reaction. Different product dissociation behaviors were observed depending on the Au cluster size dealing to different reaction mechanism [36].

Besides these reactions, extensive work on the cluster size effect on liquid phase oxidation reactions has been studied by several groups [18, 31, 37, 38]. Among them, for example, cyclohexane oxidation to cyclohexanone and cyclohexanol (Ketone/Alcohol or KA oil), which is relevant for the nylon industry.

Studies using Au nanoparticles supported on several types of oxides already showed over 90% selectivity to the desired products (K/A) [39-41]. The role of the Au particles is debatable, however. Hereijgers et al. [42] stated that Au was not active in cyclohexane oxidation and attributed the reaction to autoxidation. Liu et al. [18] revealed high activity/selectivity once gold nanoclusters were used. A blank test (without Au) did not show any cyclohexane conversion. Wu et al. [43] explored the role of Au particles supported on mesoporous silica on the reaction mechanism, showing the activation of O_2 molecules by gold. This provided active surface oxygen

species for the reaction. All these studies demonstrate the critical role of nano size gold particles in the oxidation of cyclohexane.

Tsukuda et al extensively explored the catalytic activity of supported Au_n nanoclusters in oxidation reactions [18, 37, 44, 45]. Carbon supported $Au_n(SG)_m$ clusters (n=5, 10, 18, 25, 39, ~ 85), after ligand removal, were all active in the aerobic oxidation of cyclohexane to cyclohexanol and cyclohexanone, but with a volcano-type dependence with a maximum at n=39[18]. This result clearly shows how a difference in cluster size of several atoms affects the catalytic activity. In a study of benzyl alcohol oxidation with extended cluster size (n= 2, 25, 38, 144, 330) Au_{144} exhibited the highest activity [44]. The size dependence was ascribed to differences in the geometric structure of the various clusters. For example, $Au_{25}(SR)_{18}$ has an icosahedral Au_{13} core, protected by characteristic long staples (–SR-Au-SR-Au-SR-) [46, 47]. In contrast, $Au_{144}(SR)_{60}$ has a hollow icosahedral Au_{114} core, in this case protected by short staples (-SR-Au-SR-) [48, 49]. (Fig. 4.22)
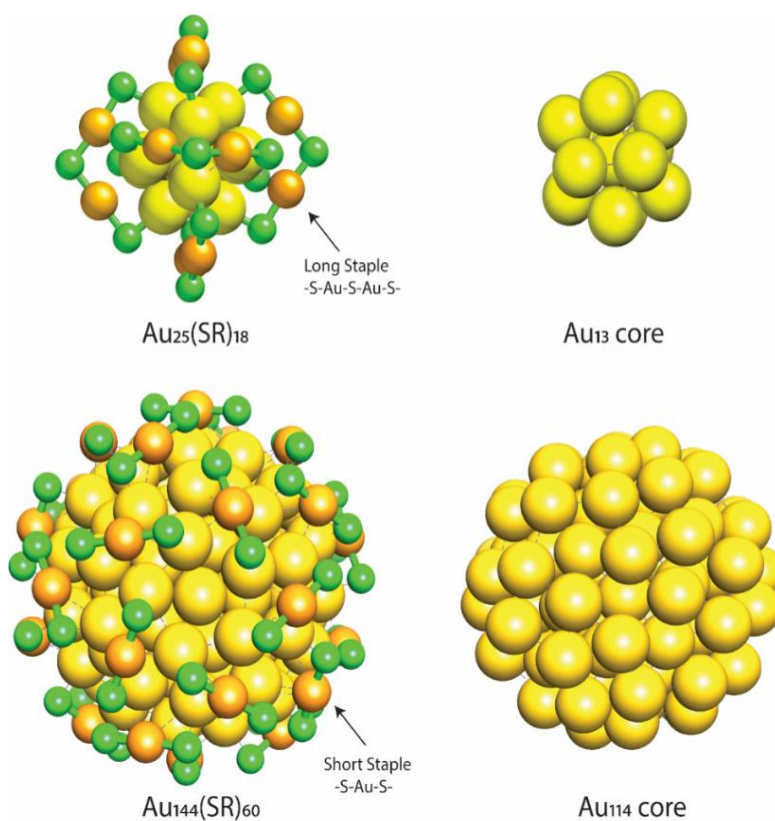
Figure 4-22 *Structure representation of $Au_{25}(SR)_{18}$ cluster and a $_{Au144}(SR)_{60}$ (R omitted for clarity) (⬤ Au (0) in the core cluster; ⬤ Au (I) in the staple; ⬤ S)*

The thiolate ligands on the clusters also influence their catalytic properties [32, 45]. Generally, they are considered to poison the active Au sites [25, 32]. Consequently, the ligands are often removed by oxidative thermal pretreatments to produce a more accessible Au surface [50]. Metal oxides are commonly used as supports to stabilize the cluster core structure during pretreatment and reaction conditions. The influence of the ligand coverage around the gold core on the activity in cyclohexane oxidation was studied by Zhang et al [51] using $Au_{38}(SR)_{24}$ clusters supported on CeO_2 and Al_2O_3. Pretreated catalysts were more active than untreated ones, once more showing that the removal of thiolates creates more active sites. Despite identical thermal treatments, Au_{38} clusters supported on CeO_2 were more active than the ones on Al_2O_3 with higher K/A selectivity. This suggests different cluster support interactions for CeO_2 and Al_2O_3.

For Au_{25} clusters, support effects were also studied by Fang et al. [52], using hydroxyapatite (HAP), TiO_2 (P25), activated carbon (AC), pyrolyzed graphene oxide (PGO) and fumed SiO_2. It was found that certain supports (like HAP and TiO_2) effectively prevented the sintering of Au nanoclusters during pretreatments due to the strength of Au-support interaction, whereas cluster growth occurred for AC,PGO and SiO_2. In contrast, Ma et al.[53] and Das et al.[54] reported that no sintering occurred for Au_{25} and Au_{144} supported on a different kind of mesoporous silica upon thiolate ligand removal (again ascribed to a strong interaction between Au and silica). Therefore, complementary studies on cluster stability supported on TiO_2 and SiO_2 are required to clarify different observations from previous reported studies.[52-54]

It should be noted that in almost all previous studies the effect of thermal pretreatment on cluster size stability was only evaluated by electron microscopy (TEM). Only Zhang et al. [51] and Shivhare et al. [55] reported detailed X-ray Absorption Spectroscopy (XAS) studies of structure changes of supported thiolate gold nanoclusters upon pretreatment. XAS represents a powerful technique for structure investigations of unsupported [56-61] and supported [51, 55] monolayer protected nanoclusters.

In this work, two different cluster sizes ($Au_{25}(SC_2H_4Ph)_{18}$ and $Au_{144}(SC_2H_4Ph)_{60}$) on two different supports (TiO_2 and SiO_2) were examined. These clusters represent both extremes in common cluster size studied in catalysts with different staple configuration (long and short),

which are related to the stability of the structure. Then, special emphasis is put on the structure evolution of clusters upon deposition on the oxide materials, upon thermal pretreatment (ligand removal) and during liquid phase cyclohexane oxidation. For the first time structural changes of supported clusters before and after a liquid phase reaction are monitored by high- energy resolution fluorescence detected x-ray absorption spectroscopy (HERFD-XAS). HERFS-XAS is ideal for samples with low concentrations, with the analyzer crystal pushing the resolution and detection limits far beyond those of regular XAS [62]. Cluster stability was thoroughly evaluated by diffuse reflectance spectroscopy (DRS), scanning transmission electron microscopy (STEM), x-ray absorption spectroscopy (XAS) and HERFD-XAS. Catalytic performance was determined by batch reactor kinetics and in situ ATR studies. Relevant differences were observed between both clusters and supports, in terms of stability and reactivity.

3. Results

3.1 Cluster stability upon deposition

The purity of the synthesized $Au_{25}(SC_2H_4Ph)_{18}$ and $Au_{144}(SC_2H_4Ph)_{60}$ cluster solutions was confirmed by UV-Vis (insets of) and MALDI mass spectroscopy (Figure in Appendix) [9, 10]. The absorption spectra of Au nanoclusters exhibit characteristic features caused by electronic transitions between different molecular orbitals, being directly related to the cluster structure. The stability of the clusters upon deposition is confirmed by the preserved characteristic features in the supported catalysts spectra (Figure 4-23). The characteristic bands are slightly shifted for $Au_{25}(SC_2H_4Ph)_{18}$ on SiO_2: the maxima shift from 398 to 400 nm, 447 to 466 nm, 520 to 550 nm and 682 to 684 nm. For $Au_{144}(SC_2H_4Ph)_{60}$ on SiO_2, a shift is still present, but less pronounced: 569 to 581 nm and 689 to 690 nm. These shifts are due to electronic cluster-support interactions. In the case of the TiO_2 support shifts are again present (442, 448 and 680 nm for $Au_{25}(SC_2H_4Ph)_{18}$ and 473, 522, 576 and 685 nm for $Au_{144}(SC_2H_4Ph)_{60}$) (Figure 4-23, inset)
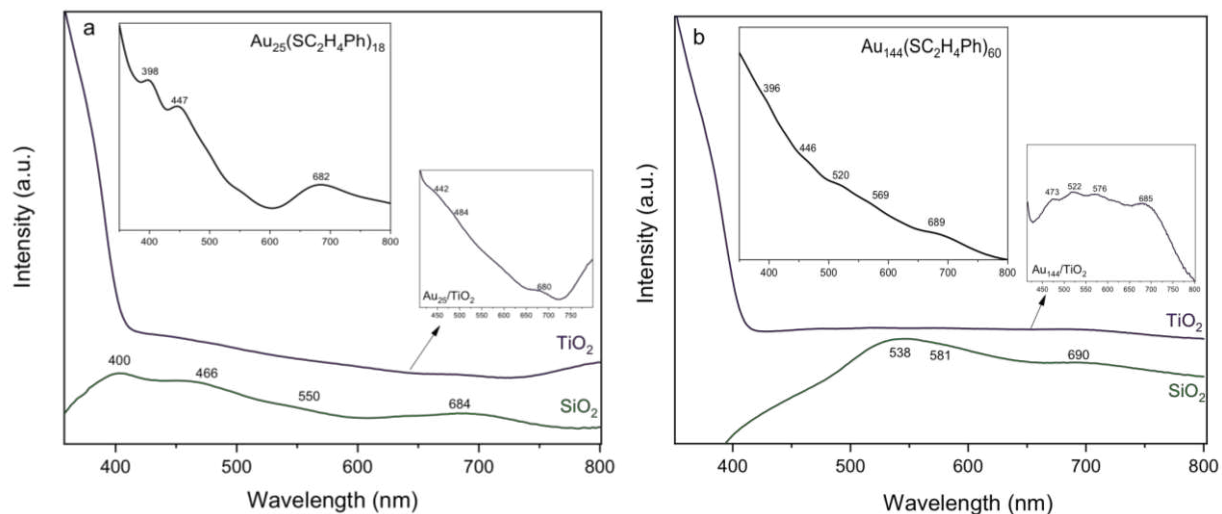
Figure 4-23 *Diffuse reflectance spectra: (a) 2% $Au_{25}(SC_2H_4Ph)_{18}$ in solution (inset) and supported on SiO_2 (green line) and TiO_2 (purple line); (b): 2% $Au_{144}(SC_2H_4Ph)_{60}$ in solution (inset) and supported on SiO_2 (green line) and TiO_2 (purple line).*

Table 4-1 *Au% weight tare of the prepared catalysts, as determinate by Total Reflexion X-ray Fluorescence (TXRF)*

Catalysts	%wt Au
$Au_{25}(SR)_{18}/TiO_2$	0.54
$Au_{144}(SR)_{60}/TiO_2$	0.36
$Au_{25}(SR)_{18}/SiO_2$	0.34
$Au_{144}(SR)_{60}/SiO_2$	0.25
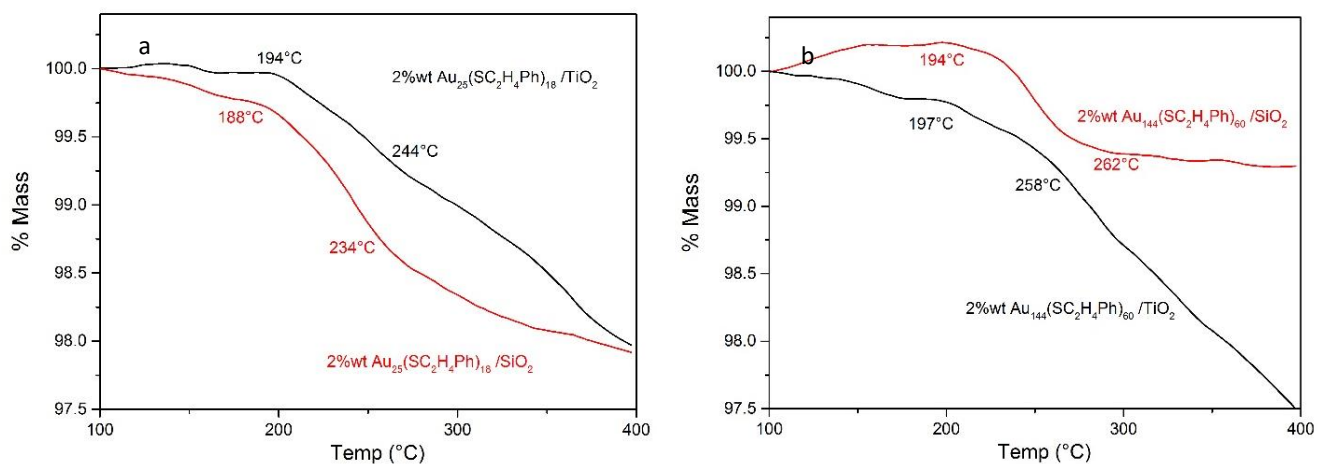
Figure 4-24 *TGA of (a) supported $Au_{25}(SC_2H_4Ph)_{18}$ supported on TiO_2 or SiO_2 and (b) $Au_{144}(SC_2H_4Ph)_{60}$ supported on TiO_2 or SiO_2*

3.2 Cluster Stability upon thermal pretreatment

Thermal pretreatment in air or oxygen is often used for ligand removal from supported clusters [32]. The temperature range typically varies between 150 °C and 400 °C. TGA analysis of both types of cluster samples (Figure 4-24) revealed that ligand desorption/decomposition started at~150 °C and was complete at~ 250 °C . The profile of the ligand desorption depended on the support [52], which indicates differences in the cluster support interaction. Previous studies of supported Au_{25} by Shivhare et al. [55] and Au_{38} by Zhang [51] et al. evidenced multistep ligand desorption in line with our observations. Accordingly, a pretreatment temperature of 150°C was selected.
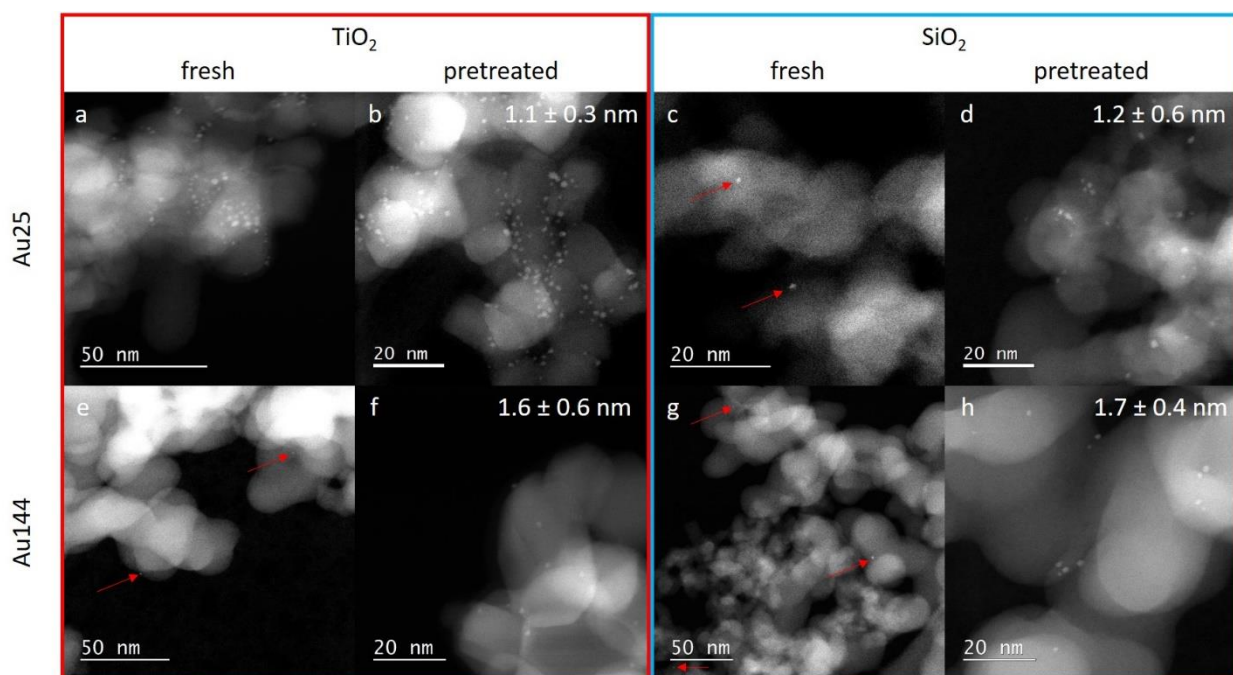
Figure 4-25 *HAADF-STEM images of (a-d) $Au_{25}(SC_2H_4Ph)_{18}$ and (e-h) $Au_{144}(SC_2H_4Ph)_{60}$, supported either on TiO_2 (a,b,e,f) or SiO_2 (c,d,g,h). Samples were either fresh (a,c,e,g) or pretreated in air at 150°C (b,d,f,h).*

Figure 4-25 compares STEM images of the supported clusters in the fresh (untreated) state and after air pretreatment at 150°C (pret). A homogeneous cluster size was observed after deposition, centred around 1.1 nm for $Au_{25}(SR)_{18}$ (Figs. 4-25a,e) and 1.6 nm for $Au_{144}(SCH_2Ph)_{60}$

(Figs. 4-25 c,g), clearly showing that the deposition did not change the cluster size (monodispersitivity). Moreover, the clusters were well dispersed on the support. After pretreatment at 150°C only a negligible increase of cluster size was observed for both types of clusters and supports (Figs. 4-25 b,d,f,h). For 250°C pretreatment temperature, significant particle size increase occurred (from 3.5 to 5.5 nm; Fig.in appendix)

Size increase upon 250°C treatment can also be inferred from diffuse reflectance spectroscopy (Fig. in appendix) because characteristic cluster features changed, leading to a new band at 520 nm due to surface plasmon resonance [63] [64]. Clusters supported on TiO_2 agglomerated more than the ones on SiO_2. The STEM and DRS results thus confirmed that pretreatment at 150°C preserved the cluster size and induced a partial ligand removal (confirmed by TGA). The structural modifications induced by 150°C air pretreatment were further studied by XANES at Au L3-edge. In Figure 4-26, features at 11922 eV, 11933 eV and 11946 eV become more intense, which are typical for Au foil, having a reduced population of unoccupied valence d-states. The number of valence d electrons mainly affects the white line, whereas the post-edge features are also related to the structure. This clearly indicates that after pretreatment stronger metallic Au features are present due to the S removal. For Au_{25}, post-edge features (11933 and 11946 eV) are affected upon pretreatment, which can be explained by cluster structure changes. This agrees with studies by Zhang et al. of supported gold nanoclusters on different supports [61] and by Anderson et al. of Au clusters on titania [65]. Our measurements show higher stability of the supported thiolate Au_{144} clusters upon pretreatment, independent of the support material.
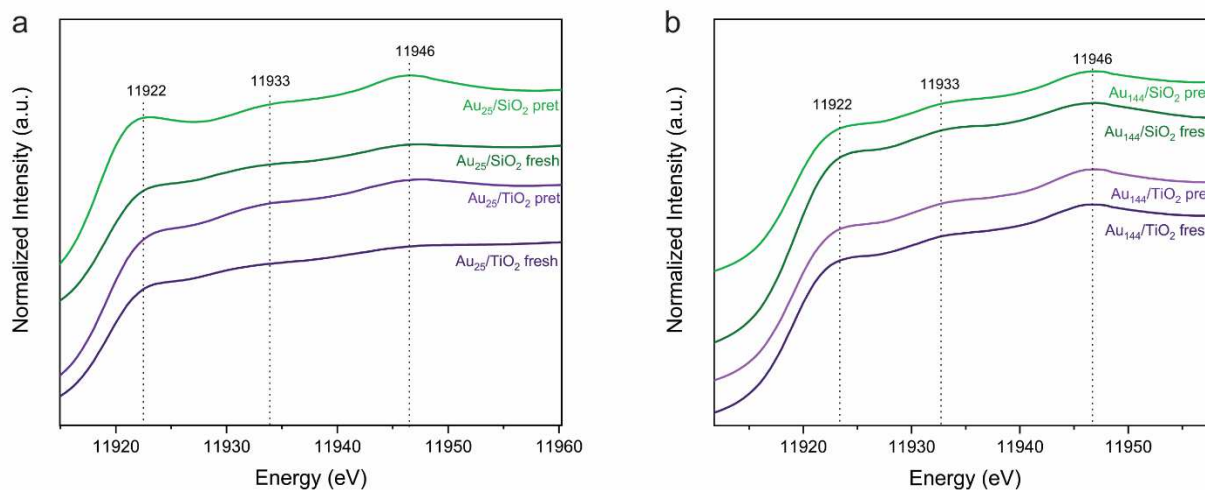
Figure 4-26 *Au L3 edge XANES spectra of a) Au₂₅ clusters supported on SiO₂ (green) or TiO₂ (purple), fresh and after air pretreatment at 150°C. (b) The same for Au₁₄₄ cluster catalysts.*

3.3 Catalytic activity in cyclohexane oxidation

To learn more about the effects of cluster size/structure and support on catalytic activity, Au_{25} and Au_{144} clusters supported on TiO_2 or SiO_2 were used for liquid phase cyclohexane oxidation. In light of our pretreatment studies, all catalysts were heated in air to 150°C before the catalytic tests. Cyclohexane oxidation, with molecular O_2 as oxidant, was performed at 75°C for 10h over the supported cluster catalysts (100 mg, 2%wt Au) in the absence of solvent, using TBHP as initiator. Results are summarized in Figure 4-27 and Figure 4-28, in terms of turnover frequency (TOF; (based on the total Au loading) and distribution of the main products (cyclohexanol and cyclohexanone) vs. by-products (analysed by GC-MS and shown in appendix). For comparison, the pure supports (without Au clusters), and commercial Au/TiO_2 (mean Au particle size 4.1 nm) were also examined.
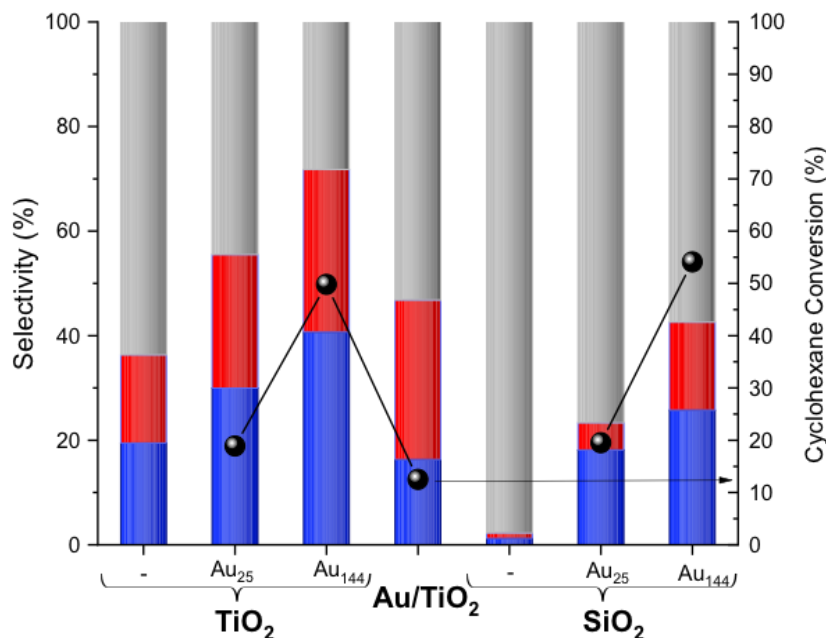
Figure 4-27 *Catalytic activity of supported Au$_{25}$ and Au$_{144}$ clusters (pretreated at 150°C) in the catalytic oxidation of cyclohexane: (a) (●) cyclohexane conversion per mg Au (except in the blank measurements) (left axis); product distribution (right axis): (■) cyclohexanol (Ol); (■) cyclohexanone (One); and (■) by-products (R).*
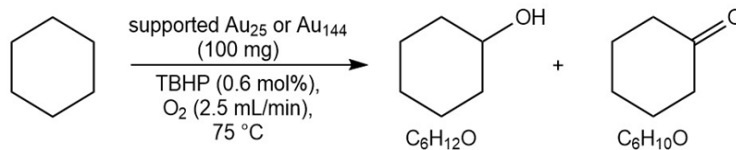
Catalyst	TOF (1/ h^{-1} mol Au^{-1})	Product distribution			
		% C$_6$H$_{12}$O	% C$_6$H$_{10}$O	% rest	KA product
TiO$_2$	-	19.5	16.8	63.7	36.4
Au$_{25}$/TiO$_2$	1495.1	30.0	25.5	44.5	55.5
Au$_{144}$/TiO$_2$	3932.6	40.7	31.1	28.2	71.7
Au/ TiO$_2$	985.4	16.3	30.5	53.2	46.8
SiO$_2$	-	1.2	1.1	97.7	2.3
Au$_{25}$/SiO$_2$	1542.5	18.2	5.2	76.6	23.4
Au$_{144}$/SiO$_2$	4273.9	25.8	16.8	57.4	42.6

Figure 4-28 *Reaction scheme, TOF's, product selectivity for the different catalysts (all pretreated in air at 150°C)*

Supported Au_{144} cluster catalysts exhibit about twice the TOFs of Au_{25} (based on the total Au loading, see Figure 4-28), which is very similar to reports by Tsukuda and co for benzyl alcohol oxidation [44, 66]. The higher activity was ascribed to better benzyl alcohol adsorption on large gold facets and to the Au_{144} electronic structure. However, the activation of molecular oxygen is considered to be a rate-limiting step of aerobic cyclohexane oxidation, for which nano-sized gold around 5 nm seems highly active [67, 68]. Therefore, the combined effects of adsorption, structure and oxygen activation may explain the higher activity of Au_{144}.

In terms of type of support, SiO_2 supported cluster catalysts show slightly higher activity than TiO_2 ones. However, higher (KA) selectivity toward cyclohexanole and cyclohexanone is obtained with TiO_2 as opposed to SiO_2 supported ones. TiO_2 has been extensively studied due to its redox properties, which may facilitate the formation of (surface) peroxide intermediates which could influence the reaction pathway - as observed by the ATR measurements discussed below.

Looking at it in more detail, it can be seen that the time dependent formation in Figure 4-29 clearly shows higher values of cyclohexanol and cyclohexanone for both Au_{144} and Au_{25} clusters supported on TiO_2 (0,17 mmol of cyclohexanol and 0,13 mmol of cyclohexanone for Au_{144}, 0,13 mmol of cyclohexanol and 0,11 mmol of cyclohexanone for Au_{25}), whereas for SiO_2 it only reached 0,10 mmol of cyclohexanol and 0,07 mmol of cyclohexanone for Au_{144} and 0,07 mmol of cyclohexanol and 0,02 mmol of cyclohexanone for Au_{25}.

Leaching experiments confirmed that the deposition/pretreatment permanently fixed the Au clusters to the support oxides. After 10h reaction time the reaction mixture was centrifuged to separate solid and liquid phases. The liquid phase (still containing unreacted cyclohexane) was then reintroduced into the reactor with samples being taken in 1h intervals and then analyzed. After the removal of the catalyst only negligible conversion (<1%) was

observed for all samples (1 to 8h). It can therefore be safely assumed that no Au species where present in the liquid phase, excluding leaching.
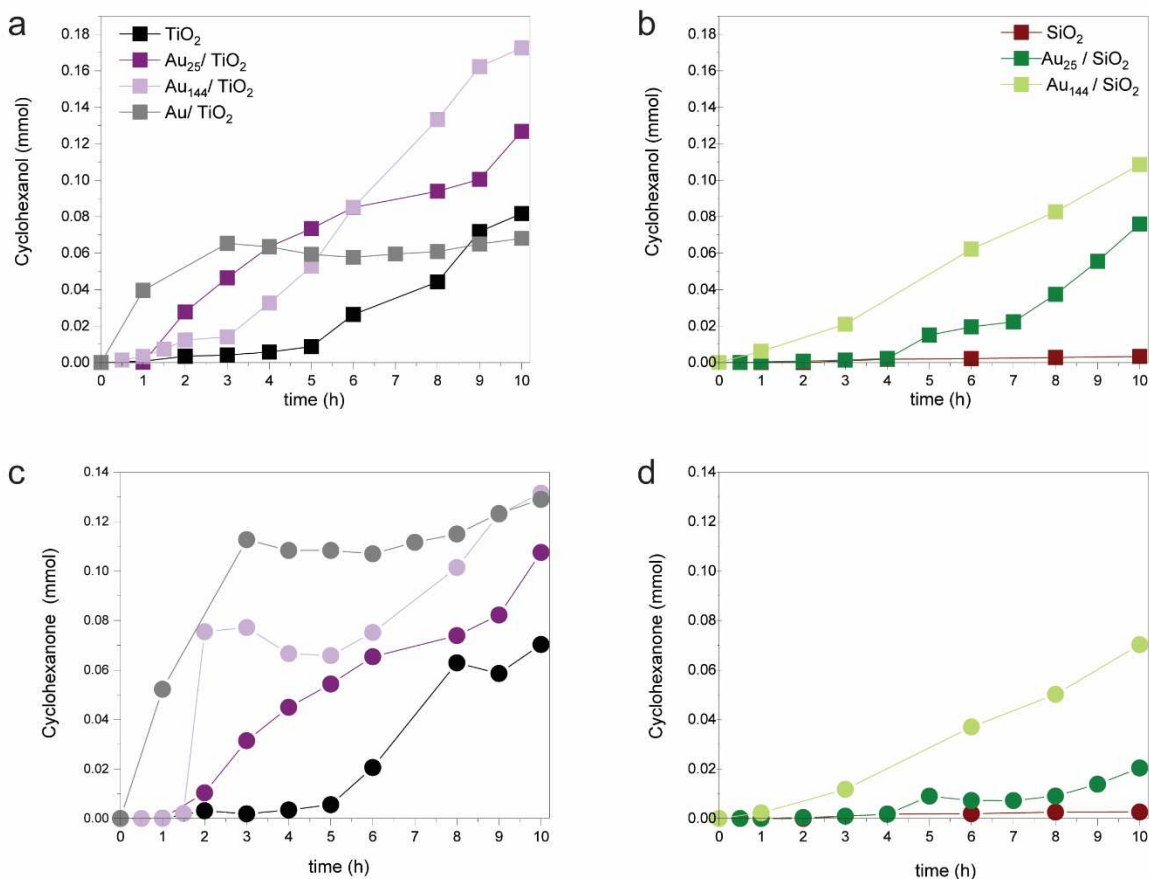
Figure 4-29 *Time dependence of products formation with (a,c) Au_n/TiO_2 and (b.d) Au_n/SiO_2 catalyst. (■) cyclohexanol and (●) cyclohexanone.*

The commercial aurolite catalyst (2% wt Au nanoparticles with 4.1 nm mean size on TiO_2) was also pretreated at 150°C and the reaction conducted analogously. A TOF of 394 mol Au^{-1} h^{-1} and relatively high selectivity (16.3% to cyclohexanol and 30.5% to cyclohexanone) was observed, but the TOF and selectivity of Au_{144}/TiO_2 were not reached. Very interestingly, the reaction with aurolite is faster in the first three hours, but suddenly slows down, possibly due to catalyst deactivation.

To summarize the present catalytic test: Au_{144} supported on SiO_2 clusters are the most active for liquid phase cyclohexane oxidation although TiO_2 supported ones lead to higher selectivity towards KA. To learn more about the underlying reasons, an operando study was performed.

3.4 Operando ATR spectroscopy of cyclohexane oxidation

Surface species present during cyclohexane oxidation on the more active Au_{144} clusters on TiO_2 or SiO_2 were studied by ATR-IR spectroscopy. The catalysts were deposited as thin films on a Ge crystal and mounted in a batch-reactor like in situ cell. The reaction mixture was then refluxed over the films.

Figure 4-30 shows in-situ ATR-IR spectra acquired during cyclohexane oxidation on Au_{144}/TiO_2 along with the evolution of the characteristic cyclohexane vibrations in the range of $_v$(C-H) vibrations evidence reactivity during the oxidation process. At around 2948 and 2836 cm^{-1} respectively symmetric and asymmetric stretching vibrations of the cyclohexane CH_2 groups are detected. In the lower wavenumber regions, cyclohexane scissoring, twisting and rocking vibrations are observed (negative bands at 1450, 1410 and 1020 cm^{-1}), as well as bending modes (positive peak at 1260 cm^{-1}) [69].
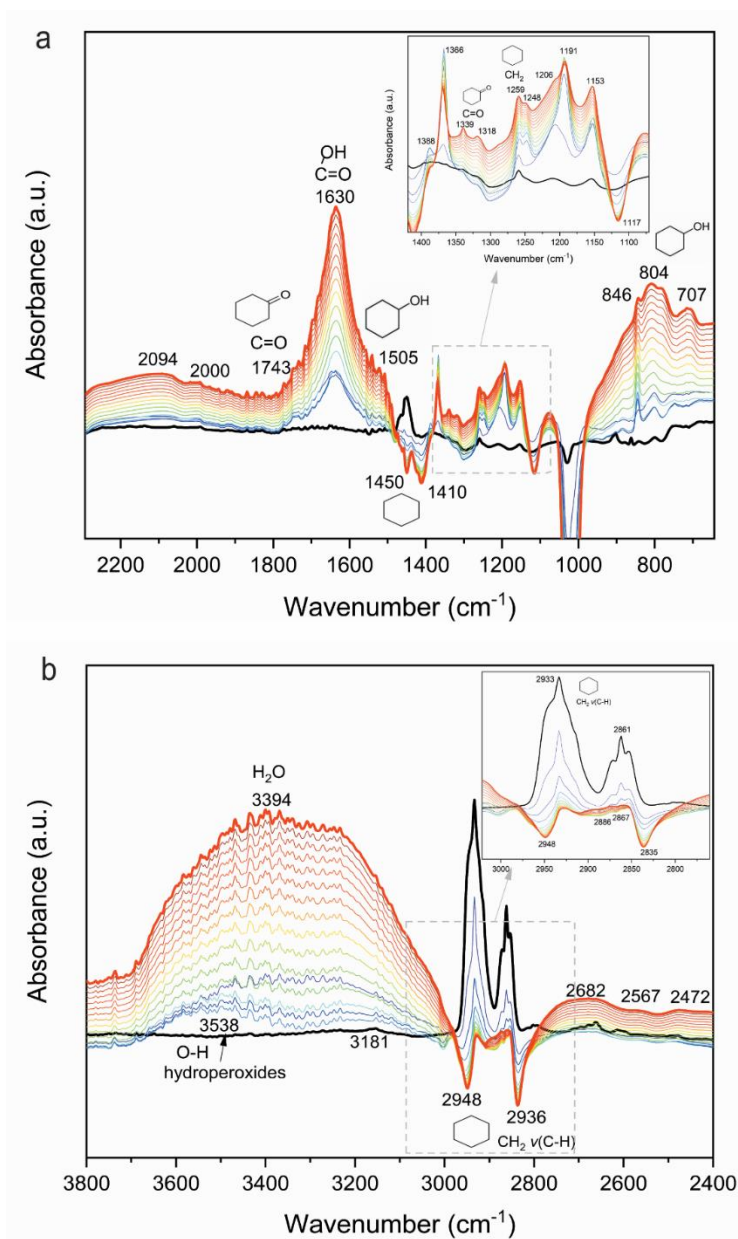
Figure 4-30 Operando ATR spectra of liquid phase cyclohexane oxidation on Au$_{144}$/ TiO$_2$

The bands at 3538 and 3181cm^{-1} in the OH stretching vibrations region grew continuously before merging into a broad band at 3394 cm^{-1}. The band at 3538 cm^{-1} is attributed to hydroperoxide intermediates on TiO$_2$, which originate from the reaction initiator (tert-butyl hydroperoxide) in line with reported infrared studies [69, 70]. The initiator reacts with cyclohexane forming the cyclohexylhydroperoxide intermediate, showing bands at 1366 and

1191 cm^{-1}. During the first 30 minutes of reaction, these bands grow but then decrease in intensity.

The generally reported accepted reaction pathway involves the formation of cyclohexylhydroperoxide as the primary oxidation product but also small amounts of cyclohexanol and cyclohexanone. The formation of cyclohexanone can be followed by the characteristic ν(C=O) vibrations between 1630-1750 cm^{-1} and around 1339 cm^{-1}, and that of cyclohexanol by the increasing bands around 800 cm^{-1} and a shoulder at 1505 cm^{-1}. The regions of the bands are in line with literature values [69, 71, 72] and with our own reference measurements (Figs. in appendix).

Bands around 3394 cm^{-1} are due to water molecules on the TiO_2 surface as observed in IR studies of cyclohexane photo-oxidation on TiO_2 [69, 70]. In these studies, carbonates and carboxylates were observed which were not detected in our experiments. The strong adsorption of carbonates and carboxylates resulted in a decrease in the cyclohexanone rate and an increase in by-products. The absence of these species in our ATR spectra conforms the high selectivity of Au_{144}/TiO_2 for the desired products (Figure 4-30).

Figure 4-31 displays the in-situ ATR experiment with the Au_{144}/SiO_2 catalyst, revealing considerable differences to the Au_{144}/TiO_2 system. Between 2970 and 2780 cm^{-1} stretching vibrations of the cyclohexane CH_2 groups can be clearly observed, as well as bands around 1450, 1258 and 901 cm^{-1}, related to scissoring, twisting and rocking vibrations [69, 71]. In comparison with Au_{144}/TiO_2 slightly shifted wavenumbers were detected, as well as pronounced differences in the intensity changes, which could be a result of the lower cyclohexane reactivity, in line with the kinetic tests.

The formation of cyclohexanone can be followed by the characteristic ν(C=O) vibrations between 1680-1780 cm^{-1} and around 1321 cm^{-1}; and of cyclohexanol by ν(O-H) around 3330 cm^{-1}. Figure 4-30a (inset) displays the formation of both adsorbed and dissolved cyclohexanone, the former at 1698 and 1683 cm^{-1} and the latter at 1716 cm^{-1}, as well as of cyclohexanol at 1734 and 1705 cm^{-1}, all of them showing intensities increasing with reaction time. This is further confirmed by the evolvement of a band characteristic of cyclohexane at 1450 cm^{-1}, and new bands at 1440,

1462 and 1470 cm^{-1} corresponding to the reaction products, in line with reference measurements (Figs. In appendix) and previous work [69, 71, 72].
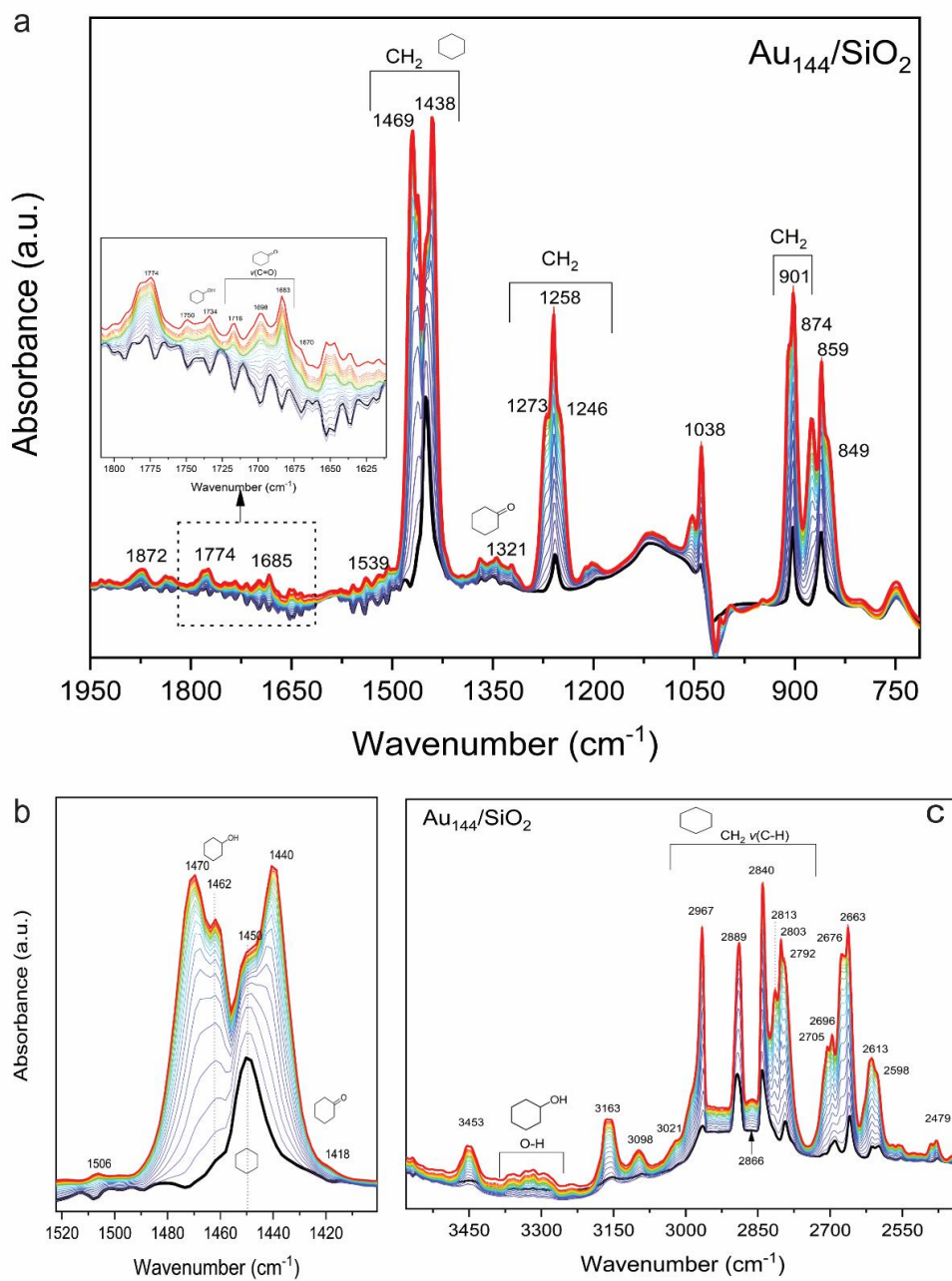
Figure 4-31 *Operando ATR spectra of liquid phase cyclohexane oxidation on Au$_{144}$/SiO$_2$*

The catalytic activity studies (Figure 4-31 Operando ATR spectra of liquid phase cyclohexane oxidation on Au144/SiO2indicated more by-products for Au$_{144}$/SiO$_2$ and as such

carbonates or carboxylates species would be expected. However, they were not observed (not even for Au_{144}/TiO_2). The strong cyclohexane bands on SiO_2 may indicate longer residence time and this could allow side reactions.

Figure 4-32 displays the evolution of reaction products of cyclohexane oxidation as determined by operando ATR. The characteristic bands of cyclohexanone are located around $1321cm^{-1}$ and for cyclohexanol are around $1506\ cm^{-1}$ for Au_{144}/TiO_2 and $1734\ cm^{-1}$ for Au_{144}/SiO_2. The trends of catalytic activity obtained by the kinetic tests were confirmed by the infrared experiments, with higher K/A selectivity for Au_{144}/TiO_2 catalysts.
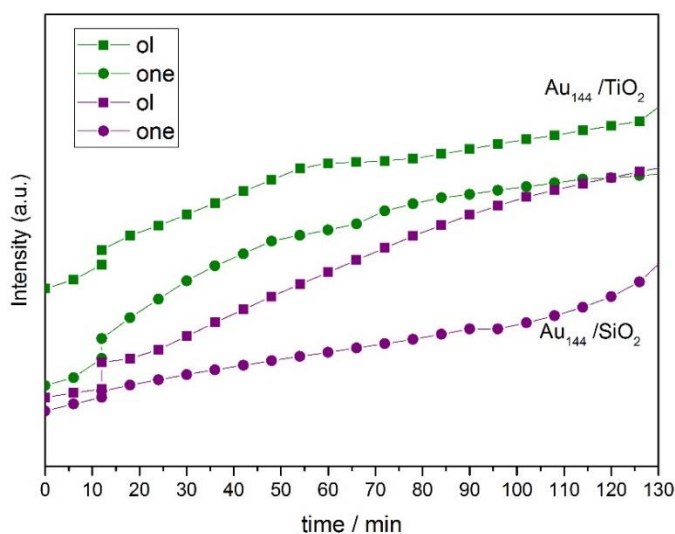
Figure 4-32 Intensity of characteristic bands of reaction products developing during cyclohexane oxidation as determined by in situ ATR (cyclohexanol 1506 cm^{-1} for Au$_{144}$/TiO$_2$ and 1734 cm^{-1} for Au$_{144}$/SiO$_2$; cyclohexanone: 1321cm^{-1})

3.5 Cluster Stability study via HERFD-XAS

High resolution XAS spectra — which are better at discriminating the different cluster structures — was obtained via HERFD-XAS This in turn allowed for the study of supported clusters after they had been used for liquid phase cyclohexane oxidation. Figure 4-33 shows the spectra of Au_{144}/TiO_2 and Au_{144}/SiO_2 before the reaction (pretreated at 150°C, "pret") and after 10 hours reaction ("used"). Clear differences were observed in the three main structure related features:

the white line intensity and energy (around 11921 eV), and the peaks at 11945 eV and 11968 eV became more intense as the structure became more bulk-like. These three features can be identified by using reference compounds (Figure 4-33c). The white line intensity is related to transitions from 2p to 5d and 6s, denoting the number of empty states [73]. Therefore, a more intense white line is thus observed for oxidized compounds [74] [75] or when the 5d electron density is decreased by bonding of electron-withdrawing ligands [76-78]. Bulk gold has a small white line due to hybridisation of s, p and d orbitals, which creates some d holes. In small clusters, oxidation and bonding to electron-withdrawing thiolate ligands can result in d holes. The white line intensity can also decrease as the size of the Au particles decrease. This was observed for bare Au nanoparticles on oxide supports [79].
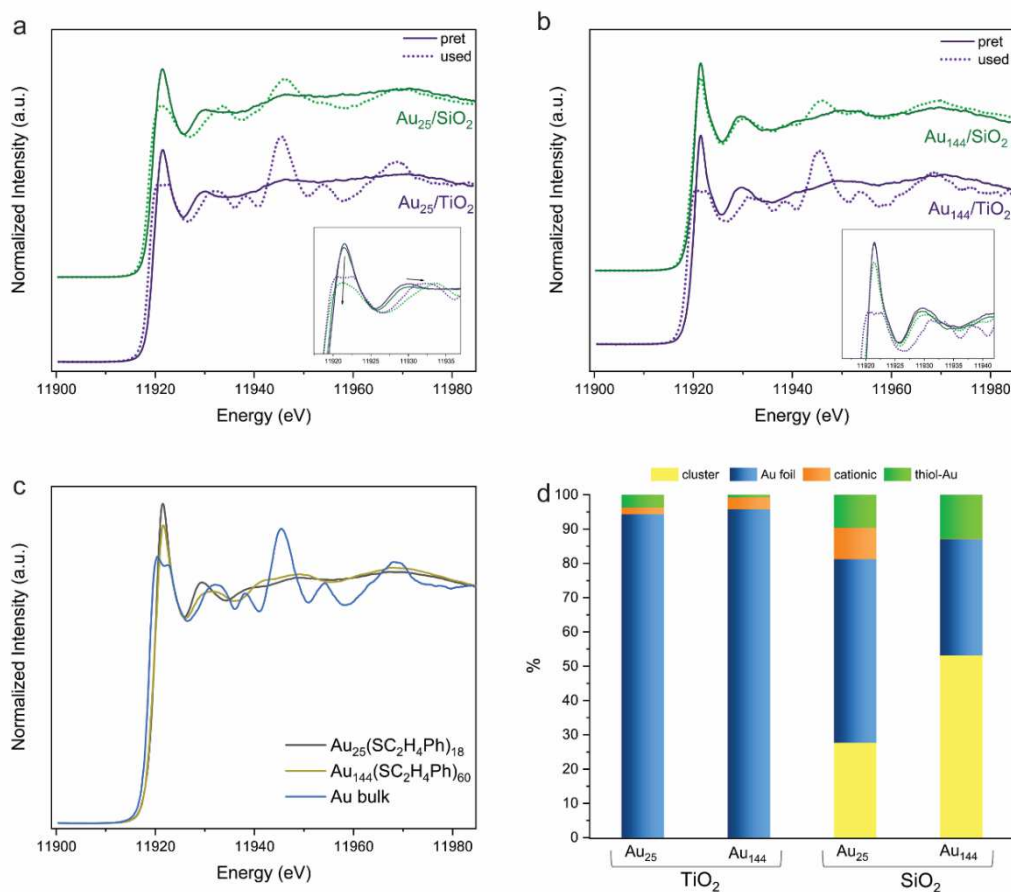
Figure 4-33 (a) HERFDS-XAS spectra of pretreated and used catalysts: (a) Au$_{25}$ supported on TiO$_2$ (purple) and SiO$_2$ (green); (b) Au$_{144}$ supported on TiO$_2$ (purple) and SiO$_2$ (green); (c) references Au$_{25}$, Au$_{144}$ and bulk Au (foil) and (d) linear combination of XANES spectra of used catalysts in the cyclohexane oxidation reaction after 10h

The pretreatment studies by XANES indicated lower stability of Au_{25} clusters than for Au_{144}, which is further confirmed by HERFD-XAS, also revealing the development of bulk-like gold structures after reaction on both supports (Figure 4-33). Surprisingly, for the SiO_2 supported catalysts a high stability was observed upon reaction. Figure 4-35b clearly shows that the cluster structure of Au_{144}/SiO_2 was largely preserved, even after 10h reaction.

A more detailed spectral analysis was performed by linear combination. Reference spectra of different oxidation states and particle structures of gold were measured to enable quantification: pure clusters, bulk fcc gold (Au foil), partially oxidized gold (asin the cluster staple (-SR-Au-SR-) of a thiolated complex (Au(I)) and cationic gold (Au(III)). The fitting of the used catalysts spectra led to the composition distribution displayed in Figure 4-33c. It showed that 53% of Au_{144}/SiO_2 were intact (unchanged), 28% were preserved in Au_{25}/SiO_2, whereas both Au_{144} and Au_{25} clusters on TiO_2 had developed bulk gold structure.

4. Appendix

Materials. Hydrogen tetrachloroaurate(III) hydrate ($HAuCl_4 \cdot 3H_2O$), tetraoctylammonium bromide (TOABr), and sodium borohydride ($NaBH_4$) were purchased from Aldrich. TiO_2 (Degussa P25), zirconia oxide (Jansen chimica) and fumed silica were used as support materials. Methanol (absolute for analysis), toluene, tetrahydrofuran (THF), cyclohexane, cyclohexanol,cyclohexanone and dichloromethane were purchased from Roth. A Millipore SAS water system was employed, with a 185nm UV lamp and membrane filters.
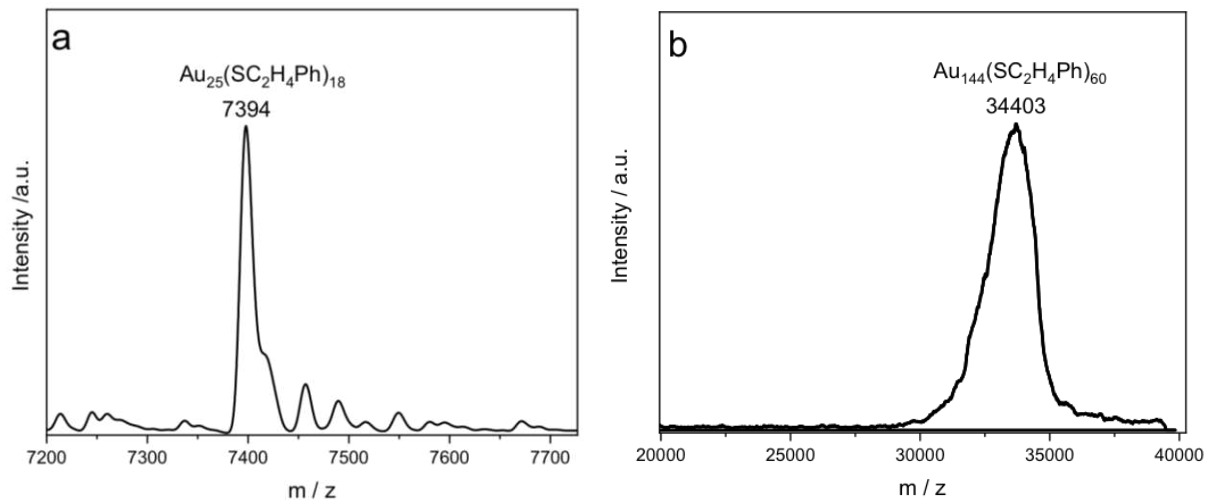
Figure 4-34 *Positive ion MALDI mass spectrum of (a) $Au_{25}(SC_2H_4Ph)_{18}$ and (b) $Au_{144}(SC_2H_4Ph)_{60}$*

Table 4-2 *Au % wt of the prepared catalysts as determined by Total Reflection X-ray Fluorescence (TXRF).*

Catalysts	%wt Au
$Au_{25}(SR)_{18}/TiO_2$	0.54
$Au_{144}(SR)_{60}/TiO_2$	0.36
$Au_{25}(SR)_{18}/SiO_2$	0.34
$Au_{144}(SR)_{60}/SiO_2$	0.25
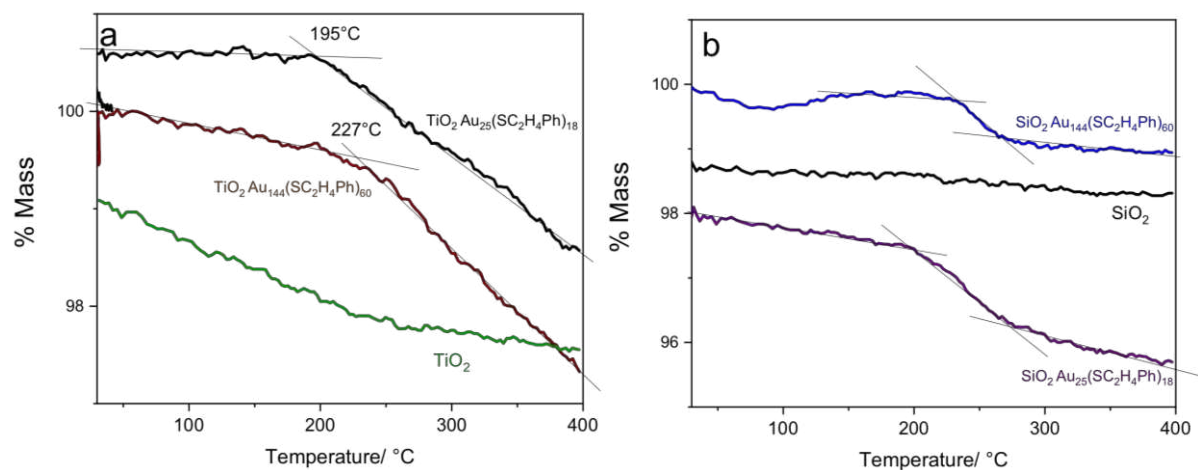
Figure 4-35 *TGA of (a) supported clusters on TiO₂ and (b) SiO₂.*
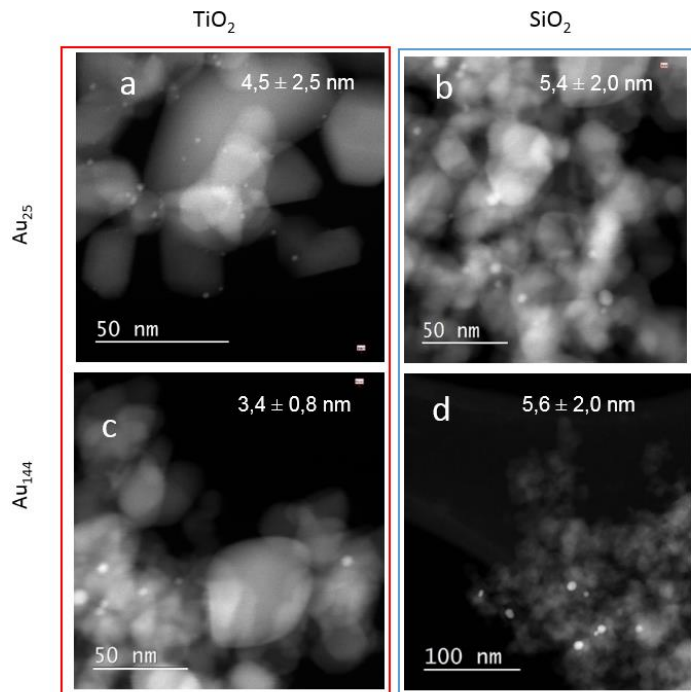
Figure 4-36 *TEM images of (a, b) Au₂₅(SC₂H4Ph)₁₈ supported on TiO₂ or SiO₂ and (c, d) Au₁₄₄(SC₂H₄Ph)₆₀ supported on TiO₂ or SiO₂, all pretreated in air at 250°C.*
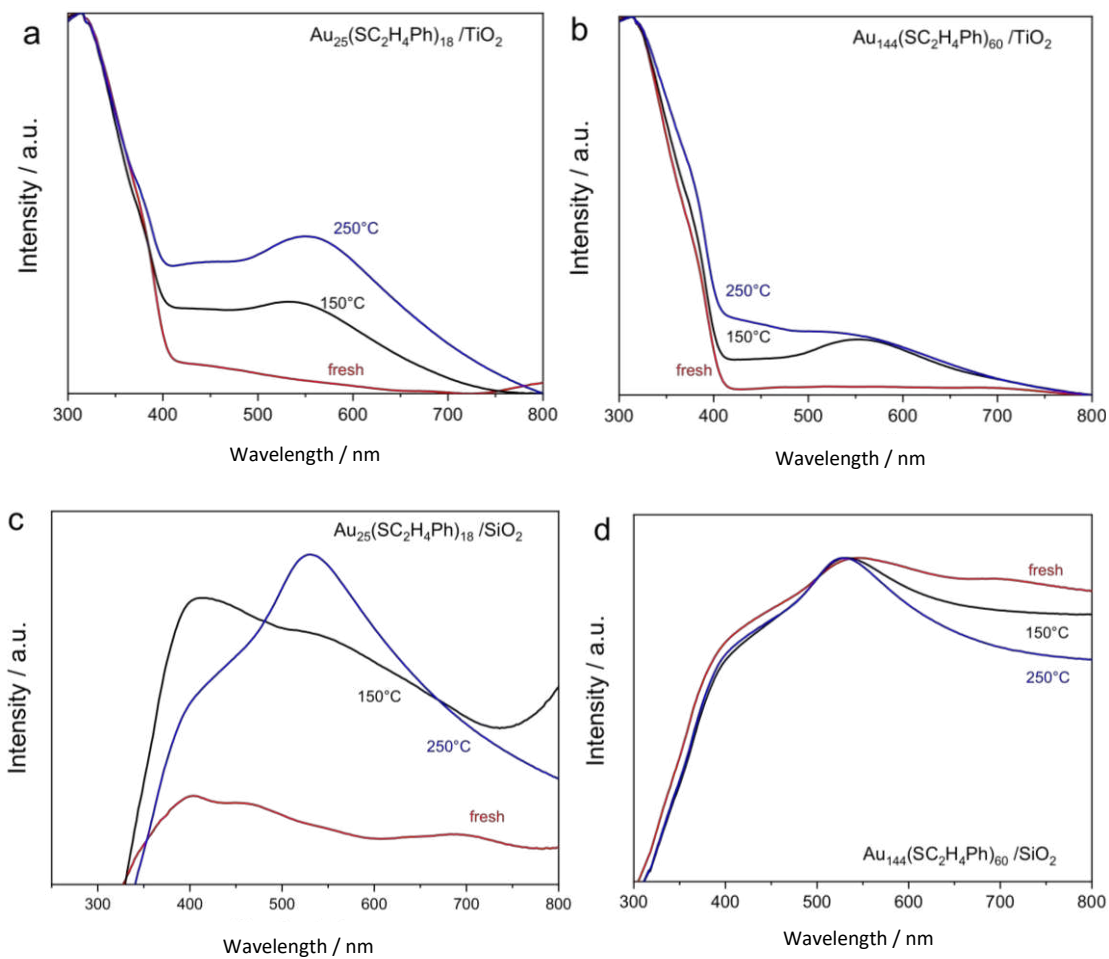
Figure 4-37 *Diffuse reflectance spectra of Au$_{25}$(SC$_2$H4Ph)$_{18}$ and Au$_{144}$(SC$_2$H$_4$Ph)$_{60}$, fresh and after air pretreatments at 150 and 250°C supported on TiO$_2$ (a, b) and SiO$_2$ (c, d).*
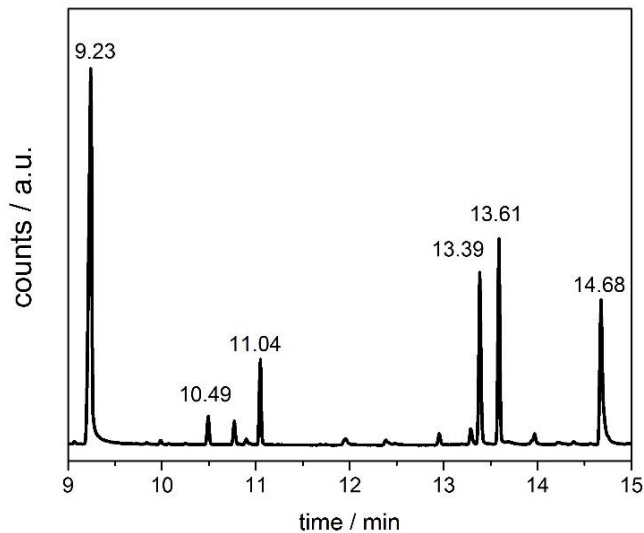
Figure 4-38 *GC-MS spectra, taken after 10h reaction on Au$_{144}$(SC$_2$H$_4$Ph)$_{60}$/TiO$_2$.*

Intermediates and by-products were identified by GC-MS: the largest peak corresponds to the main intermediate, cyclohexylperoxide (9.23 min), methyl-ethyl-cyclohexane was identified at 10.49 min, the peak at 11.05 min is a silicon polymer due to peroxides in the GC column; the other 3 peaks were found to be 1,1'-bicyclohexyl (13.39 min), cis-2-2hydroxyethyl-cyclohexanol (13.61 min) and 1-cyclohexylcyclohexanol (14.68 min).
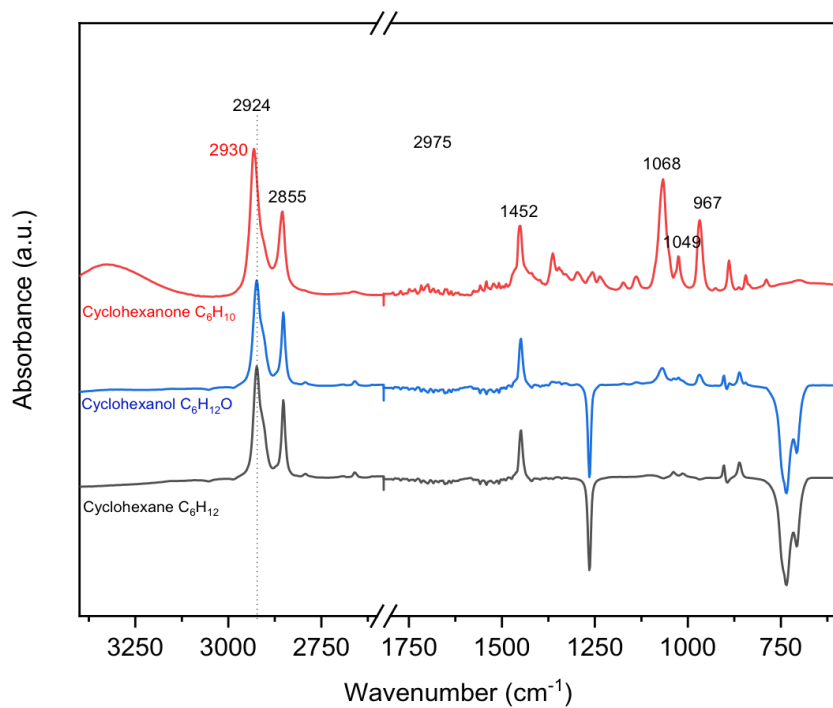
Figure 4-39 *ATR reference spectra of the reactant and main reaction products.*
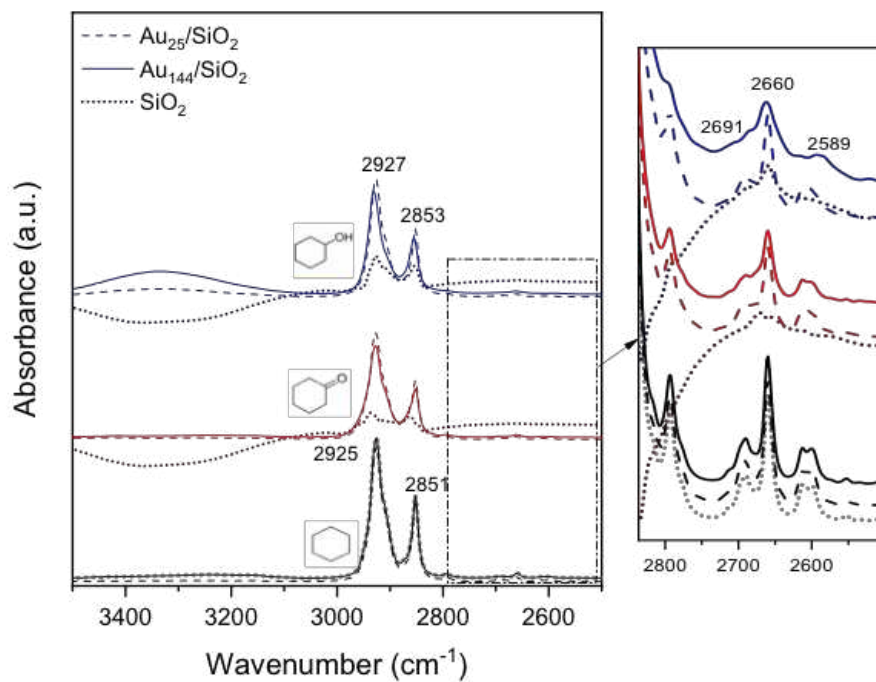
Figure 4-40 *ATR reference spectra of cyclohexane, cyclohexanol and cyclohexanone, adsorbed on SiO_2 or Au_n/SiO_2 catalysts.*
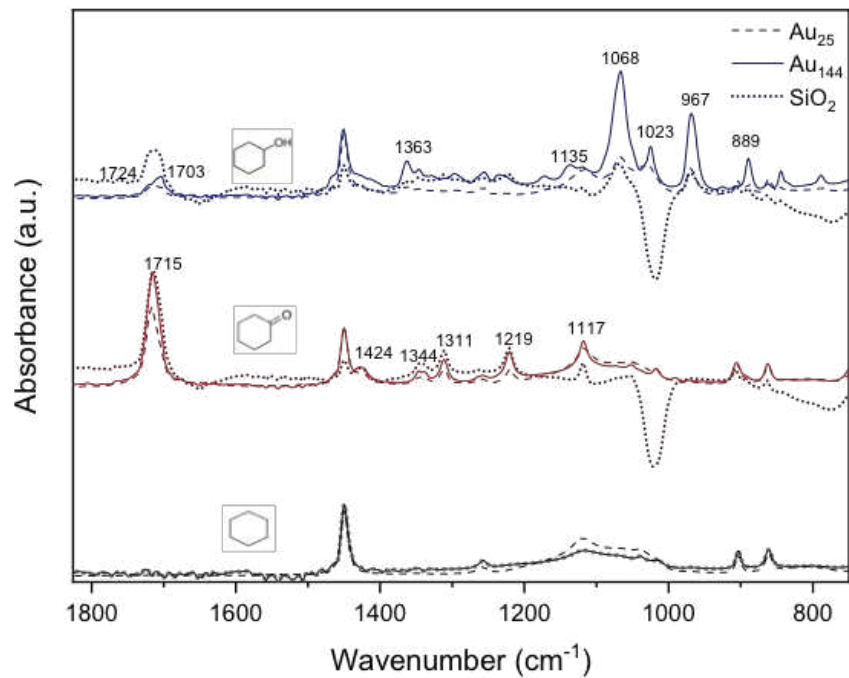
Figure 4-41 *ATR reference spectra of cyclohexane, cyclohexanol and cyclohexanone, adsorbed on SiO$_2$ or Au$_n$/SiO$_2$ catalysts.*
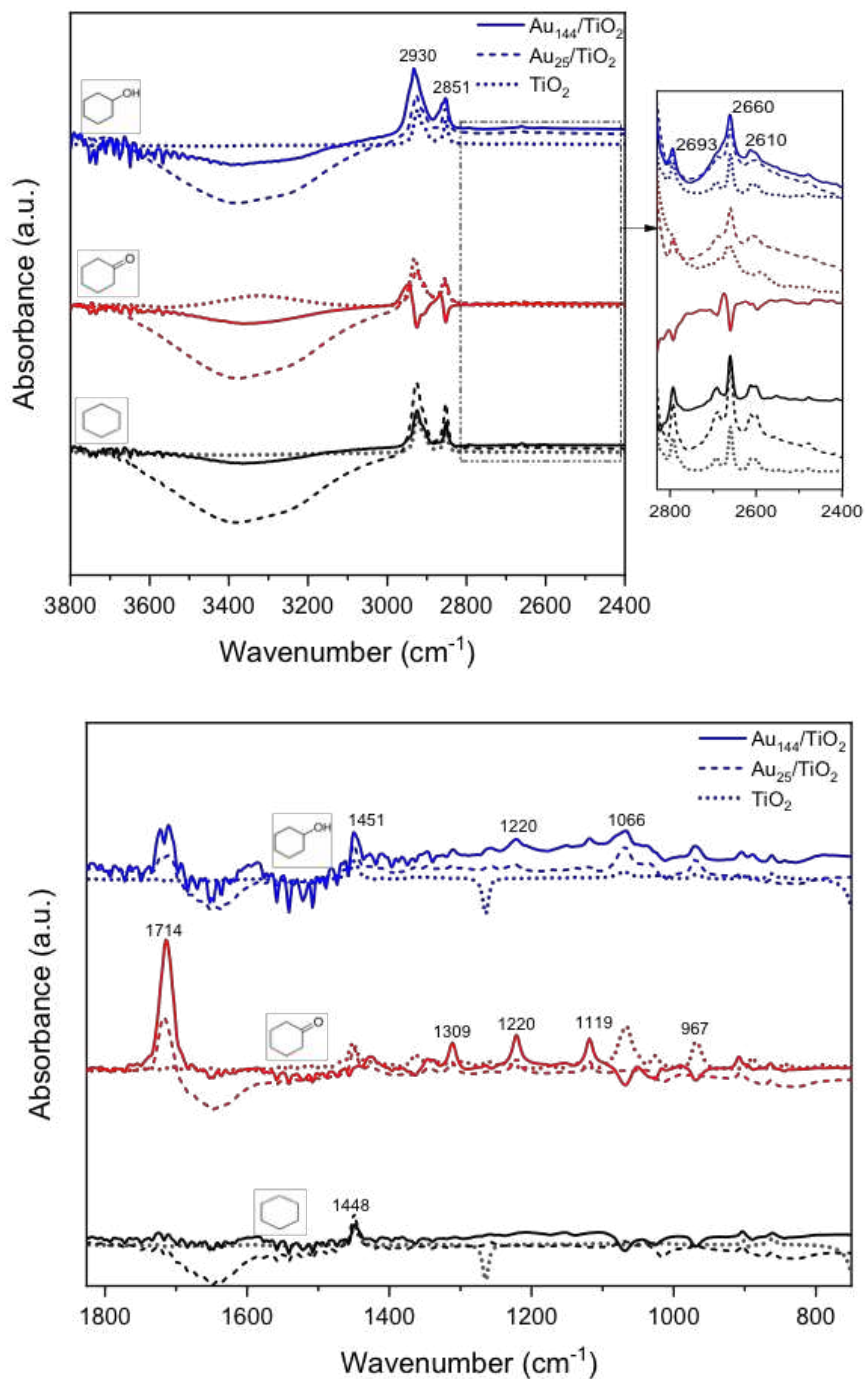
Figure 4-42 *ATR reference spectra of cyclohexane, cyclohexanol and cyclohexanone, adsorbed on TiO_2 or Au_n/TiO_2 catalysts.*
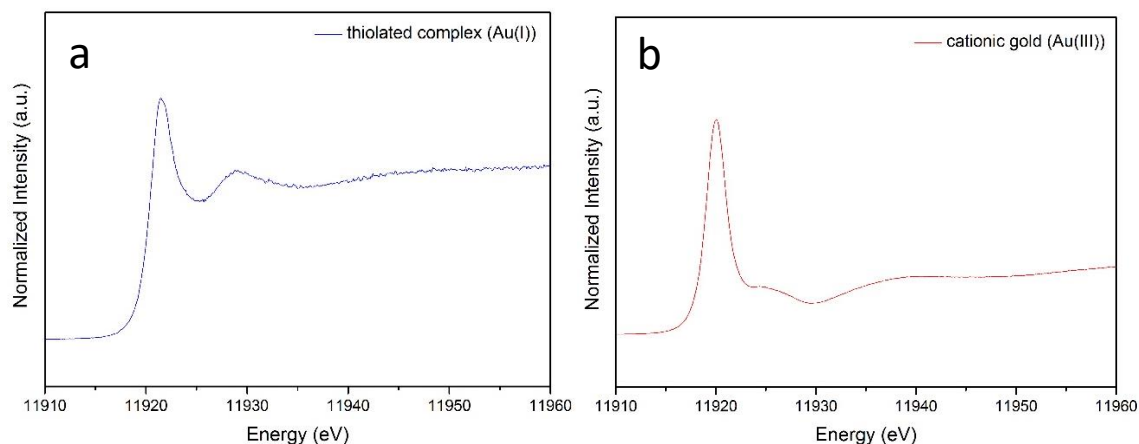
Figure 4-43 *Reference HERFD-XAS spectra used for the lineal combination fitting: (a) thiolate complex and (b) cationic gold (Au(III)).*

References

[1] A. Sels, N. Barrabes, S. Knoppe, T. Burgi, Isolation of atomically precise mixed ligand shell PdAu24 clusters, Nanoscale, 8 (2016) 11130-11135.

[2] A. Sels, G. Salassa, S. Pollitt, C. Guglieri, G. Rupprechter, N. Barrabés, T. Bürgi, Structural Investigation of the Ligand Exchange Reaction with Rigid Dithiol on Doped (Pt, Pd) Au25 Clusters, The Journal of Physical Chemistry C, 121 (2017) 10919-10926.

[3] X.-K. Wan, J.-Q. Wang, Z.-A. Nan, Q.-M. Wang, Ligand effects in catalysis by atomically precise gold nanoclusters, Science Advances, 3 (2017).

[4] J. Fang, J.G. Li, B. Zhang, X. Yuan, H. Asakura, T. Tanaka, K. Teramura, J.P. Xie, N. Yan, The support effect on the size and catalytic activity of thiolated Au-25 nanoclusters as precatalysts, Nanoscale, 7 (2015) 6325-6333.

[5] A. Shivhare, D.M. Chevrier, R.W. Purves, R.W.J. Scott, Following the Thermal Activation of Au-25(SR)(18) Clusters for Catalysis by X-ray Absorption Spectroscopy, J Phys Chem C, 117 (2013) 20007-20016.

[6] B. Zhang, S. Kaziz, H. Li, M.G. Hevia, D. Wodka, C. Mazet, T. Burgi, N. Barrabes, Modulation of Active Sites in Supported Au-38(SC2H4Ph)(24) Cluster Catalysts: Effect of Atmosphere and Support Material, J Phys Chem C, 119 (2015) 11193-11199.

[7] M. Zhou, C.J. Zeng, Y.X. Chen, S. Zhao, M.Y. Sfeir, M.Z. Zhu, R.C. Jin, Evolution from the plasmon to exciton state in ligand-protected atomically precise gold nanoparticles, Nat Commun, 7 (2016).

[8] S. Malola, L. Lehtovaara, J. Enkovaara, H. Hakkinen, Birth of the Localized Surface Plasmon Resonance in Mono layer-Protected Gold Nanoclusters, Acs Nano, 7 (2013) 10263-10270.

[9] P. Zhang, X-ray Spectroscopy of Gold–Thiolate Nanoclusters, The Journal of Physical Chemistry C, 118 (2014) 25291-25299.

[10] D.P. Anderson, R.H. Adnan, J.F. Alvino, O. Shipper, B. Donoeva, J.Y. Ruzicka, H. Al Qahtani, H.H. Harris, B. Cowie, J.B. Aitken, V.B. Golovko, G.F. Metha, G.G. Andersson, Chemically

synthesised atomically precise gold clusters deposited and activated on titania. Part II, Phys Chem Chem Phys, 15 (2013) 14806-14813.

[11] S. Yamazoe, T. Yoskamtorn, S. Takano, S. Yadnum, J. Limtrakul, T. Tsukuda, Controlled Synthesis of Carbon-Supported Gold Clusters for Rational Catalyst Design, The Chemical Record, 16 (2016) 2338-2348.

[12] Contributors, in: T. Tsukuda, H. Häkkinen (Eds.) Frontiers of Nanoscience, Elsevier2015, pp. xi-xii.

[13] L.-X. Xu, C.-H. He, M.-Q. Zhu, K.-J. Wu, Y.-L. Lai, Silica-Supported Gold Catalyst Modified by Doping with Titania for Cyclohexane Oxidation, Catalysis Letters, 118 (2007) 248-253.

[14] P.P. Wu, P. Bai, Z.F. Yan, G.X.S. Zhao, Gold nanoparticles supported on mesoporous silica: origin of high activity and role of Au NPs in selective oxidation of cyclohexane, Sci Rep-Uk, 6 (2016).

[15] A.R. Almeida, J.A. Moulijn, G. Mul, In Situ ATR-FTIR Study on the Selective Photo-oxidation of Cyclohexane over Anatase TiO2, The Journal of Physical Chemistry C, 112 (2008) 1552-1561.

[16] A.R. Almeida, R. Berger, J.A. Moulijn, G. Mul, Photo-catalytic oxidation of cyclohexane over TiO2: a novel interpretation of temperature dependent performance, Physical Chemistry Chemical Physics, 13 (2011) 1345-1355.

[17] Tables of molecular vibrational frequencies. Consolidated volume II, Journal of Physical and Chemical Reference Data, 6 (1977) 993-1102.

[18] G. Socrates, Infrared and Raman Characteristic Group Frequencies: Tables and Charts, Wiley2004.

[19] A.N. Mansour, J.W. Cook, D.E. Sayers, Quantitative technique for the determination of the number of unoccupied d-electron states in a platinum catalyst using the L2,3 x-ray absorption edge spectra, The Journal of Physical Chemistry, 88 (1984) 2330-2334.

[20] A. Pantelouris, G. Kueper, J. Hormes, C. Feldmann, M. Jansen, Anionic Gold in Cs3AuO and Rb3AuO Established by X-ray Absorption Spectroscopy, Journal of the American Chemical Society, 117 (1995) 11749-11753.

[21] M.F. Lengke, B. Ravel, M.E. Fleet, G. Wanger, R.A. Gordon, G. Southam, Mechanisms of Gold Bioaccumulation by Filamentous Cyanobacteria from Gold(III)–Chloride Complex, Environmental Science & Technology, 40 (2006) 6304-6309.

[22] P. Zhang, T.K. Sham, Tuning the electronic behavior of Au nanoparticles with capping molecules, Appl Phys Lett, 81 (2002) 736-738.

[23] P. Zhang, T.K. Sham, X-Ray Studies of the Structure and Electronic Behavior of Alkanethiolate-Capped Gold Nanoparticles: The Interplay of Size and Surface Effects, Physical Review Letters, 90 (2003) 245502.

[24] J.A. van Bokhoven, J.T. Miller, d Electron Density and Reactivity of the d Band as a Function of Particle Size in Supported Gold Catalysts, The Journal of Physical Chemistry C, 111 (2007) 9245-9249.

[25] J.A. van Bokhoven, C. Louis, J.T. Miller, M. Tromp, O.V. Safonova, P. Glatzel, Activation of oxygen on gold/alumina catalysts: in situ high-energy-resolution fluorescence and time-resolved X-ray spectroscopy, Angewandte Chemie (International ed. in English), 45 (2006) 4651-4654.

Chapter 5

Palladium doping effect on the catalytic activity and stability of $Au_{25}(SR)_{18}$ nanocluster catalysts in oxidation reactions

1. Abstract

Heteroatom doping on the Au nanocluster structure lead to the possibility of fine tuning of their physical chemical properties. In the case of Pd doping, enhanced stability and reactivity have been observed. Pd doped $Au_{25}(SR)_{18}$ nanoclusters have been prepared and deposited on oxide materials (TiO_2 and SiO_2).

The catalytic activity of the bimetallic nanocluster catalysts has been studied in two different oxidation reactions, CO oxidation in gas phase and cyclohexane oxidation in liquid phase. Insights into structure-reactivity relationship has been investigated by *in situ* spectroscopic techniques (DRIFTS and XAFS).

$PdAu_{24}$ nanoclusters, with the Pd dopant atom located at the centre of the Au cluster core, were supported on titania and applied in catalytic CO oxidation, showing significantly higher activity than monometallic Au_{25} nanoclusters. After pretreatment, CO adsorbed on Pd was detected by in-situ DRIFTS spectroscopy during CO oxidation conditions, indicating a migration of the Pd dopant from the Au cluster core to the cluster surface. Increasing the number of Pd dopant atoms in the Au structure led to a preferential incorporation of Pd in the S-(M-S)n protecting staples of the cluster. A combination of oxidative and reductive thermal pretreatment resulted in the formation of isolated Pd surface sites within Au, as evidenced by in-situ XAFS and ex-situ XPS. Thus, the structural evolution of the bimetallic PdAu nanoclusters led to a Pd single-site catalyst with enhanced activity in CO oxidation.

In case of cyclohexane oxidation, an increase in the reactivity and selectivity is observed for the doped cluster, more relevant in case of SiO_2, and a significant aggregation is observed after reaction by XAFS.

2. Dynamics of Pd atoms inside Au nanoclusters under catalytic CO oxidation reaction conditions

2.1 Introduction

Heterogeneous Au nanoparticle catalysis has been increasingly studied in the last decades, owing to gold´s versatile catalytic activity, for example in oxidation,[1-3] hydrogenation[1-4] or C-C coupling reactions.[2, 4] To understand and control catalytic performance of nanoparticles at the molecular level remains a major challenge. Developing novel nanostructures with atomically controlled key structure parameters are required, such as the number of atoms (size), elemental composition and surface modification by functional groups. This can be achieved with monolayer protected gold nanoclusters ($Au_n(L)_m$), which have led to advances in nanoscience.[5] Heterogeneous catalytic research of atomically precise gold nanoclusters is an emerging field opening new opportunities for accurate studies of size-dependent properties, atomic structure effects and reaction mechanisms in catalysis.[3, 6-7]. Moreover, due to these properties combined with small particle sizes below 2 nm, nanoclusters exhibit high activity for several catalytic reactions.[7]

The physical-chemical properties of gold nanoclusters can be fine-tuned by heteroatom doping, which has a strong influence on their stability and catalysis.[8] Knowledge of the number of incorporated dopant atoms, their exact location in the cluster, as well as structure-property relationships are required for a thorough understanding. Depending on the nature of the dopant atom, different positions within the Au cluster have been identified, e.g. in the center (Pd, Pt, Cd), in the outer core shell (Ag, Cd) or in the protecting Au(I)-thiolate staple motifs (Cu, Hg) surrounding the core.[6, 9-12]

Previous studies of Ag_xAu_y nanoclusters revealed the dynamic nature of bimetallic nanocluster structures. Initially reported by Pradeep and coworkers, mobility of atoms between $Au_{25}(SR)_{18}$ and $Ag_{44}(SR)_{30}$ in solution was observed, forming $Au_{25-x}Ag_x(SR)_{18}$ species.[13] This initiated a series of studies on intercluster reactions.[13-23] Recently, Bürgi and coworkers reported

that metal exchange reactions could also be observed between Au nanoclusters and metal foils (Ag, Cd, Cu), leading to bimetallic nanoclusters.[24] Metal migration in Ag_2Au_{25} clusters was found to occur also intramolecularly, when exposed to a thiol solution.[25] Altogether, this demonstrated that, in solution, the structure of doped nanoclusters is not static, but evolves under different conditions.

In the case of Au_{25} clusters, heteroatom doping with Pd, Pt or Cd induced a drastic change of its redox properties[26-27] and increased its stability.[8, 26, 28-29] In addition, the reactivity in catalytic reactions was also altered,[6] and in several cases, doped M_1Au_{24} (M= Pd, Pt, Cd) clusters performed superior to their homogold analogues.[26, 28-32]

Pd-doped Au nanostructures have been applied in catalysis due to their favorable catalytic properties.[33-34] Their high activity was often ascribed to electronic effects, i.e. the Pd site(s) being slightly electron-deficient compared to the Au ones.[29, 31, 35-36] Pd dopant atoms are typically in center positions, but other locations have also been reported: Monopalladium doping into Au:PVP nanoclusters lead to preferential formation of $PdAu_{33}$ and $PdAu_{43}$ particles, with the Pd dopant on the particle surface, leading to a drastic increase in benzyl alcohol oxidation activity.[37] Scott and coworkers showed that multiple Pd doping can be achieved by mixing $Au_{25}(SR)_{18}$ clusters with a Pd(II) compound, leading to the replacement of Au atoms in the staples by Pd, in addition to the usual Pd center position.[38-40] After ligand removal treatment, isolated Pd atoms were obtained at the surface of the Au nanoparticles, which led to significantly enhanced allyl alcohol hydrogenation reactivity.[38] The presence of monomer (pair) Pd surface sites instead of larger ensembles was also found to increase the activity of Pd/Au(100) and Pd/Au(111) surfaces for acetoxylation of ethylene.[34]

CO oxidation is one of most extensively studied reactions, also in Au nanoparticle catalysis, reflected in recent reviews.[1-2] The exact reaction mechanism, especially with regard to O_2 activation, is still intensively debated. Among many support materials, reducible oxides such as TiO_2 have been found particularly suitable for CO oxidation.[1-2, 41-42] In contrast, for Au nanoclusters, CO oxidation has so far focused on CeO_2 as support material,[43-49] because $Au_{25}(SR)_{18}/TiO_2$ was found to be almost inactive.[44]

Furthermore, heteroatom doping of Au clusters for CO oxidation was so far limited to replacing multiple Au atoms by Cu or Ag. This was found to alter the CO oxidation activity, with $Cu_xAu_{25-x}(SR)_{18}/CeO_2$ performing slightly better, but $Ag_xAu_{25-x}(SR)_{18}/CeO_2$ worse than $Au_{25}(SR)_{18}/CeO_2$. This was attributed to the different CO adsorption energies on the metal surfaces.[49] Similar effects had already been reported for CO oxidation on bimetallic AuPd(100) surfaces, with their low temperature efficiency ascribed to a decrease in CO adsorption energy (and thus weaker CO poisoning).[50]

Multiple studies have also indicated that for heterogeneous nanocluster catalysis, the (partial) removal of the thiolate protecting groups is necessary.[36, 38, 46, 51-53] Several strategies are known to expose the active metal surfaces of the clusters,[52, 54] among which thermal pretreatments[36, 38, 46, 48, 51, 55] are probably most often applied. For CO oxidation on CeO_2 supported Au_{38} nanoclusters, Jin and coworkers reported that the reaction can only take place if the ligands at the cluster-support border were removed by O_2 pretreatments.[46] $Au_{38}(SR)_{24}/CeO_2$ catalysts were found to be most active for CO oxidation after an oxidative pretreatment at 250 °C, which resulted in exposing the bare Au metal surface. The same procedure at 150 °C only led to a collapse of the clusters' staple structure, with S still poisoning the Au core.[55] A combination of O_2 and a reductive pretreatment (with CO or H_2) at 80 °C led to the best results for $Au_{144}(SR)_{60}/CeO_2$ catalysts in CO oxidation.[48] An oxidative pretreatment in air followed by reducing in H_2 atmosphere (both at 250°C) also led to the best results in activating AuPd particles by formation of segregated Pd sites by Scott an coworkers.[38] The benefit of a reductive pretreatment step before CO oxidation was also observed for $PdAu/TiO_2$ nanoparticle systems.[56]

Kurashige *et al.*[29] recently investigated water splitting with $Au_{24}M$-$BaLa_4Ti_4O_{15}$ (M = Pd, Pt) catalysts. Both Pd and Pt heteroatom doping were found to strongly influence the catalytic activity. The exact location of the dopant atom played a critical role. As revealed by Extended X-ray Absorption Fine Structure (EXAFS) measurements at the Pd K-edge and Pt L_3-edge, the heteroatom dopants migrated upon ligand removal at 300 °C, finally occupying a position at the Au cluster/support interface (Pt) or a Au cluster surface position (Pd). In the case of Pd, Pd-S interaction was still observed after pretreatment, but disappeared during the water splitting reaction, indicating the presence of exposed Pd metal. Luneau *et al.* observed a redistribution of

Pd in silica supported $Pd_{0.04}Au_{0.96}$ from internal to surface sites, stabilized by formation of Pd-O interactions. Exposure to H_2 atmospheres at elevated temperatures led to reoccupation of subsurface positions.[57] Pd surface segregation was also found in several PdAu nanoparticle systems when exposed to CO atmospheres.[50, 58-60] Accordingly, to be able to correlate and understand the catalytic behavior of bimetal nanocluster systems, studies of their structural evolution during pretreatment and reaction are of tremendous importance.

Therefore, within this study, we have employed titania supported Pd-doped Au nanoclusters to investigate structural changes upon pretreatment and reaction. The influence of pretreatment was studied for $PdAu_{24}/TiO_2$, and its CO oxidation activity compared to that of Au_{25}/TiO_2. The bimetallic cluster was found to strongly increase the CO conversion, which seems to be related to Pd atom migration from the cluster center to the outer surface. In order to test this hypothesis, we have also prepared multiply-doped Pd_xAu_y clusters (Pd/Au: 0.25) and conducted *in-situ* diffuse reflectance infrared Fourier transform spectroscopy (DRIFTS), as well as EXAFS (Pd-K and Au-L_3 edges) and X-ray photoelectron spectroscopy (XPS) after pretreatment and reaction. The observation of Pd-S interactions clearly indicated that Pd atoms were initially located in the staples, but then migrated to the cluster surface, forming a PdAu alloy exhibiting isolated Pd sites. Altogether, these studies should aid an improved understanding of the specific catalytic activity of Pd-doped Au nanoclusters.
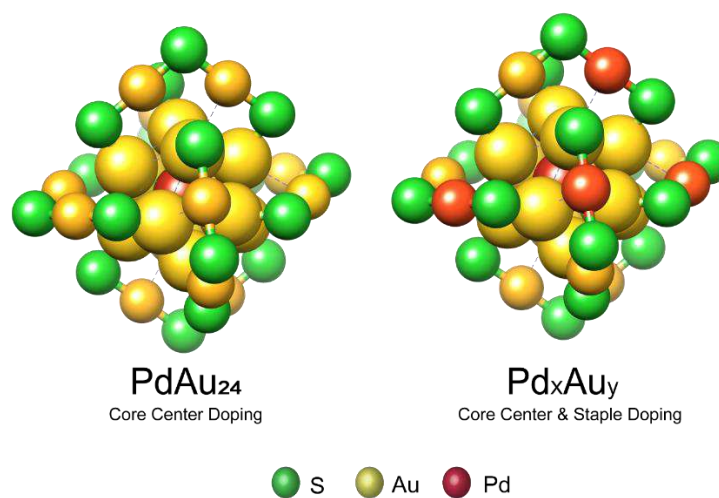
Figure 5-44 *Illustration of the structure of $PdAu_{24}$ and Pd_xAu_y (for an example of Pd_5Au_{20}) with the different possible locations of the Pd doping atom(s) $PdAu_{24}$ features only core center doping, whereas both doping at the core center and in the staples is possible for Pd_xAu_y. The hydrocarbon backbone of the ligands is not shown.*

2.2   Results and Discussion

2.2.1 Pretreatment effect on PdAu$_{24}$/TiO$_2$ nanocluster catalysts

As discussed in the introduction, optimal activation of a catalyst is crucial to achieve high reactivity. Our and other groups´ previous studies have indicated that the local removal of the thiolate ligands from Au is best achieved by oxidative pretreatment at 250 °C, exposing clean Au clusters surfaces.[51, 55, 66] However, for bimetallic PdAu catalysts, due to the easier oxidation of Pd, an additional reductive step is required to create Pd^0 active sites.[56] To find optimal catalyst activation conditions, four different thermal pretreatments were tested for the PdAu$_{24}$(SR)$_{18}$ (SR = 2-PET) clusters supported on titanium dioxide, differing in the gas types and sequence (pretAr, pretO$_2$, pretH$_2$, pretO$_2$-H$_2$), before carrying out CO oxidation.

As evident from Figure 5-45, the type of pretreatment plays a significate role. Thermal pretreatment in argon was not able to remove the thiol ligands which then blocked the active sites even at 250 °C reaction temperature. Pure oxidation or reduction improved activity at 250 °C, but the maximum and lower temperature activity was obtained by a combination of oxidation and reduction (pretO$_2$-H$_2$). Oxidation allows for removal of ligands[44, 67] and surface impurities (synthesis residues), while the subsequent H$_2$ treatment reduces oxidized Pd (and Au) atoms.[56] Activity set in at 225 °C, which agrees with CO oxidation on (impregnated) Pd/Al$_2$O$_3$ catalysts (below 225 °C, the actives sites are poisoned by CO).[68-69] Figure 5-45a also shows the effect of longer heating times (e.g. pretO$_2$ vs. pretO$_2$-Ar).
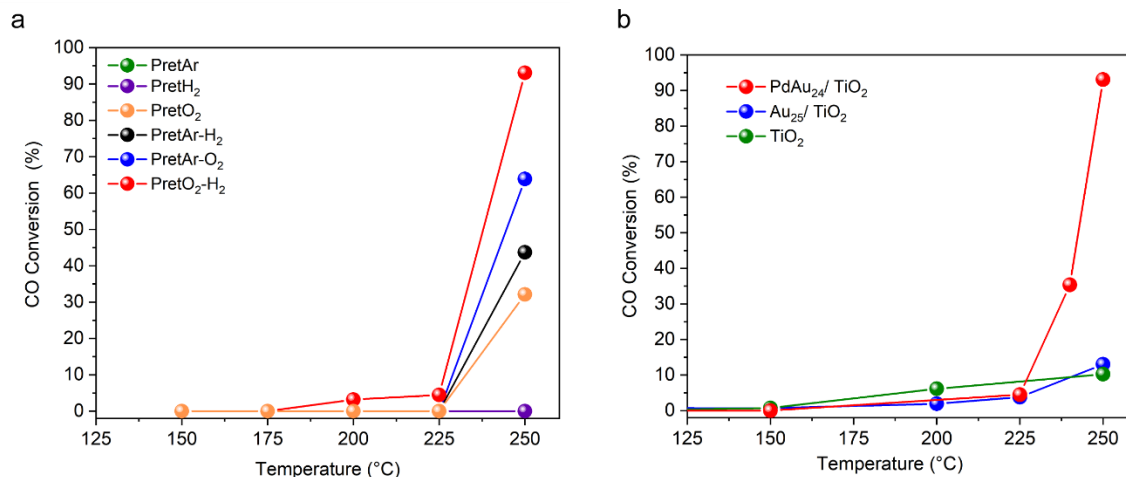
Figure 5-45 (a) Effect of pretreatment on the catalytic CO oxidation activity of PdAu$_{24}$/TiO$_2$. (b) Catalytic CO oxidation activity of PdAu$_{24}$/TiO$_2$, Au$_{25}$/TiO$_2$ and the pure support (all after pretO$_2$-H$_2$).

2.2.2 Comparison of PdAu$_{24}$/TiO$_2$ to Au$_{25}$/TiO$_2$ and TiO$_2$

To evaluate the effect of Pd doping on the nanoclusters' reactivity, PdAu$_{24}$/TiO$_2$ was contrasted to undoped Au$_{25}$/TiO$_2$ and the pure titania support, with pretO$_2$-H$_2$ applied to all samples. As evident from Figure 5-45b the catalytic activity was very low below 200 °C, both for PdAu$_{24}$/TiO$_2$ and Au$_{25}$/TiO$_2$. For the palladium doped catalyst, the onset of activity was at 225 °C, reaching more than 90% conversion at 250 °C. Only around 10% conversion was detected for Au$_{25}$/TiO$_2$ at 250 °C, slightly higher than that of the bare TiO$_2$ support. As oxidation at 250 °C should remove the ligands from Au, the inactivity of Au$_{25}$/TiO$_2$ can likely be attributed to continued S-poisoning of the support. PretO$_2$ works well for Au$_{25}$/CeO$_2$[44] or Au$_{38}$/CeO$_2$,[55] but it is insufficient for Au$_{25}$/TiO$_2$, which was also reported before. Inactivity of ligands-on Au$_{25}$/TiO$_2$ catalysts in CO oxidation has also been reported before.[44] Nevertheless, the strong effect of adding only *one* single Pd dopant atom to a Au nanocluster is evident.

2.2.3 In-situ DRIFTS of CO oxidation on PdAu$_{24}$/TiO$_2$

To further examine the effect of doping, *operando* DRIFTS during CO oxidation was performed on PdAu$_{24}$/TiO$_2$ after a one step pretreatment with oxygen (pretO$_2$) and after a pretreatment with both an oxidative and a reductive step (pretO$_2$-H$_2$), representing a catalyst with a relatively low *vs.* the maximum level of activity obtained in the catalytic tests (Figure 5-45a). Figure 5-46 shows temperature-dependent (stepwise heating) infrared spectra of PdAu$_{24}$/TiO$_2$ after pretO$_2$-H$_2$ (a) and after pretO$_2$ (b).
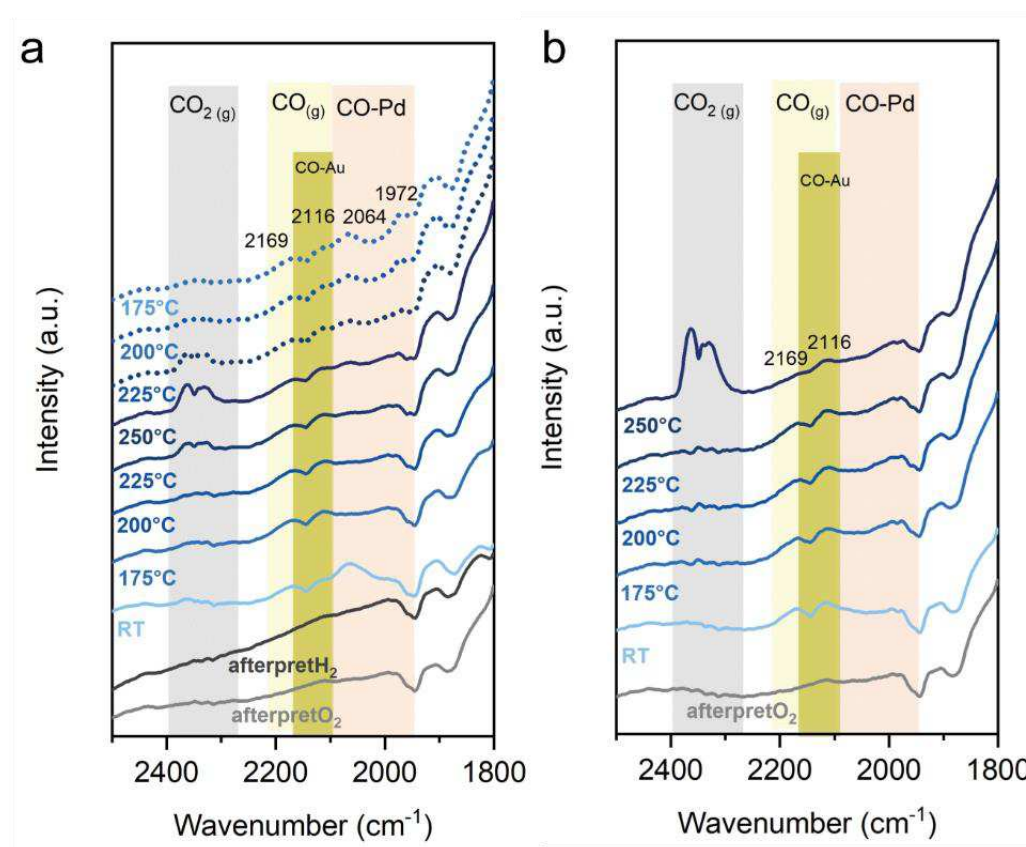
Figure 5-46 In-situ DRIFTS spectra of TiO$_2$ supported catalysts during CO oxidation: (a) PdAu$_{24}$/TiO$_2$ after pretO$_2$-H$_2$ and (b) PdAu$_{24}$/TiO$_2$ after pretO$_2$. Spectra taken upon cooling are indicated by dotted lines. Operando DRIFTS spectra of PdAu$_{24}$/TiO$_2$ catalysts during CO oxidation: (a) after pretO$_2$-H$_2$ and (b) after pretO$_2$. Spectra taken upon cooling are indicated by dotted lines. Spectra of the reference operando DRIFTS measurements of TiO$_2$ can be found in the Appendix. Note that absolute intensities of different samples cannot be compared.

Focusing first on catalytic activity, indicated by the CO$_2$ gas phase bands (2400–2300 cm^{-1}), for PdAu$_{24}$/TiO$_2$ (pretO$_2$-H$_2$) catalytic activity set in above 200 °C (Figure 5-46a). The

PdAu$_{24}$/TiO$_2$ catalyst after pure oxygen pretreatment became active at 250 °C (cf. the CO$_2$ bands in Figure 5-46 b). The activity trends indicated by the CO$_2$ gas phase bands were corroborated by mass spectroscopic (MS) analysis of the DRIFTS cell exhaust gas (Figure in Appendix), both being in line with the GC measurements in Figure 5-45b.

Turning to adsorbed species, there were significant differences between pretO$_2$-H$_2$ and pretO$_2$. After pretO$_2$-H$_2$, PdAu$_{24}$/TiO$_2$ showed a band at 2067 cm^{-1}, clearly indicating CO adsorbed on Pd. No CO adsorption on the TiO$_2$ support could be detected (see Figure 5-61 in Appendix).

Based on previous studies of Pd[75] and PdAu alloy[59] nanoparticles, 2067 cm^{-1} points to atop CO on *isolated* Pd atoms. After synthesis (and before pretreatment), the Pd dopant atom is located in the center of the Au nanocluster core (Figure 5-46 a).[9, 12] This would indicate that the Pd atom should not be accessible to CO bonding. This seems to hold true for the pretO$_2$ sample (Figure 5-46 b), for which no Pd-related bands could be detected.

Therefore, the CO-Pd band in Figure 5-46a indicates that pretO$_2$-H$_2$ induces migration of the Pd atom from the cluster center position to the surface of the Au core. Mobility of metal atoms within a nanocluster structure[13-23, 29] and Pd segregation of to the surface of alloy PdAu particles were indeed reported before.[57-59, 76] The band around 1962 cm^{-1} at 250 °C became more pronounced after cooling (dotted traces in Figure 5-46a) and was assigned to bridging CO on Pd-Au alloy sites, based on experimental and theoretical studies.[58, 68, 77-78] Zhu *et al*. corroborated DFT calculations by several groups by experimental DRIFTS measurements, assigning the bands between 1950 and 1969 cm^{-1} to bridged CO on PdAu sites.[58, 77, 79]

The formation of PdAu observed by *operando* DRIFTS is also consistent with the higher activity of PdAu$_{24}$/TiO$_2$ below 250 °C, when CO oxidation is continued. Not only pretO$_2$-H$_2$, but also the reaction conditions led to further activation of the PdAu$_{24}$(SR)$_{18}$/TiO$_2$ catalyst. This is in agreement with the observations by Luneau *et al*., who reported changes in the palladium surface content of PdAu nanomaterials, induced by two consecutive treatments (O$_2$ and H$_2$) or under CO exposure.[57] Upon H$_2$ treatment, Pd moved subsurface but migrated back to the Au surface in the presence of CO.

The region of the CO gas phase bands overlaps with possible bands associated to CO-Au vibrations. Slight shifts to higher wavenumbers were observed, from 2169 and 2115 cm^{-1} (gas phase CO, see Figure 5-62 in Appendix) to 2175 and 2120 cm^{-1}, that may be related to the contribution of CO-Au bands. Therefore, CO dosing experiments were performed with the samples after different pretreatments (Figure 5-62), detecting low intensity CO-Au bands around 2108 and 2118 cm^{-1}. For PdAu$_{24}$/TiO$_2$ after pretO$_2$-H$_2$, an intense CO-Pd band at 2046 cm^{-1} was detected, confirming the observations of the *operando* DRIFTS measurements. No additional bands in the region around 1900cm^{-1} appeared, neither in the CO-dosing experiments (Figure 5-62b-c), which rules out the presence of bridge/hollow CO-Pd vibrations, characteristic of larger Pd ensembles.

2.2.4 Structural evolution of Pd$_x$Au$_y$/TiO$_2$ catalysts

In the following, catalysts with more than one Pd dopant atom per cluster were prepared in order to investigate how the structure of supported bimetallic PdAu nanoclusters evolved during CO oxidation. Clusters with Pd:Au ratios of about 1:4 or 1:3 were prepared, as determined
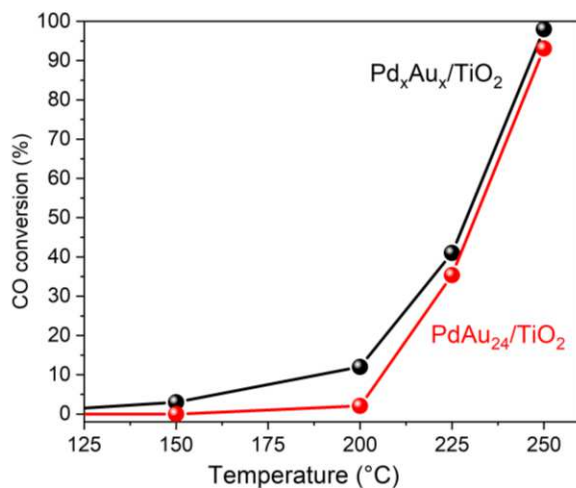
Figure 5-47 *Comparison of the catalytic activity of PdAu$_{24}$/TiO$_2$ and Pd$_x$Au$_y$/TiO$_2$ (x=~6; y=~30) catalysts (both pretO$_2$-H$_2$).*

by TXRF and XPS (see Appendix), supported and pretreated (pretO$_2$-H$_2$). According to STEM, the particle size of Pd$_x$Au$_y$ on TiO$_2$ was around 1.3 nm, indicating that the clusters contained ~25-30 metals atoms. Changes in size were noted after pretreatment, with particle sizes of around 2.7 nm observed by HAADF-STEM (Figure 5-59). The catalytic activity of Pd$_x$Au$_y$/TiO$_2$ is compared to that of mono-palladium PdAu$_{24}$/TiO$_2$ in Figure 5-46 (both after pretO$_2$-H$_2$). The higher number of (~6) Pd dopant atoms resulted in a small increase of catalytic activity.

2.2.5 In-situ DRIFTS of CO oxidation on Pd$_x$Au$_y$/TiO$_2$

The higher catalytic activity obtained by multiple Pd doping was confirmed by *in-situ* DRIFTS via stronger CO$_2$ bands at respective temperatures (Figure 5-48a). The CO gas phase bands at 2168 and 2122 cm^{-1} are overlapping potential CO-Au bands (≈2130 cm^{-1}), however, there existence is confirmed by post reaction CO dosing experiments (Figure 5-48c). The region related to CO-Pd vibrations displayed a strong component at 2060 and a shoulder at 2075 cm^{-1}, due to different on-top CO species on Pd atoms, with the vibrational frequency depending on the coordination numbers of Pd in the Au$_x$Pd$_y$ alloy clusters.[131, 142]

Under reaction conditions, the on-top and bridge CO on Pd (2076 cm^{-1}) became even more pronounced. This points to rearrangements, resulting from Pd and Au mobility, and possible formation of Pd dimers and larger ensembles. The latter are known to be effectively dissociate O$_2$.[142]
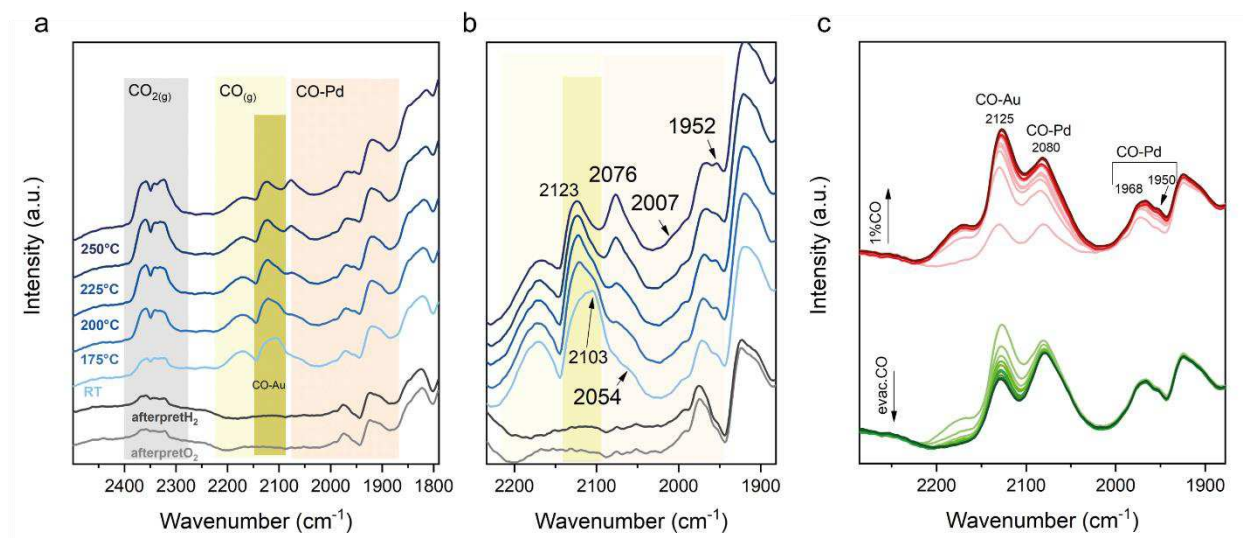
Figure 5-48(a-b) In-situ DRIFTS spectra during CO oxidation on Pd_xAu_y/TiO_2 (pretO$_2$-H$_2$). (c) Post-reaction DRIFTS spectra upon 1% CO dosing and evacuation.

Figure 5-48 b shows the post-reaction characterization of Pd_xAu_y/TiO_2 (pretO$_2$-H$_2$) after cool down and purging with He. Upon CO dosing, the same bands as observed under reaction conditions appeared, slightly shifted due to the different gas atmosphere. CO-Au and CO-Pd vibrations can be identified at 2125 cm^{-1} and 2080 cm^{-1}, respectively. The bands at 1968 cm^{-1} and 1950 cm^{-1} confirm Pd segregation and formation of dimer and larger sites.[126, 131, 132] However, other studies reported that these bands originated from PdAu alloy sites instead [143]. This seems to apply to our Pd_xAu_y/TiO_2 also, as EXAFS measurements (discussed below) detected no significant contribution of Pd-Pd bonds. After pretreatment and CO oxidation, Pd is therefore expected to be located on the surface of the Au cluster in the form of isolated and/or neighboring Pd atoms/sites.

2.2.6 Ex-situ XPS

The composition and oxidation state of Pd and Au in the Pd_xAu_y nanoclusters were investigated by *ex-situ* XPS.
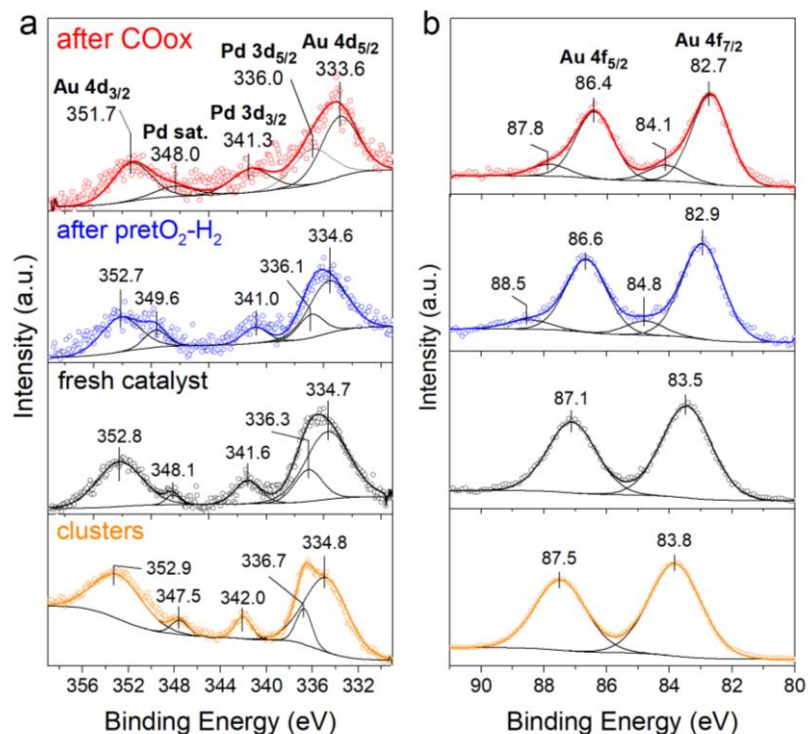
Figure 5-49 Ex-situ *XPS spectra of the Pd$_x$Au$_y$ catalyst: (a) Pd 3d and Au 4d region, (b) Au 4f region: clusters supported on HOPG (clusters), clusters supported on TiO$_2$ (fresh catalyst), the latter after pretreatment (after pretO$_2$-H$_2$) and after reaction (after COox).*

For the Pd$_x$Au$_y$ bimetallics the Pd 3d and Au 4d region is most informative (Figure 5-49a). When the as-prepared (untreated) clusters were deposited on HOPG, the Pd 3d binding energies suggested oxidized Pd species. This is in accordance with the expected location of the Pd dopants in the staples of the clusters (as only one Pd atom can be at the core center). Upon supporting, a small (~0.4 eV) shift was observed. In the Au 4f region (Figure5-49b), changing from a HOPG to TiO$_2$ support, the peaks also shifted, leading to BEs typical of ligand-protected nanoclusters (Au^0 in the core and Au$^+$ in the staples).[51]

After pretreatment (pretO$_2$-H$_2$), the Pd 3d signal was shifted to even lower binding energy (336.1 eV), indicative of metallic Pd in PdAu alloy.[60, 80-81] Small shifts to more negative binding energies were also found for the Au 4d signal. The Au 4f spectra corroborated these compositional changes and confirmed PdAu alloy formation. After reaction, Pd seemed oxidized (337.2 eV). Overall, the XPS measurements agreed with the *operando* DRIFTS spectra (Figure 5-48a-b), indicating surface Pd species and PdAu alloy formation.[60, 80-82]

2.2.7 In-situ EXAFS

The structural evolution of the TiO_2 supported bimetallic Pd_xAu_y nanoclusters was studied by *in-situ* XAFS at the Pd K-edge and the Au L_3-edge. Figure 5-50 and Table 5-3 show results of the Pd K-edge EXAFS fitting for each step. Supporting the Pd_xAu_y clusters on TiO_2 by impregnation does not lead to significant changes, confirming the stability of the cluster structure. Pd K-edge EXAFS of the as-prepared sample showed a strong peak at 2.33 Å, followed by low intensity peak at 2.81 Å, related to Pd-S and Pd-Au bonds, respectively. Together with the coordination numbers (CNs) obtained (2.2 and 0.9, respectively), this indicates a preference for Pd atoms in the staples, in agreement with previous reports.[59, 116, 149] The absence of Pd-Pd bonds indicates isolated Pd atoms in the clusters and apparently a lower percentage of Pd than Au, based on TXRF, XPS and previous studies on PdAu nanoparticles.[115, 129, 132, 146] This is also confirmed by the fitting results at Au L_3-edge, where no Au-Pd bonds were detected in the fresh sample.

After $pretO_2$-H_2, most Pd-S and Au-S bonds disappeared, denoting the removal of S from the cluster. However, some remaining Pd-S presence could be related to the staples collapsing on the cluster core surface, already observed in previous works.[128, 134] Simultaneously, Pd-Au bonds were established, denoting PdAu alloy formation. The alloying process initiated by the migration of Pd from the staples to the Au core surface (maybe in the staple-collapse step) continues under CO oxidation reaction conditions. No evidence for Pd-Pd bond formation was detected (also corroborated by EXAFS simulations; see Supporting Information). Therefore, results indicate isolated Pd single atom surface sites in PdAu nanoalloys.[110, 117, 146] The fitting results at Au L_3-edge over the CO oxidation reaction denoted a higher CN number of Au-Au in comparison to Au-Pd, corroborating the good dispersion of the Pd atoms across the nanocluster surface.[132]

The particle size of the Au_xPd_y particles after pretreatment and reaction was then extracted based on the CN numbers of the Au L_3-edge EXAFS, considering the Au-Au and Au-Pd CNs from the first shell, related to the number of next neighbor atoms. For bulk fcc gold, the Au-Au CN = 12, but it is significantly lower for nanoclusters (CN ~3-9).[116, 150, 151] The coordination numbers of the

first shell (Au-Au and Au-Pd) varied from around 8 to 9 for Pd_xAu_y/TiO_2 during pretreatment and reaction, denoting an increase in particle size. Based on previous studies, Pd_xAu_y clusters after reaction may consist of 40-80 atoms (depending on the structure/shape) with a particle size of ~2nm.[113, 115, 116, 148, 150, 151] A mean particle size of around 2.7 nm was observed by HAADF-STEM for the $pretO_2$-H_2 and after CO oxidation (see Appendix).
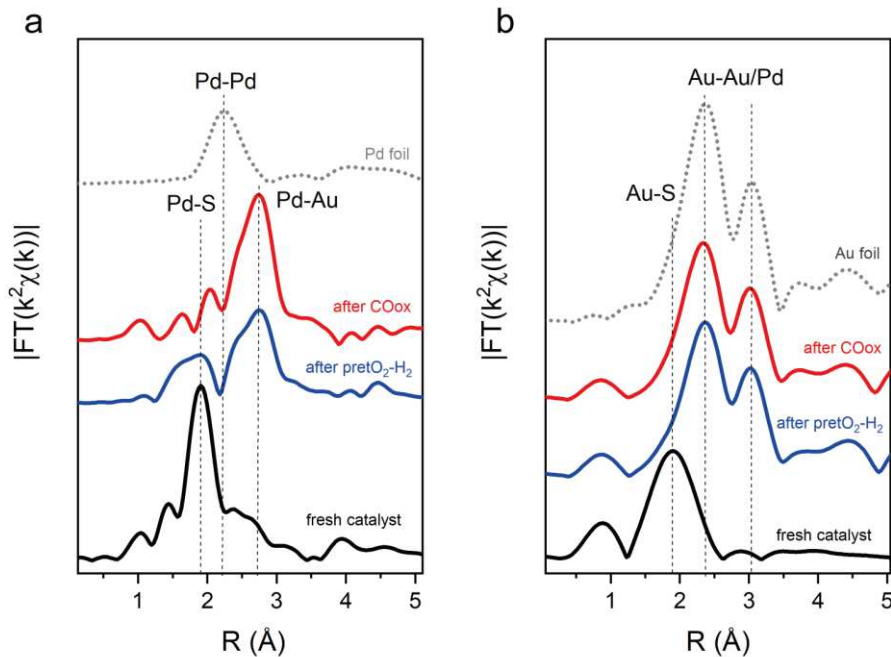
Figure 5-50 *EXAFS fitting of the k-space and R-space of in-situ spectra of the Pd_xAu_y/TiO_2 catalyst: (a) Pd K-edge, (b) Au L_3-edge. The structural evolution of the cluster structure from the fresh sample to after pretreatment and after CO oxidation reaction is depicted. Pd and Au foil are shown as references.*

Table 5-3 *EXAFS fitting results for the Pd_xAu_y/TiO_2 catalyst*

	Pd K-edge				Au L$_3$-edge					
	Pd-S		Pd-Au		Au-S		Au-Au		Au-Pd	
	CN	R (Å)	CN	R (Å)	CN	R (Å)	CN	R (Å)	CN	R (Å)
Fresh	2.3 (3)	2.33 (1)	0.9 (5)	2.81 (3)	2.1(4)	2.31 (1)	0.6 (1)	2.74 (6)	-	-
pretO$_2$-H$_2$	0.9 (3)	2.30 (2)	4.1 (6)	2.82 (1)	0.2(3)	2.31 (1)	8.5 (7)	2.84 (1)	0.6 (5)	2.80 (1)
After COox	0.2 (1)	2.30 (3)	6.2 (6)	2.80 (2)	-	-	8.7 (8)	2.83 (1)	0.9 (5)	2.80 (1)

Uncertainties in the last significant digits are given in parentheses. Detailed EXAFS analysis are in the Appendix. (CN: coordination number; R: distance).
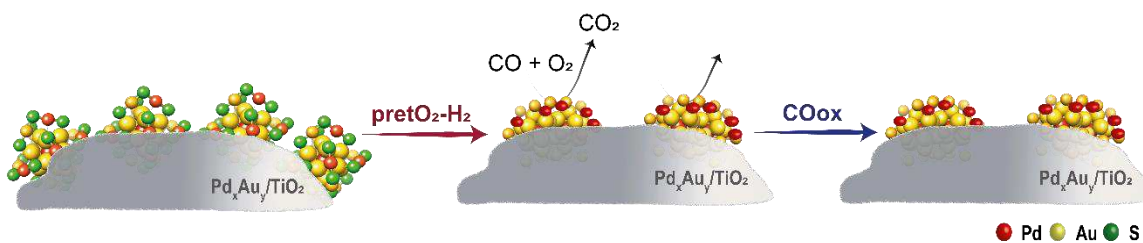
Scheme 5-1 *Illustration of the structure evolution of Pd_xAu_y supported on TiO_2 after pretreatment and CO oxidation.*

2.3   Conclusions

In summary, this work demonstrates the dynamic structure of Pd-doped Au_{25} nanoclusters upon pretreatment and catalytic reaction. When one Pd atom was doped into the center of a Au_{25} cluster, a combination of oxidative and reductive pretreatment was required to obtain maximum CO oxidation activity. This was related to the migration of the Pd atom to the surface of the cluster core. A CO-Pd vibrational band, characteristic of single site bonding, was observed by *operando* DRIFTS. Therefore, the activity enhancement of the doped system is related to a single Pd atom located on the Au cluster surface. In the case of multiply-Pd-doped Au nanoclusters, the Pd atoms were initially mainly located in the staples. Upon pretreatment, migration of Pd to the core surface was evidenced primarily by XAFS, forming a PdAu alloy. A distribution of isolated Pd single sites on the cluster surface was observed, with XAFS ruling out Pd-Pd bond, further supported by DRIFTS.

Thus, the evolution of the Pd-doped clusters to PdAu nanoalloys with single atom Pd surface sites was observed by XAFS, DRIFTS and XPS analysis. Overall, this study contributes to a better understanding of the dynamics of supported doped nanoclusters upon pretreatment and reaction, which is a key information for future design and application of bimetallic nanocluster catalysts.

3. Pd doping effect on the reactivity and stability of PdAu$_{24}$ nanoclusters in the cyclohexane oxidation reaction

3.1 Introduction

It has been observed that the exchange of one or more atoms of gold by other metal atoms induces changes in the stability and in the catalytic activity in liquid phase alcohol oxidation reactions[152]. For example, Pt$_1$Au$_{24}$(SR)$_{18}$/TiO$_2$ catalyst has a higher catalytic activity for styrene oxidation than Au$_{25}$(SR)$_{18}$/TiO$_2$, according to Qian et al.[105]. Deng et al.[103] also observed that Cd$_1$Au$_{24}$(SR)$_{18}$ nanocluster exhibited much higher activity than homogold Au$_{25}$ nanocluster in aerobic benzyl alcohol oxidation. A similar enhancement in catalytic activity was also seen in the case of Pd doping, as Xie et al. reported for Pd$_1$Au$_{24}$ clusters on multiwalled carbon nanotubes in benzyl alcohol oxidation [108]. In all cases, synergic effects are attributed to the differences in catalytic activity. The necessary next step is to study how doping with palladium can influence the catalytic activity, selectivity and the stability for cyclohexane oxidation.

3.2 Results and discussion

Pd$_1$Au$_{24}$(SR)$_{18}$ supported on TiO$_2$ and SiO$_2$ catalysts prepared and characterized following the same procedure as described above (3.1.) However, in this case, single step pretreatment at 150°C under air was applied, as in Chapter 4 [153]. DRS allows to discard a possible aggregation during the thermal pretreatment for this type of clusters. In Figure 5-51, the cluster characteristic bands can be observed confirming the cluster's presence without decomposition and a possible aggregation is discarded once more, as there is no plasmonic band around 550 nm.
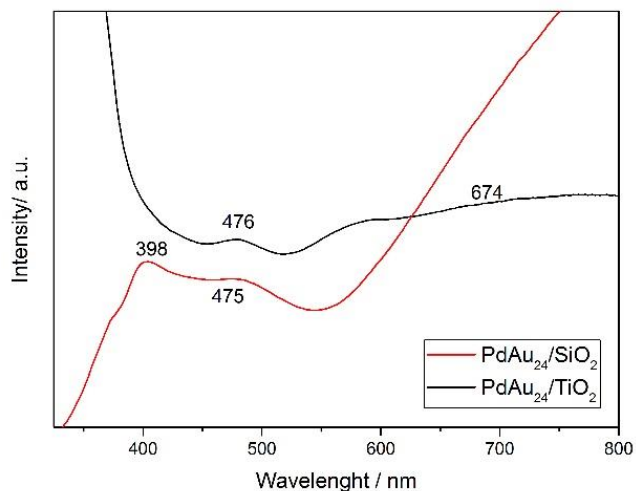
Figure 5-51 Diffuse reflectance spectroscopy of PdAu$_{24}$(SR)$_{18}$ supported on TiO$_2$ and SiO$_2$ after 150° pretreatment in air.

In order to compare the catalytic performance with the un-doped cluster catalysts (Au$_{25}$/MO$_x$) in the cyclohexane oxidation reaction, same conditions as in Chapter 4 were followed. In Figure 5-52 is shown the catalytic activity and selectivity with both set of samples, from pure support, to the Au$_{25}$ and Pd doped Au$_{25}$ catalysts. A slight increase on the cyclohexane conversion is obtained in both cases with the doped catalysts. In the case of TiO$_2$ catalysts, not relevant differences are obtained. The same trend is observed in the selectivity with a minimum increase in cyclohexanol production. Regarding SiO$_2$ catalysts, rather higher difference in conversion is achieved, from, from 6 % (Au$_{25}$/SiO$_2$) to 8 % (PdAu$_{24}$/SiO$_2$). Concerning selectivity an increased in KA (ketone and alcohol) production is observed with the doped sample (from 23% to 37%).
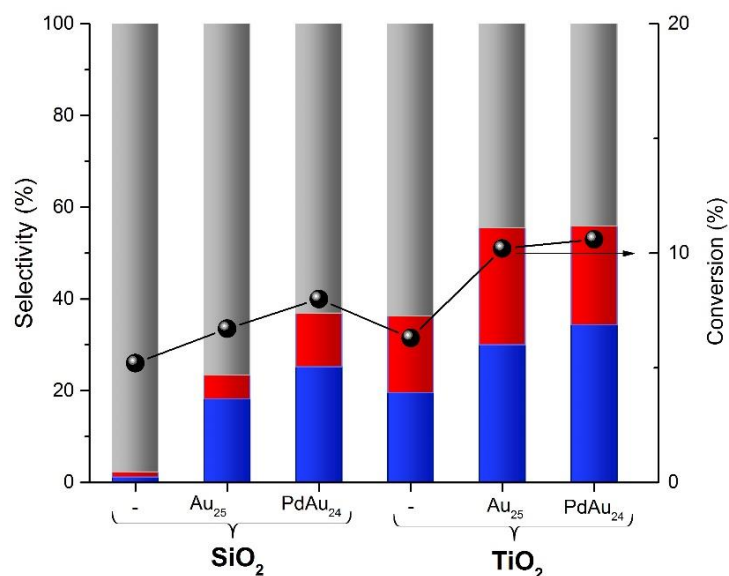
Figure 5-52 *Catalytic activity and selectivity of doped and undoped $Au_{25}(SR)_{18}$ supported on TiO_2 and SiO_2 after 10 hours reaction (blue for cyclohexanol, red for cyclohexanone, grey for byproducts)*

A structure stability study of the supported clusters after pretreatment and reaction was performed by XAFS measurments at Pd K-edge and Au L_3-edge. XANES spectra at Pd K-edge obtained from the sample at different stages are displayed in Figure 5-53 and 5-54.

In both cases, broader and shifted bands in comparison with the foil are observed. It is related to the presence of Pd-S bonds, in agreement with the expected location of the doped Pd atoms at the staple of the Au_{25} cluster. After pretreatment and reaction, not relevant changes are observed, denoting the absence of significant changes in respect of Pd-S bonds configuration. In the case of Au L_3-edge XANES (Figure 5-54) pronounced differences are noticed, that could be related to an increase in particle size and agglomeration. Following the same trend shown in Chapter 4, the spectra of the cluster supported on TiO_2 after pretreatment and after reaction is more similar to foil. It could be related to the complete loss of the cluster structure and the evolution to fcc.
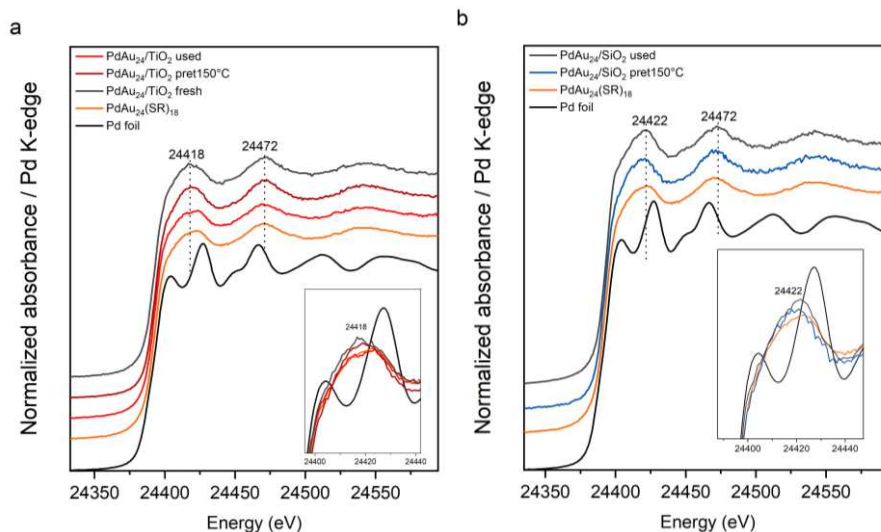
Figure 5-53 *Pd K-edge XANES spectra of the PdAu$_{24}$ samples, from pure clusters, to the supported catalysts (fresh), followed by the pretreated (pret150°C) and after the cyclohexane oxidation reaction (used), supported on TiO$_2$ (a) and SiO$_2$ (b).*
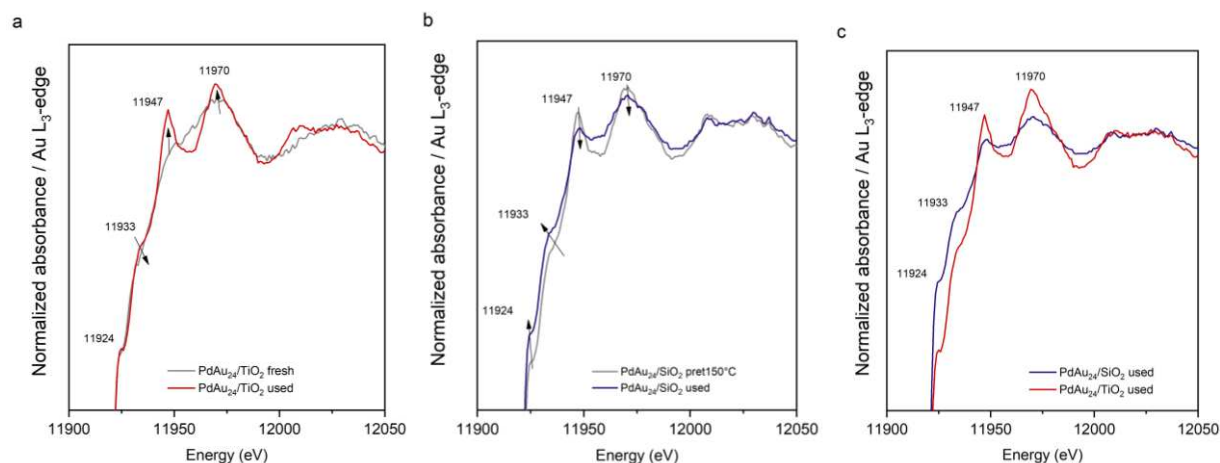
Figure 5-54 *Au L$_3$-edge XANES spectra of the PdAu24 catalysts before (pret150°C) and after the cyclohexane oxidation reaction (used), supported on TiO$_2$ (a) and SiO$_2$ (b). (c) shows the comparison of both used catalysts after the reaction*

The EXAFS fitting analysis results at Pd K-edge is shown in Figure 5-55 and in Table 5-3. Contrary to the results obtained in previous section 3.1., only one step pretreatment is not removing the Pd-S bonds, denoted by the CN values. Therefore, no migration of the Pd atoms to the Au cluster surface take place at low temperature pretreatment. Slight decrease in the CN of Pd-S is obtained just after reaction. Apparently, major part of the Pd-S bonds remain over all the stages, due to the absence of Pd-Pd or a pronounced increase of Pd-Au bonds. Contrary, major part of the Au-S bonds are removed after pretreatment and reaction, shown in the Figure 5-55.

Parallel, the peaks related to the Au-Au bonds increased, denoting the growing of the particle size.
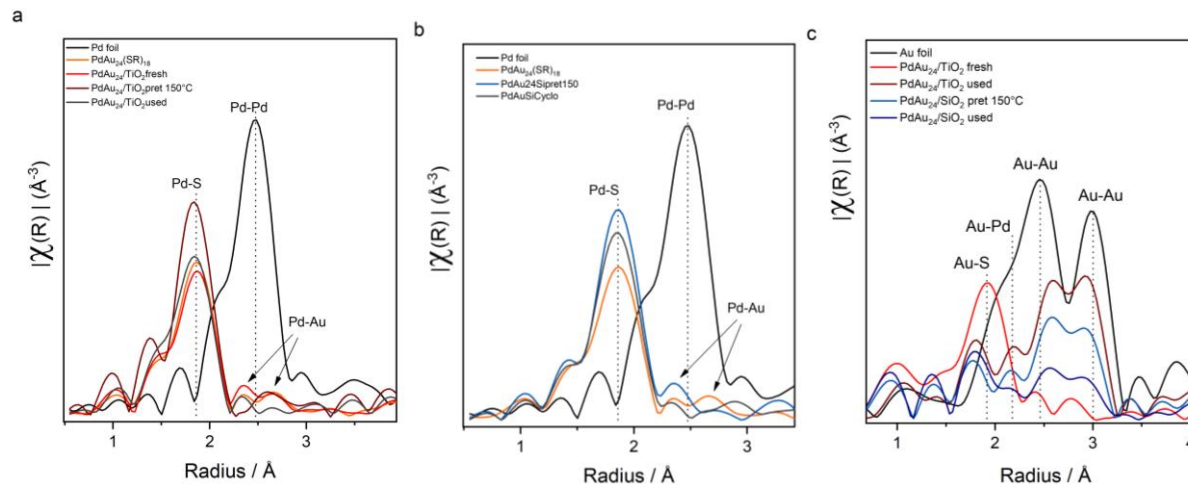
Figure 5-55 *R space of the Pd K-edge (a,b) and Au L3-edge (c) of the PdAu$_{24}$ catalysts*

Table 5-3 *EXAFS fitting results for the palladium doped clusters supported in TiO$_2$ and SiO$_2$*

		Pd K-edge			
		Pd-S		Pd-Au	
	Sample	CN	R (Å)	CN	R (Å)
TiO$_2$ catalysts	pret150°C	3.42 ± 0.4	2.32 ± 0.01	0.02 ± 0.43	-
	used	2.72 ± 0.2	2.31 ± 0.05	0.44 ± 0.7	2.83 ± 0.05
SiO$_2$ catalysts	pret150°C	3.43 ± 0.36	2.33 ± 0.02	-	-
	used	2.92 ± 0.5	2.30 ± 0.03	1.00 ± 0.6	2.81 ± 0.01

3.3 Conclusions

The catalytic activity of palladium-doped clusters supported on TiO_2 and SiO_2 has been investigated for CO oxidation and cyclohexane oxidation. In case of CO oxidation, silica supported clusters have been shown to be inactive. The catalytic activity and selectivity is enhanced in case of SiO_2 catalysts while only a slight increase is observed for TiO_2 supported catalysts. The active role of the TiO_2 in this reaction could hide the role of palladium. Furthermore, XAFS studies disclosed lower stability of cluster structure supported on TiO_2 and a clear agglomeration in all the cases after reaction.

4. Appendix

UV-Vis spectra and MALDI mass spectra of the nanocluster samples in solution

Both the UV-Vis spectrum of $[Au_{25}(SC_2H_4Ph)_{18}]^-$ (Figure 5-56, left) and the dominant peak at m/z = ≈7394 in the MALDI mass spectrum (Figure 5-56, right) are in good agreement with the reported data.[156]
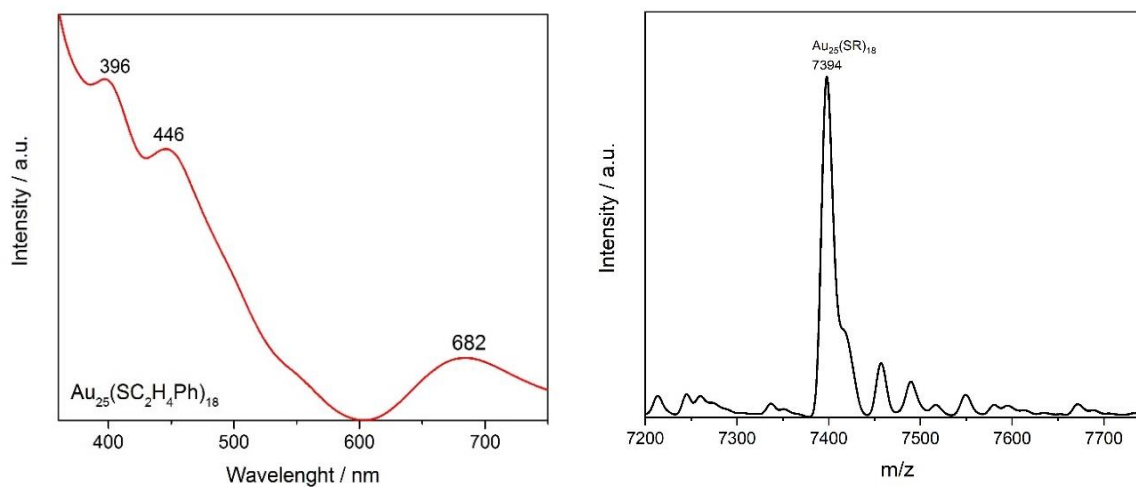
Figure 5-56 *UV-Vis (left) and MALDI mass spectrum (right) of $[Au_{25}(SC_2H_4Ph)_{18}]^-$*

The UV-Vis fingerprint of $PdAu_{24}(SC_2H_4Ph)_{18}$ (Figure 5-56, left) agrees with reported spectra.[86, 89] In addition, the mass spectrum (Figure 5-56, right) shows only a single significant peak at m/z = 7309, corresponding to $PdAu_{24}(SC_2H_4Ph)_{18}$.
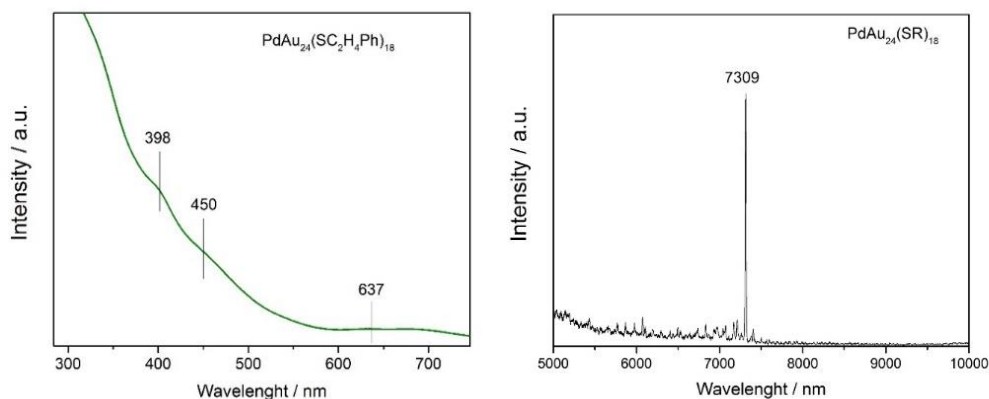
Figure 5-57 UV-Vis (left) and MALDI mass spectrum (right) of PdAu$_{24}$(SC$_2$H$_4$Ph)$_{18}$

The UV-Vis spectrum of Pd$_x$Au$_y$(SC$_2$H$_4$Ph)$_z$ shows bands in similar regions as Au$_{25}$(SC$_2$H$_4$Ph)$_{18}$ and PdAu$_{24}$(SC$_2$H$_4$Ph)$_{18}$, although broadened. Unfortunately, due to upgrade of instrumentation no MALDI-MS spectrum of the Pd$_x$Au$_y$(SC$_2$H$_4$Ph)$_z$ samples could be obtained (strong fragmentation with the new equipment). However, STEM-HAADF indicated a mean particle size of 1.3±0.2 nm, very close to the particle size of Au$_{25}$ and PdAu$_{24}$ clusters, in line with a cluster size of around 20-30 metal atoms.
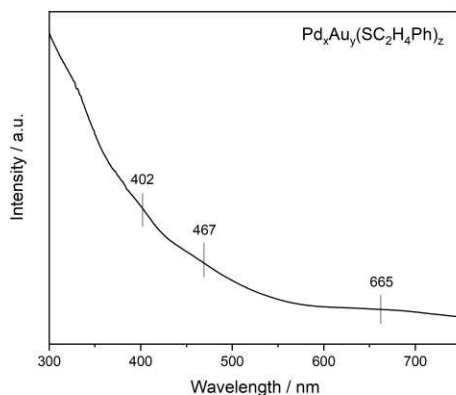
Figure 5-58 UV-Vis spectrum of Pd$_x$Au$_y$(SC$_2$H$_4$Ph)$_z$

Total metal loading & Pd/Au ratio of the nanocluster catalysts

The total metal loadings of the catalysts (Au_{25}/TiO_2, $PdAu_{24}/TiO_2$, Pd_xAu_y/TiO_2) were determined by TXRF. As seen from Table 5-4, the Pd content in $PdAu_{24}/TiO_2$ was too low for detection by TXRF.

For Pd_xAu_y/TiO_2, a Pd:Au 1:4.2±0.4 atomic ratio was determined by TXRF. XPS measurements of $Pd_xAu_y(SC_2H_4Ph)_z$ dropcast on HOPG yielded a Pd:Au ratio of 1:3.1±0.3.

Table 5-4 *Metal loading (%wt) of the nanocluster catalysts determined by TXRF*

	%wt Pd	%wt Au	%wt total	Pd:Au atomic ratio
Au_{25}/TiO_2	-	4.50	4.50	-
$PdAu_{24}/TiO_2$	n.d.*	2.70	2.70	n.a.
Pd_xAu_y/TiO_2	0.24	1.88	2.12	1:4.2±0.4

* n.d.: not detected; TXRF-measurements can have a maximum relative error of 10%.

HAADF-STEM of the TiO$_2$-supported PdAu$_{24}$, Pd$_x$Au$_y$ and Au$_{25}$ nanoclusters

HAADF-STEM images were acquired for the nanocluster catalysts to determine the average particle size (Figure 5-59). For TiO$_2$-supported Au$_{25}$ and PdAu$_{24}$ the average diameter was 1.2 ± 0.2 nm, for Pd$_x$Au$_y$ nanoclusters it was 1.3 ± 0.2 nm.
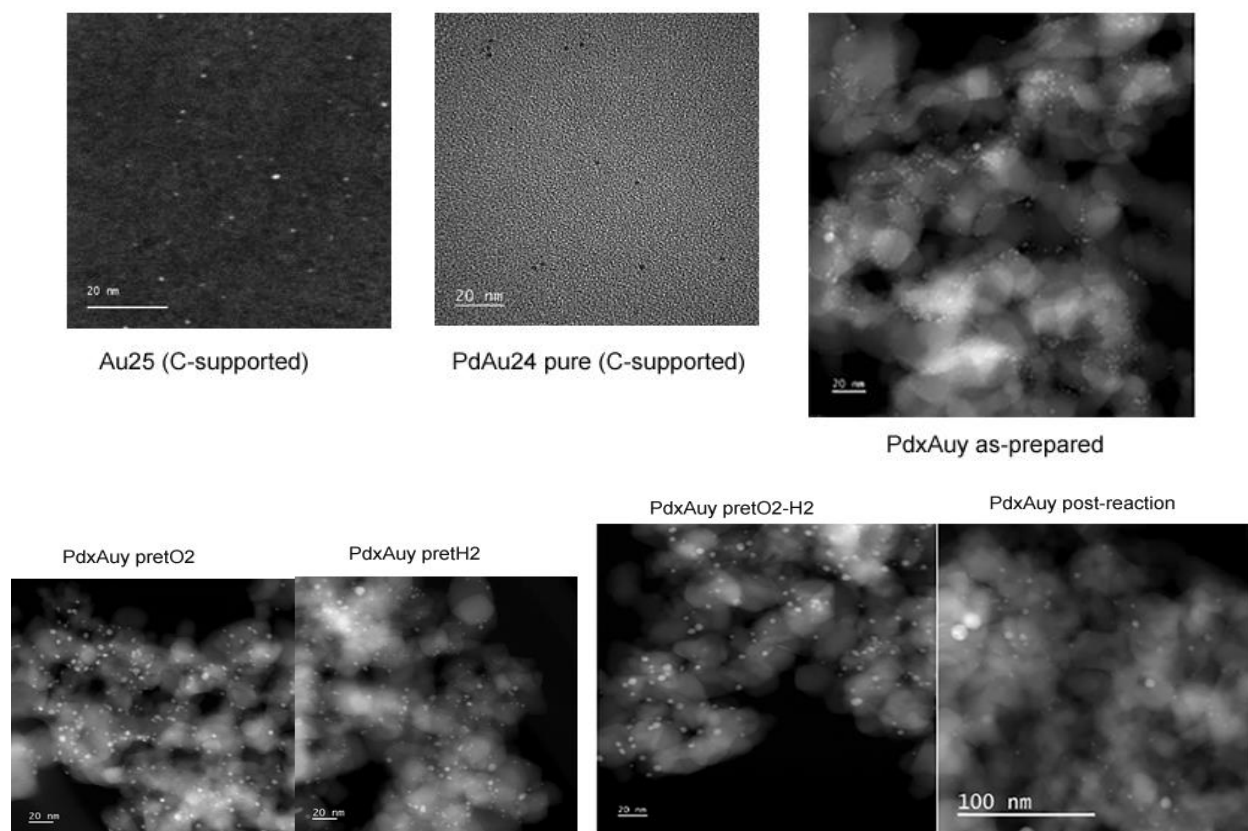
Figure 5-59 *(upper Figure) HAADF-STEM images of (a) Au_{25} and (b) $PdAu_{24}$ supported on carbon-film, and (c) Pd_xAu_y supported on TiO_2. (Lower Figure) HAADF-STEM images of Pd_xAu_y supported on TiO_2: (a) $pretO_2$, (b) $pretH_2$, (c) $pretO_2$-H_2 and (d) post-reaction.*

Table 5-5 *Mean particle sizes of the supported PdxAuy nanoclusters, as-prepared and after various treatments and reaction, estimated from HAADF-STEM.*

	fresh catalyst	after pretO₂	after pretH₂	after pretO₂-H₂	after COox
Pd_xAu_y/TiO_2	1.3 ± 0.2	2.7 ± 0.7	2.6 ± 0.6	2.7 ± 0.5	2.8 ± 0.8

For Pd_xAu_y/TiO_2 catalyst, images were also taken after oxidative, reductive, and sequential treatments ($pretO_2$-H_2) and after CO oxidation (post-reaction), as shown in Figure 5-59. Upon pretreatment and reaction (Table 5-5), the particle size approximately doubled (2.8±0.8 nm).

Reusability of PdAu$_{24}$/TiO$_2$ in CO oxidation

Reusability test with PdAu$_{24}$/TiO$_2$ were conducted by subsequent CO oxidation reactions in the flow reactor set-up without removing the catalyst in between. After the first reaction, the sample was cooled to room temperature (under Ar). Once reached, a second CO oxidation reaction was initiated (same for the third catalytic test). As can be seen in Figure 5-60, activity increases in the 2nd and 3rd run, which indicates activation of PdAu$_{24}$/TiO$_2$ at CO oxidation conditions.
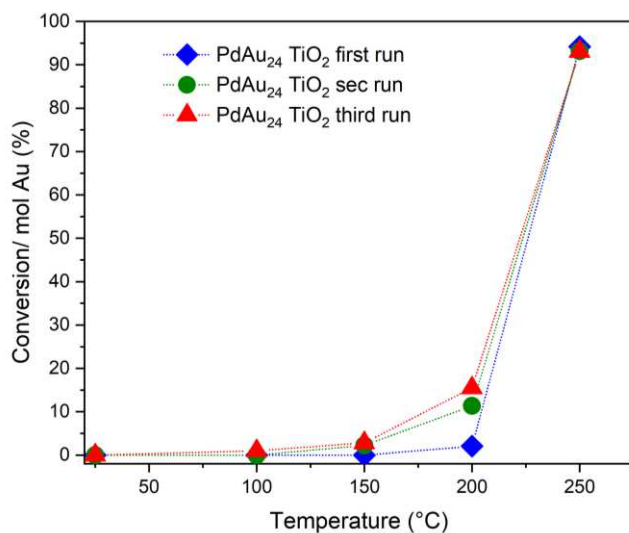
Figure 5-60 Reusability tests with PdAu$_{24}$/TiO$_2$ in CO oxidation

DRIFT spectra: CO dosing and TiO$_2$ blank

CO dosing experiments were performed with the pretreated catalysts before starting the CO oxidation reaction, which DRIFT spectra are depicted in Figure 5-61. The CO gas phase bands are clearly visible in the 1% CO atmosphere spectra at around 2170 and 2115 cm^{-1}.

For Au$_{25}$/TiO$_2$, no significant formation of CO-adsorbate species could be detected. This correlates with its low CO oxidation activity. For the PdAu$_{24}$/TiO$_2$ catalyst, the spectra strongly depended on the pretreatment conditions. After only pretO$_2$, minimal formation of CO adsorbed

on Au could be found, whereas after pretO$_2$-H$_2$, a pronounced CO-Pd band could be detected. This correlates with the better catalytic performance of the pretO$_2$-H$_2$ catalysts.

Blank experiments with the pure TiO$_2$ support without any impregnated Au clusters were performed as well (Figure 5-61). CO dosing experiments showed no formation of adsorbed CO species, yet still some CO$_2$ formation could be detected in the *in-situ* DRIFTS measurements during CO oxidation, getting stronger at higher temperature. The same trend could be observed in the kinetic tests.
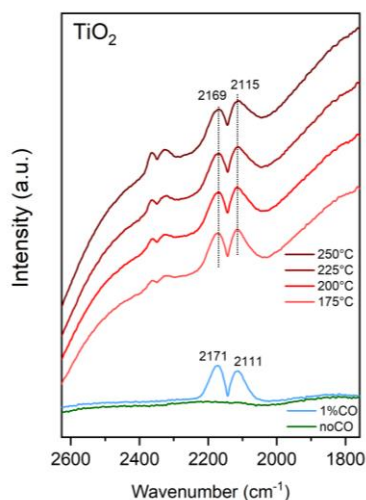
Figure 5-61 In-situ *DRIFTS spectra of a TiO$_2$ blank experiment during CO oxidation (red). CO dosing after pretreatment (blue and green)*
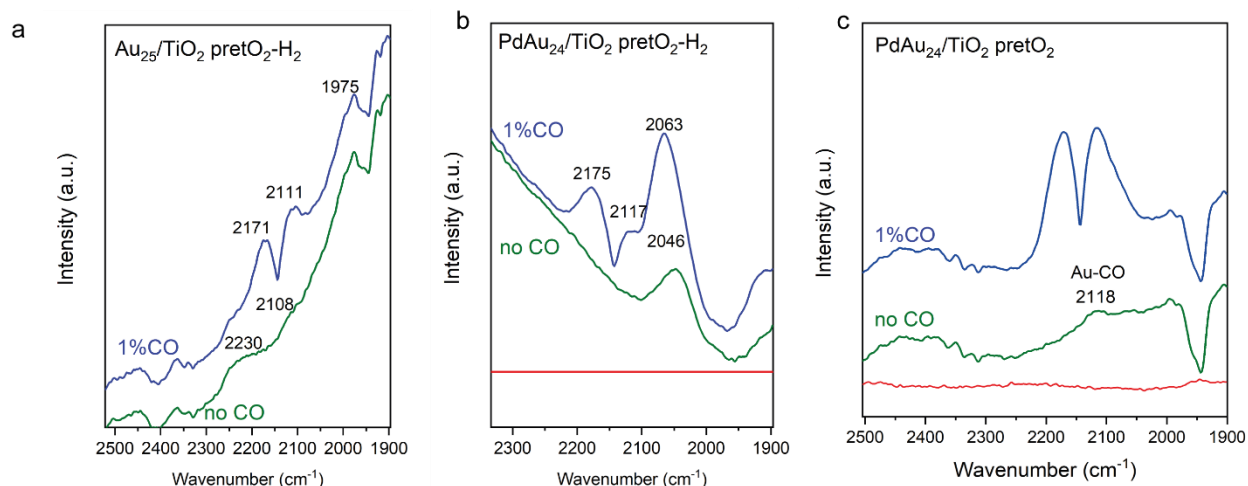
Figure 5-62 *DRIFT spectra after CO dosing and subsequent He purging: (a) Au₂₅/TiO₂ pretO₂-H₂, (b) PdAu₂₄/TiO₂ pretO₂-H₂ and (c) PdAu₂₄/TiO₂ pretO₂. The pretreated samples were exposed to a 1% CO in He gas atmosphere and afterwards purged with He at RT, until no further changes in the spectra were observed.*
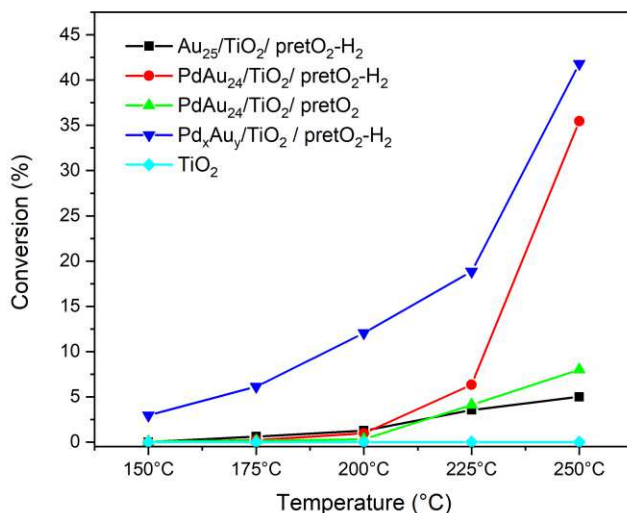
Figure 5-63 *MS analysis of CO conversion during DRIFTS experiments. Each run used 10 mg of catalyst.*

EXAFS Fitting

XAS data have been processed according to standard procedures. Au L_3 and Pd K-edge spectra have been normalized by calculating and subtracting pre-edge and post-edge backgrounds as low order polynomial smooth curves. The corresponding EXAFS signal has been then extracted, k-squared weighted, and Fourier transformed (FT) in the range 2.8 Å^{-1} and 10 Å^{-1}

and 2.6 Å^{-1} and 12.6 Å^{-1} at Au L$_3$ edge and Pd K-edge, respectively. The results are displayed in Figure 5-64.

Pd K-edge EXAFS fit. A two shell model (with Pd-S, Pd-Au contributions) has been considered to model the EXAFS data at Pd K-edge. For each spectrum of the dataset, we considered two coordination numbers CN (N$_{Pd-S}$, N$_{Pd-Au}$) as fitting parameters and two correction factors for interatomic distances (R$_{Pd-S}$ and R$_{Pd-Au}$). We decided to use only two disorder parameters (σ^2_{Pd-S} and $\sigma^2_{Pd-Au} = \sigma^2_{Au-Pd}$) for the whole dataset, plus the energy correction to photoelectron reference ΔE_0 and the passive electron reduction factors S$_0^2$.Au L$_3$-edge EXAFS fit. A three shell model (with Au-S, Au-Au, and Au-Pd contributions) has been considered to model the data. For each spectrum of the dataset, we considered three coordination numbers CN (N$_{Au-S}$, N$_{Au-Au}$, and N$_{Au-Pd}$) as fitting parameters and two correction factors for interatomic distances (R$_{Au-S}$ and R$_{Au-Au}$ = R$_{Au-Pd}$), which means that we constrained the Au-Pd and Au-Au distances. Due to the limited k range available and the strong inter-correlation between the fitting parameters, we decided to use only two disorder parameters (σ^2_{Au-S} and $\sigma^2_{Au-Au} = \sigma^2_{Au-Pd}$) kept common for all the spectra in the dataset. Such assumption can be justified considering the limited temperature range of these *in-situ* measurements (25-250 °C) and the fact that in general, the static structural disorder is higher than the temperature one for small clusters[157]. This approach assures that the coordination numbers obtained from the analysis are consistent with all the experimental information available. Finally, we fit the energy correction to photoelectron reference ΔE_0 and the passive electron reduction factors S$_0^2$, again common to all the spectra.

Pd K-edge

amp	Δe	σ²(Pd-S)	σ² (Pd-Au)
1.02 +/- 0.23	-3.74 +/ 1.22	0.0014 +/- 0.0003	0.0056 +/- 0.0005
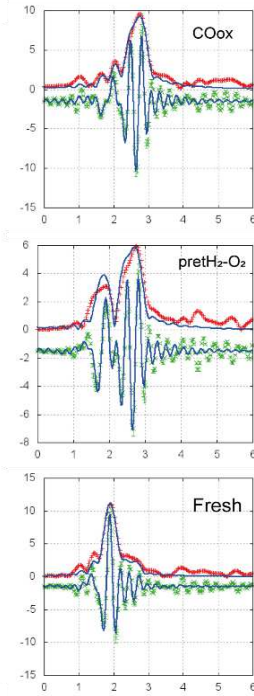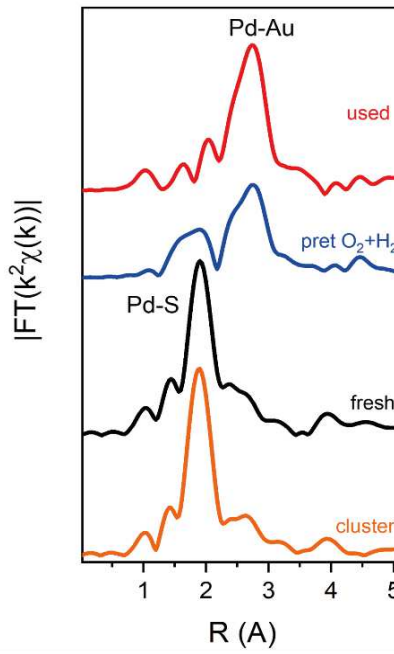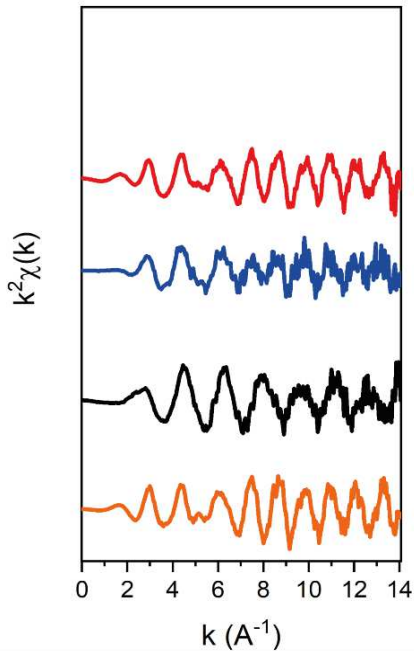
Au L₃-edge

amp	Δe	σ²(Au-S)	σ² (Au-Au) = σ² (Au-Pd)
0.88 +/- 0.27	4.62 +/ 1.35	0.0087 +/- 0.0040	0.0043 +/- 0.0012
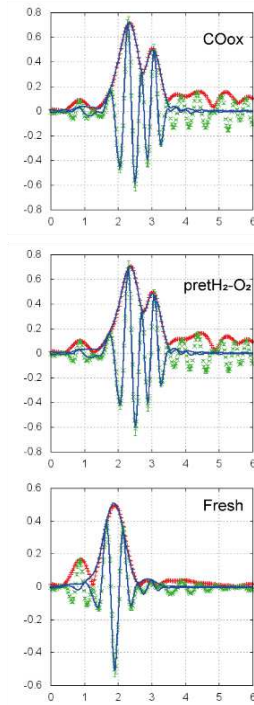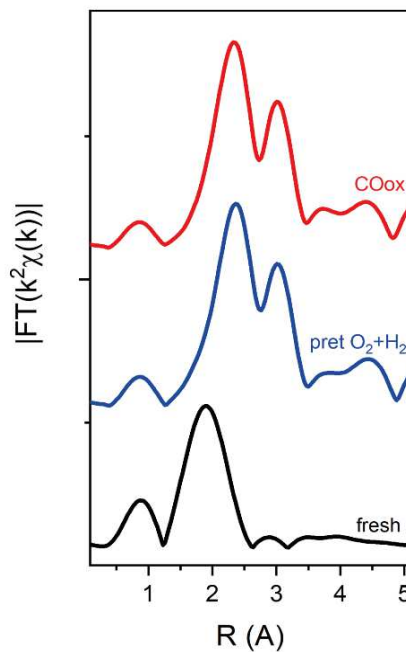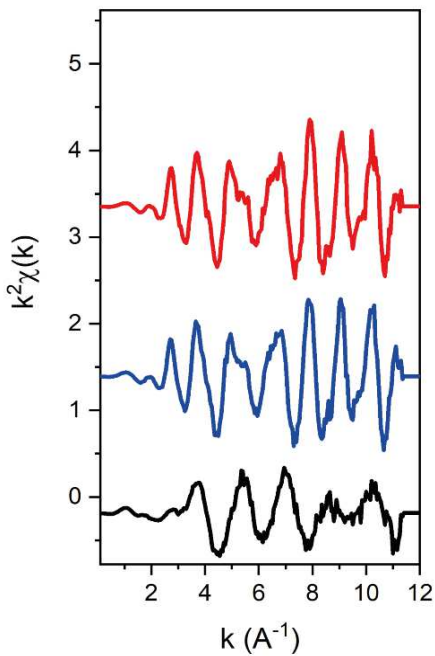
Figure 5-64 EXAFS fitting

In order to evaluate if there was a significant contribution of Pd-Pd in the EXAFS, a FEFF9 simulation was done. The results of the simulation are shown in Figure 5-65. From these simulations, it could be shown that in a bimetallic particle containing less than 30% of Pd, small presence of Pd-Pd will not be possible to distinguish between Pd-Pd and Pd-Au, only in the case that will be strong presence of Pd-Pd bonds.
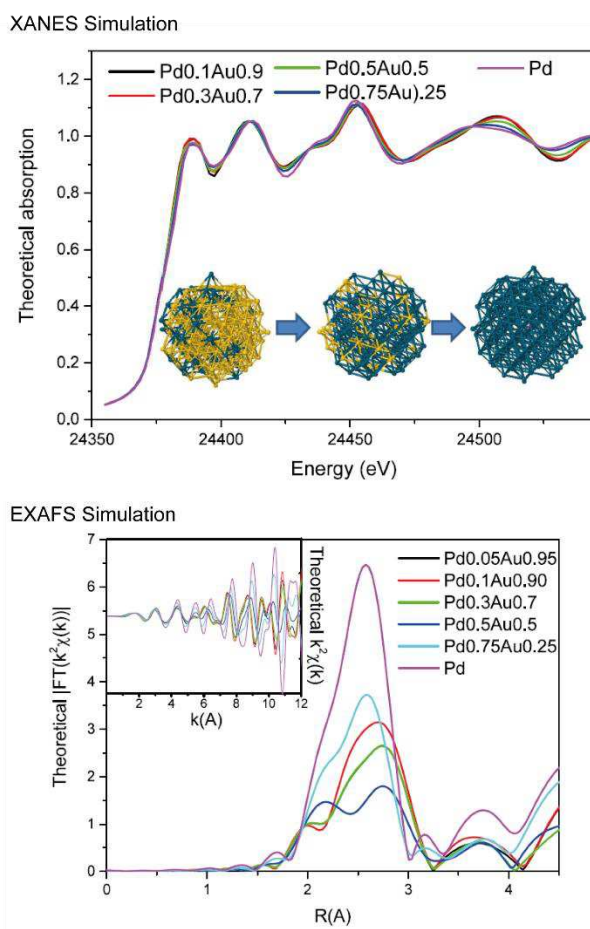
Figure 5-65 *EXAFS and XANES simulation to study Pd-Pd contributions in spectra of PdAu nanoparticles containing less than 30% of Pd.*

XPS: comparison of PdAu$_{24}$/TiO$_2$ and Pd$_x$Au$_y$TiO$_2$
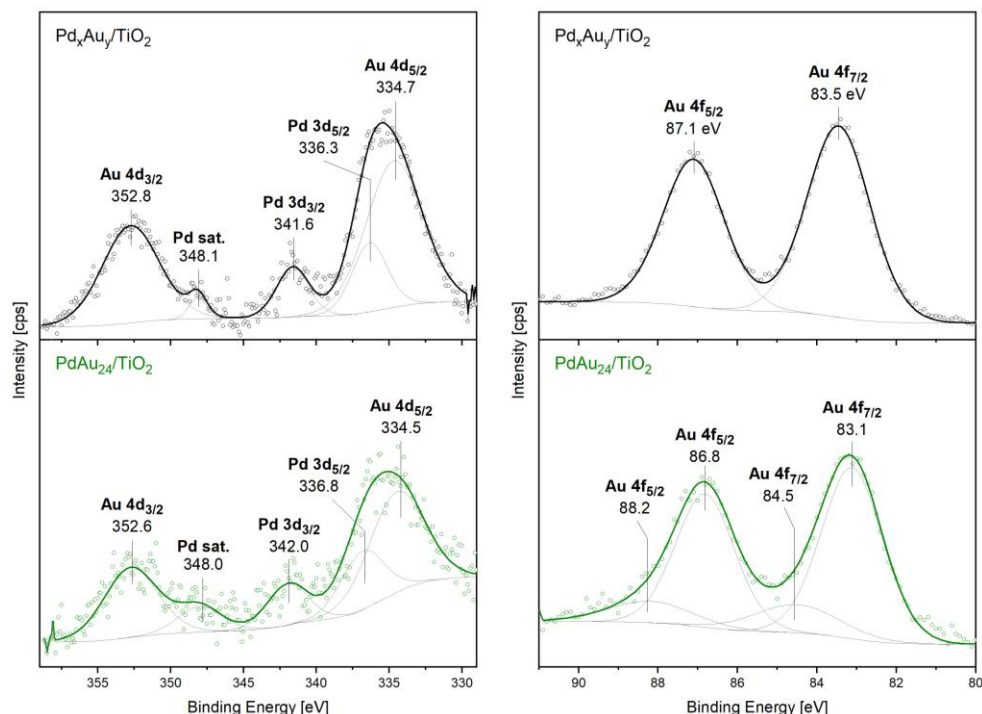
Figure 5-66 *XPS spectra of as-prepared PdAu$_{24}$/TiO$_2$ (bottom, green) and Pd$_x$Au$_y$/TiO$_2$ (top, black): Pd 3d & Au 4d region (left) and Au 4f region (right).*

Figure 5-66 compares prepared PdAu$_{24}$/TiO$_2$ and Pd$_x$Au$_y$/TiO$_2$. Differences in the Pd 3d region may be due to the different location of the Pd dopant (PdAu$_{24}$/TiO$_2$: Pd in center of Au core, Pd$_x$Au$_y$/TiO$_2$: Pd atoms preferentially in the staples). There are also differences in the Au 4f region: for PdAu$_{24}$/TiO$_2$ different contributions (at 83.1 eV and 84.5 eV) can be identified, presumably related to different environments of Au (without and with contact to the Pd center atom).

No distinctly different species could be identified for Pd$_x$Au$_y$/TiO$_2$, as Pd accumulated in the clusters' staples, with most Au atoms in the core.

Chapter 6

Synthesis of $Ag_xAu_{25-x}(SR)_{18}$ and doping effects on the catalytic activity in oxidation reactions

1. Abstract

As already observed in Chapter 5 for palladium, the doping of Au nanoclusters induced a strong effect on their physical-chemical properties, leading to changes in their catalytic activity. Depending on the metal doping different properties can be obtained. In this chapter, the effect of Ag doping is explored. In the case of Ag, several atoms can be introduced to the Au_{25} nanoclusters. Therefore, the synthesis, isolation and characterization of $Ag_xAu_{25-x}(SR)_{18}$ nanoclusters is challenging. Through an optimization of the synthesis conditions, a narrow distribution of Ag doped Au_{25} was obtained, confirmed by MALDI and UV-VIS spectroscopy. The prepared doped clusters were supported on different oxides to study their interaction and their effect on the catalytic properties. Two oxidation reactions were tested, cyclohexane oxidation in liquid phase and CO oxidation in gas phase. In both cases, lower catalytic activity was obtained with the Ag doped Au_{25} catalysts in comparison with the pure Au_{25} ones. In addition, clear influence of the oxide material used as support on the catalytic behaviour was observed (TiO_2> silicate zeolites > SiO_2 > aluminosilicate zeolites). However, further studies are required to complete these preliminary results and clarify the open questions.

2. Introduction

One way to further explore the effect of heteroatom doping on the catalytic activity of $Au_{25}(SR)_{18}$ nanocluster catalysts is to introduce more than one metal atom into the gold cluster structure. Jiang et al. [158] predicted that 16 elements are capable of being doped into $Au_{25}(SR)_{18}$ at the central position while maintaining the geometric and electronic structures of the particle. Recently, Tsukuda et al. reported that in the case of Au_{25} doped with Ag, its occupies a surface site in the icosahedral Au_{13} core leading to the most stable structure confirmed by theoretical calcualtions [88]. Therefore, in this case, the substitution of Au atoms located in the staple motifs does not occur [159, 160].

Ag and Au have contrasting physical and chemical properties despite their similarity in atomic size, structure and bulk-lattice. Doping gold clusters with silver has been proven to induce changes in the electronic structure [161], in the optical absorption [162] and in the luminescence [163]. Recently, it has also been reported that silver doping increases both structure flexibility [164] and chirality [165], and induces photoluminescence[166]. These systems are also potentially important for various applications [152, 167] because the combination of Ag and Au inside the same particle provide a balance between stability and reactivity.

Previous studies, explored the effect of Ag doping effect on the catalytic activity of Au clusters in CO oxidation. Haeck et al. observed that the activity highly depends on the number of dopant atoms [167]. Li et al. showed the tendency of $Cu_xAu_{25-x}(SR)_{18} > Au_{25}(SR)_{18} > Ag_xAu_{25-x}(SR)_{18}$ which depends on the metal nature, supported on CeO_2. [125]. However, no complementary structure-catalytic activity studies were performed to determine the reasons for the difference in performance.

In the case of liquid phase reactions, Tsukuda et al. studied silver doped clusters prepared by the co-reduction method in the presence of poly(N-vinyl-2-pyrrolidone) for aerobic oxidation of p-hydroxybenzyl alcohol. They observed an enhancement in catalytic activity for the Ag-doped clusters and correlated it with the charge state of Au observed by XPS [168]. The same system was studied by Li et al. for carbon-carbon coupling reaction revealing differences in both

conversion and selectivity, which suggests that selectivity may be influenced by the nature of the doping atom [169].

Different synthetic procedures have been reported in order to prepare Ag doped $Au_{25}(SR)_{18}$ [170, 171]. The three main approaches are the metal exchange method [172], exchange through reaction with metal surfaces [101, 173] and co-reduction [174]. In this thesis, the co-reduction method was chosen as it was possible to obtain higher yields compared with other synthetic approaches. In this case, a distribution of Ag doping atoms was obtained ($Ag_xAu_{25-x}(SR)_{18}$, x=5-8). The number of silver dopants included in the cluster depends on the reaction time and the ratio of the metal precursors.

In this chapter it is explored the effect of Ag doping on Au_{25} cluster supported in different oxides. Two reactions are employed, gas phase CO oxidation in gas phase and in the liquid phase cyclohexane oxidation. In previous chapters higher stability was obtained with SiO_2 catalysts, therefore silica based materials as zeolites have been also used in this study. Zeolites have attracted a lot of attention due to their good performance as hydrocracking catalysts and their tunable structure as the ratio between silica and alumina can be varied during the synthesis in order to enhance some of their properties [175]. Zeolites are composed of SiO_2 and AlO_2 tetrahedrons and build a defined three-dimensional framework where the corners of the tetrahedrons are connected with common oxygen atoms. The general formula of zeolites can be written as:

$$A^{m+}_{y/m}[(SiO_2)_x \cdot (AlO_2{}^-)_y] \cdot zH_2O$$
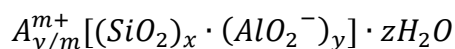
Equation 6-6 Zeolites composition

It is not possible for two aluminium tetrahedra to be linked together directly; therefore the minimum Si:Al-ratio is 1:1.The linked tetrahedrons then form distinct structures such as channels and cages. An example for a cage and the resulting 3D-framework in can be seen in Figure 6-67.
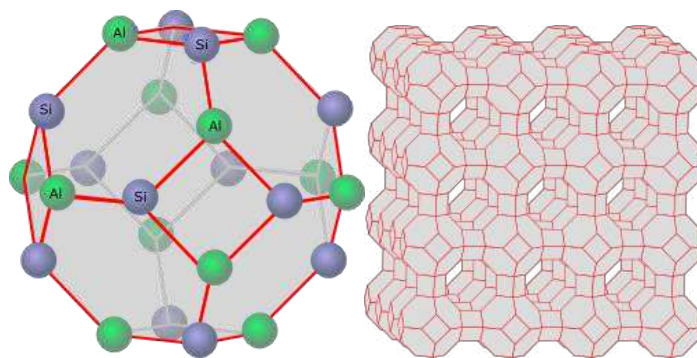
Figure 6-67 *Zeolite structure: sodalite unit (left) and framework of zeolite containing many sodalite units (right)*

Inside these channels and cages water and cations can be found. Cations are necessary because every aluminium tetrahedron carries a negative charge that needs to be compensated for. Thus, the framework itself has acidic properties with acid sites on the surface being particularly essential for the catalytic activity of zeolites. An important aspect of classifying zeolites and examining their behaviour is the structure of their pore system. This can be characterized by their orientation (like unidimensional or three-dimensional pores) and the number of tetrahedrons that build such a pore. The most common ones are 8-, 10- and 12-membered ring pores. Since their diameter is usually below 2 nm, zeolites are generally considered to be microporous materials, although mesoporous zeolites are also available.

The zeolites have a high catalytic activity due to their catalytically active acid sites; these have to be accessed through uniformly sized pores and voids thereby imposing size constraints on the accessibility to reactants and the nature of the intermediates and products. Providing access for larger molecules to the catalytic sites would expand the range of reactions that zeolites can catalyse. With the delamination of the zeolite a layered structure can be obtained with the zeolite-type catalytic sites contained within. With this delamination process the accessibility of the catalytic sites is improved without affecting the activity of the catalyst. The idea of a delaminated zeolite is shown below in Figure 6-68 [176].
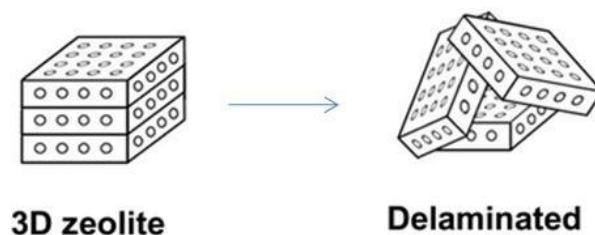
Figure 6-68: *Delaminated zeolite. Graphic reproduced from Opananseko, V., et al.*

Besides zeolites, there are some other materials that have similar characteristics regarding their structure, e.g. aluminophosphates.

In this chapter, we compare these supports (silicate zeolites and aluminosilicate zeolites) with titanium oxide and silica oxide in order to observe the differences in stability and reactivity. This work was part of a collaboration with The Institute of Chemistry and Technology (ITQ) —part of The Polytechnic University of Valencia. The results have been published in the journal, "Catalysis Today" [177].

3.   Results and discussion

3.1.   Characterization of $Ag_xAu_{25-x}(SR)_{18}$ nanoclusters

Ag_xAu_{25-x} clusters were synthesized and isolated by the procedures described in Chapter 3. and characterized by UV-Vis and MALDI spectroscopy (Figure 6-69). UV-Vis spectra show bands at 475, 520 and 673 nm related to the Ag_xAu_{25-x} in agreement with previously characteristic absorption spectra reported [102]. The exact composition of the doped cluster obtained was identified by MALDI spectroscopy (Figure 6-69). The results show a distribution in the number of dopants introduced in the structure between 6 to 8, as it can be observed in Figure 6-69 (right).
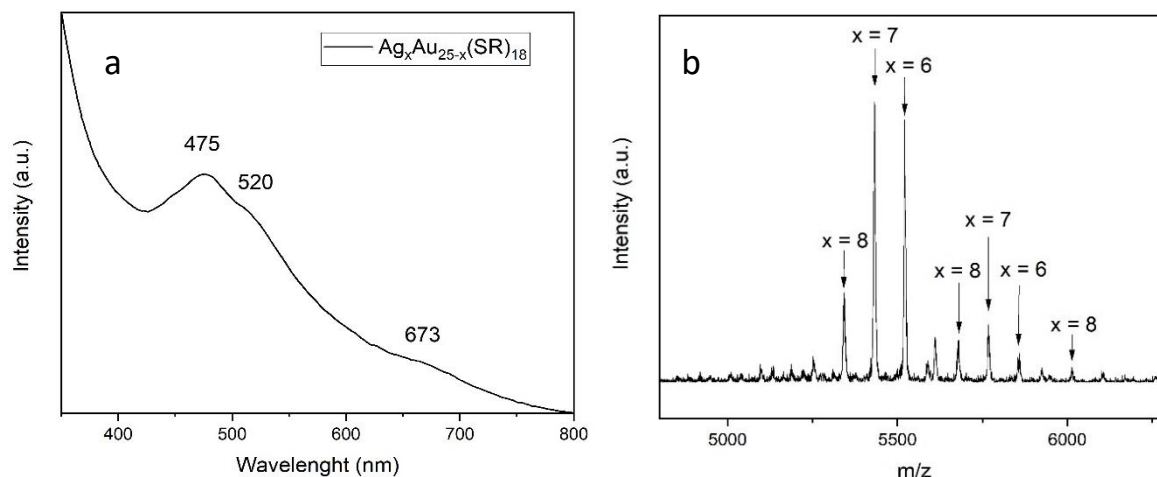
Figure 6-69 *Figure composed by two figures: a) Uv-Vis spectra of pure $Ag_xAu_{24-x}(SR)_{18}$ (final product) and b) MALDI-TOF spectra*

Particle size of the synthesized cluster was studied by HAADF-STEM and shown in Figure 6-70. A range lower than 2 nm can be observed, in agreement with previous studies.
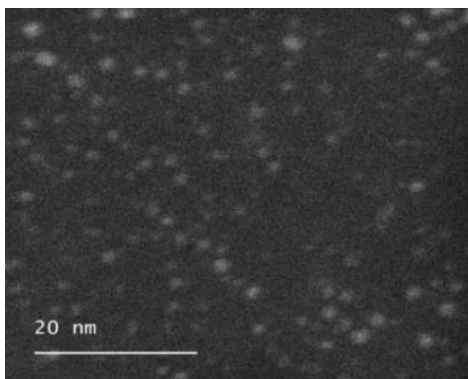
Figure 6-70 *HAADF-STEM image of the pure Ag_xAu_{25-x} clusters*

3.2. Catalysts characterization

Following previously used protocols and as described in Chapter 3, the obtained Ag doped clusters were supported on three different oxides: TiO_2, SiO_2, and zeolites. TiO_2 and SiO_2 have already been covered in Chapter 4, where it was found that they had a strong effect on the

stability and catalytic properties of the gold nanocluster catalysts. The zeolites — which were synthesized and supplied by The Institute of Chemistry and Technology (ITQ) —are delaminated and have a different Si/Al ratio, one of them (RTQU46) being pure silica and the other (RTQ511) having a relation Si/Al ratio of 10.

Following the previous approach, the catalysts were pretreated at 150°C to partially remove the ligands [127]. Figure 6-72, and 6-73 show the DRS spectra obtained from the samples with no relevant changes to the cluster structure after deposition and after pretreatment at 150°C.

In the case of silica, the characteristic bands show a slightly shift to lower wavelenghts in comparison to the pure cluster spectra (Figure 6-71).
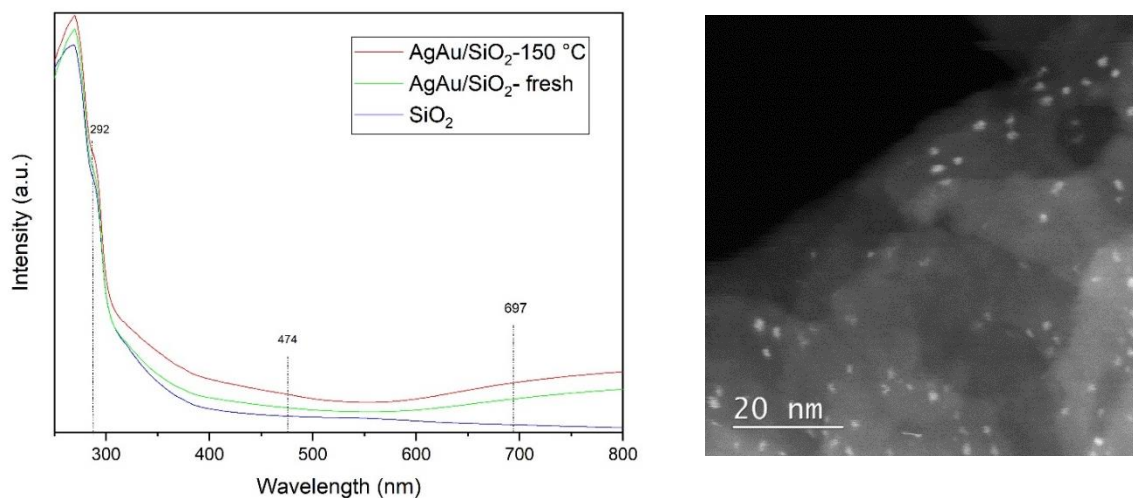
Figure 6-71 *DR-spectra of SiO$_2$ and Ag$_x$Au$_{25-x}$(SR)$_{18}$ supported on SiO$_2$ before and after the pretreatment (left) and HAADF-STEM of the same sample before pretreatment (right)*
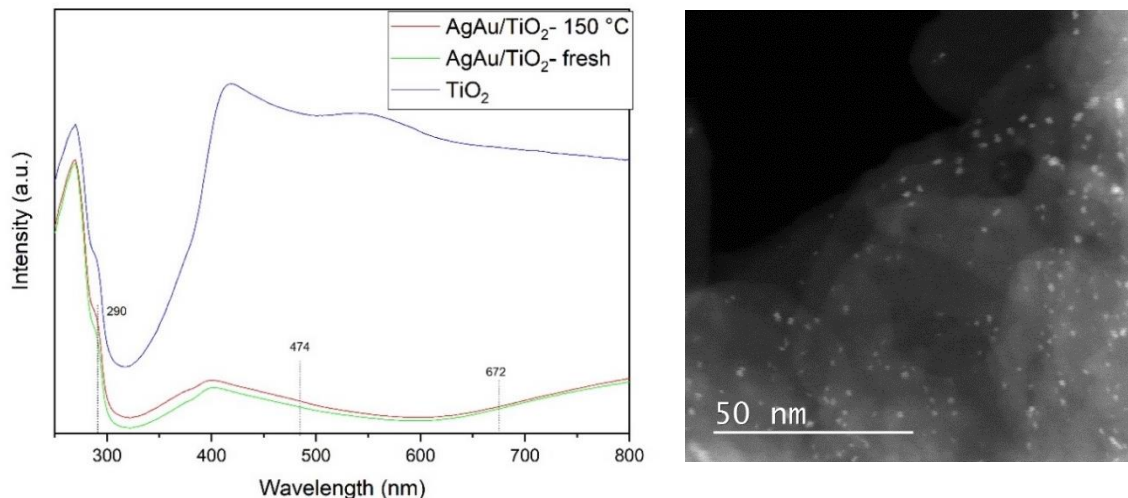
Figure 6-72 DR-spectra of TiO_2 and $Ag_xAu_{25-x}(SR)_{18}$ supported on TiO_2 before and after the pretreatment (left) and HAADF-STEM of the same sample before pretreatment (right)

In the case of titanium oxide, some bands were not visible due to strong absorption of the support, e.g. the band around 400 nm for TiO_2. It is relevant to point out that no plasmonic resonance bands — which would denote agglomeration or particle size increase — were observed at any point. HAADF-STEM confirmed the high dispersion and the controlled size, as shown in Figures 6-71, 6-72 and 6-73 for all the supports. The particle size corresponds to the pure cluster measurement in Figure 6-70(1-2 nm particle size).
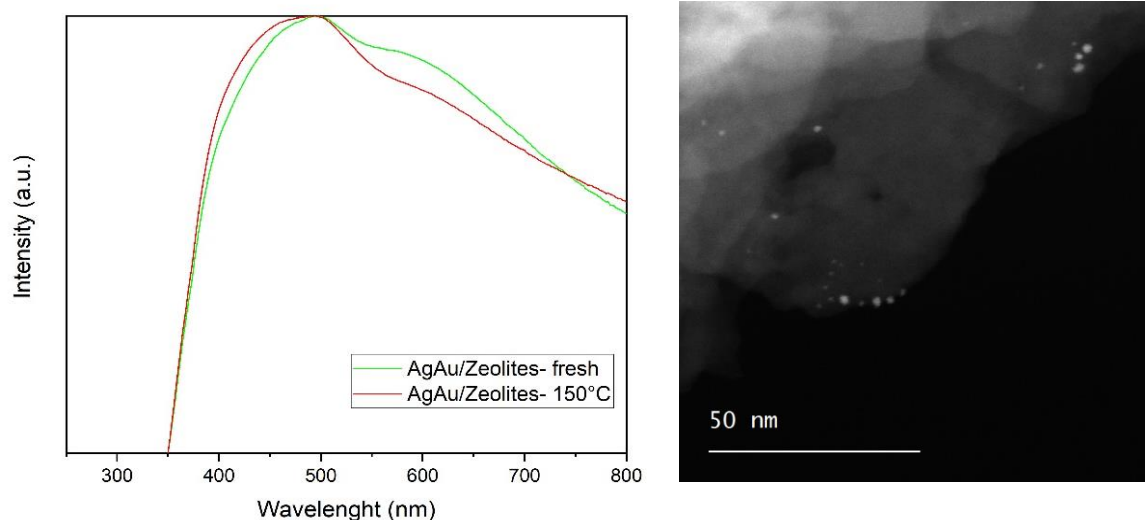
Figure 6-73 DR-spectra of $Ag_xAu_{25-x}(SR)_{18}$ supported on zeolites before and after the pretreatment (left) and HAADF-STEM of the same sample before pretreatment (right)

Figure 6-70 shows an example of the DRS spectra of fresh and pretreated zeolite supported clusters. As with the titanium oxide supported clusters, some bands are hidden due to the strong absorption of the support. Aluminosilicate zeolites have a characteristic band around 500 nm, as can also be seen in our measurements. Also in this case, no agglomeration or particle size increase is observed due to the impregnation or during pretreatment. HAADF-STEM confirmed the high dispersion and expected particle size.

3.3. Catalytic Activity Studies

The catalytic activity in oxidation reaction of the prepared samples was studied following the same procedure as in previous chapters. The metallic charged on the catalysts is around 2%wt, confirmed by XRF.

3.3.1. Cyclohexane oxidation

Cyclohexane oxidation in liquid phase requires the presence of gold to activate the oxygen, as was discussed in Chapter 3. Moreover, catalytic activity and selectivity highly depend on the support and on the particle size. In Chapter 4 a relevant improvement in the catalytic properties was also observed as the structure was doped with one or more atoms of palladium.

In this section, we shall explore the effect of Ag doping. The reaction conditions were 100 mg catalyst, 10 ml of cyclohexane and 80 µl of tert-butyl hydroperoxide (initiator). The reaction was carried out in a quartz beaker with a 2.5 ml/min O_2 flow and the temperature was 75 °C. Reactants and products were identified by GC-MS.

3.3.1.1. Ag doped Au_{25} nanoclusters on TiO_2 and SiO_2 as supports

Figure 6-74 summarizes the values of conversion and selectivity after 10 hours reaction. Significant decrease in the catalytic activity, in terms of cyclohexane conversion with the Ag doped Au cluster catalysts is obtained, independent on the support employed. However, in the case of TiO_2 catalysts, pronounced increase in the selectivity to the desired products (ketone and alcohol) with the Ag_xAu_{25-x} clusters is obtained. Therefore, clear influence in the reaction mechanism of the Ag presence in the catalysts is expected. Complementary studies are required to clarify this effect.
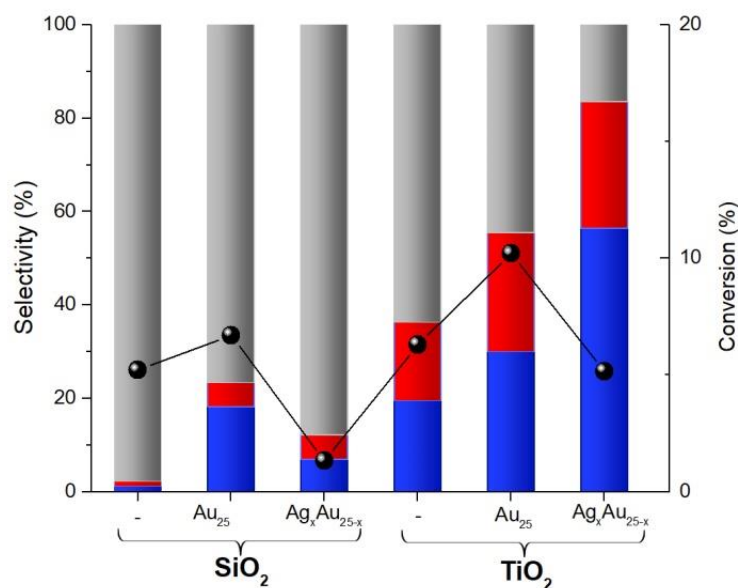
Figure 6-74 *Catalytic activity of supported Ag$_x$Au$_{25-x}$ and Au$_{25}$ clusters in the oxidation of cyclohexane: cyclohexane conversion (black) (right axis); product selectivity (left axis) for cyclohexanol (blue); cyclohexanone (red); by-products (grey)*

Table 6-5 *Catalytic ac activity of supported Ag$_x$Au$_{25-x}$ and Au$_{25}$ clusters in the oxidation of cyclohexane expressed in terms of yield*

	Catalysts	Yield (%)	
		Cyclohexanol	Cyclohexanone
TiO$_2$ catalyst	support	1.23	1.06
	Au$_{252}$	3.05	2.61
	Ag$_x$Au$_{25-x}$	5.82	2.80
SiO$_2$ catalyst	support	0.06	0.06
	Au$_{25}$	1.21	0.37
	Ag$_x$Au$_{25-x}$	0.19	0.14

3.3.1.2. Ag doped Au$_{25}$ nanoclusters on zeolites as supports

The use of zeolites (silicates and aluminosilicates Si/Al) as support for Au$_{25}$ and Ag$_x$Au$_{25-x}$ nanoclusters was explored as a complementary study. The catalytic activity results show that as a support silicate zeolites are more active than commercial silica while titanium oxide remains the most active. The aluminosilicates lead to low values of conversion. The high catalytic activity related to the silicate zeolites can be ascribed to the acidic sites on the surface [175].Figure **6-75** Catalytic activity of zeolite supported AgxAu25-x and Au25 clusters in the oxidation of cyclohexane: cyclohexane conversion (black) (right axis); product selectivity (left axis) for cyclohexanol (blue); cyclohexanone (red); by products (grey). The zeolites are silicates (left) and aluminosilicates (right)6-75 shows that the tendencies observed for the other two supports are also followed here: doping with silver leads to a decrease in catalytic activity but an increase in selectivity. More in detail, we observe that in case of zeolites without alumina, the conversion is already 40% for the support, and this value is increase to 63% for gold clusters, while it decreases
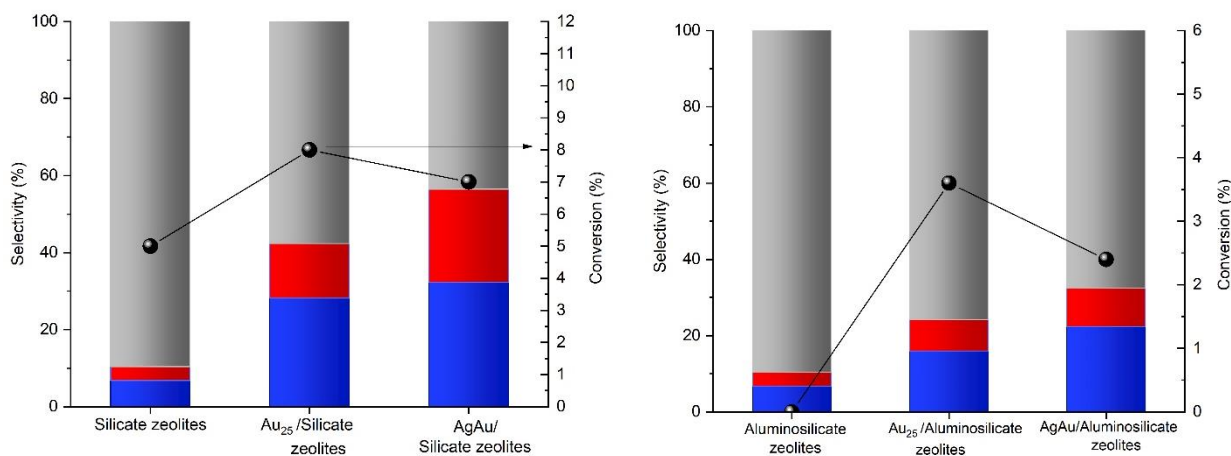
to 57% for the silver doped cluster. In the other case, zeolites with alumina and silica content, the conversion is almost negligible for the support, slightly higher for gold clusters (76%) and it is again decrease for the silver doped cluster (43%).

The stability was analysed by HAADF-STEM. In Figure 6-76 it can be observed that the particle size is increases to 3-4 nm after 10 hours reaction time at 75°C, although further measurements should be performed to express this value with more precision. The work with zeolites suggests that this material could be a promising support for further investigations.

Figure 6-75 *Catalytic activity of zeolite supported Ag$_x$Au$_{25-x}$ and Au$_{25}$ clusters in the oxidation of cyclohexane: cyclohexane conversion (black) (right axis); product selectivity (left axis) for cyclohexanol (blue); cyclohexanone (red); by products (grey). The zeolites are silicates (left) and aluminosilicates (right)*
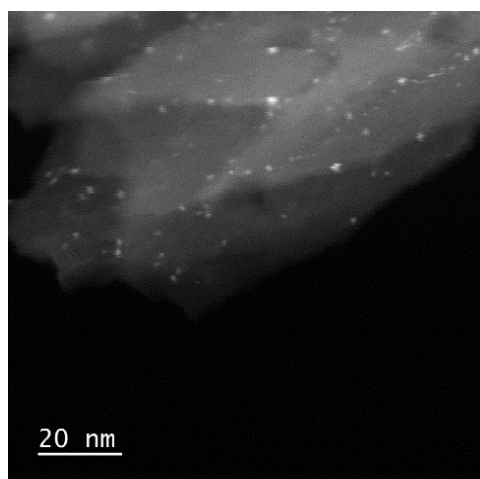
Figure 6-76 *HAADF-STEM images of Ag$_x$Au$_{25-x}$(SR)$_{18}$ supported on zeolites after reaction*

3.3.2. CO oxidation

In order to further investigate how doping with silver affects catalytic properties, it is interesting to analyse a well-known simplified system such as gas phase CO oxidation, as was previously done with palladium in Chapter 4. For CO oxidation, a strong pretreatment (250°C) is required to effectively activate the catalyst. Moreover, the pretreatment composition also affects the catalytic activity (see Chapter 4). According to our observations, the optimal

pretreatment is a combination of an oxidation treatment (under oxygen flow) at 250°C for 40 minutes followed by a reduction treatment (under hydrogen flow) at 250°C for 40 minutes. Here the same two steps pretreatment was used before each catalytic test. This test consists of a mixture of 1% CO and 2% O_2 balance with He, heat up stepwise, each step was kept until a steady state was reached. The reaction products were analysed by an online micro-GC (see Chapter 2).
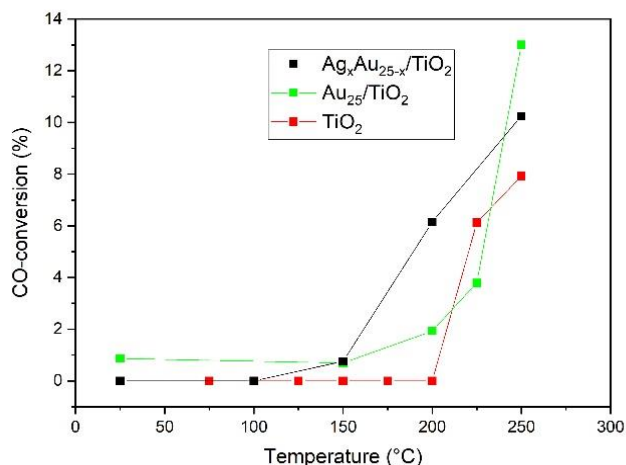
Figure 6-77 CO conversion for $Ag_xAu_{25-x}(SR)_{18}$ supported on TiO_2, $Au_{25}(SR)_{18}$ supported on both on TiO_2

The preliminary results of the CO conversion depending on the reaction temperature with the TiO_2 catalysts are displayed in Figure 6-77 CO conversion for AgxAu25-x(SR)$_{18}$ supported on TiO2, Au25(SR)$_{18}$ supported on both on TiO2. After 150°C the activation of the metal catalysts starts, being more pronounced in the case of Ag doped catalysts than in the case of pure Au catalysts at 200°C. However, in the case of Au_{25} catalysts the conversion drastically increases from 225°C to 250°C, reaching higher values than Ag doped catalysts under the same conditions. Therefore, a different evolution of the metal clusters during reaction conditions may occur and as such complementary studies are required.

4. Conclusion

The Ag_xAu_{25-x} clusters were successfully synthesized using the co-reduction method. The presence of the dopant was confirmed by several analytical methods, such as UV-VIS and MALDI. A possible aggregation after deposition was discarded, given that the HAADF-STEM and DRS measurements confirmed the size to be 1-2 nanometers for all the supports. In the catalytic test for the liquid phase oxidation the TiO_2 supported clusters gave the best values, followed by the zeolites. For this support, silver doped clusters lead to lower activity than pure gold but a higher selectivity for the desired products. Between the two zeolites employed, the best results obtain for the silicate zeolites, as they lead to a higher conversion for the cyclohexane oxidation reaction than the conventional SiO_2.

The CO oxidation catalytic measurements in gas phase, $Au_{25}(SR)_{18}$ and $Ag_xAu_{25-x}(SR)_{18}$ supported on SiO_2 ʻshowed no catalytic activity in the oxidation of CO. With $Ag_xAu_{25-x}(SR)_{18}$ supported on TiO_2, a CO conversion of around 10% was observed at 250°C— lower than the undoped clusters. This could be ascribed to lower stability under reaction conditions.

5. Appendix

Figure 6-78 and 6-79 shows the quantification of cyclohexanol and cyclohexanone time resolved.
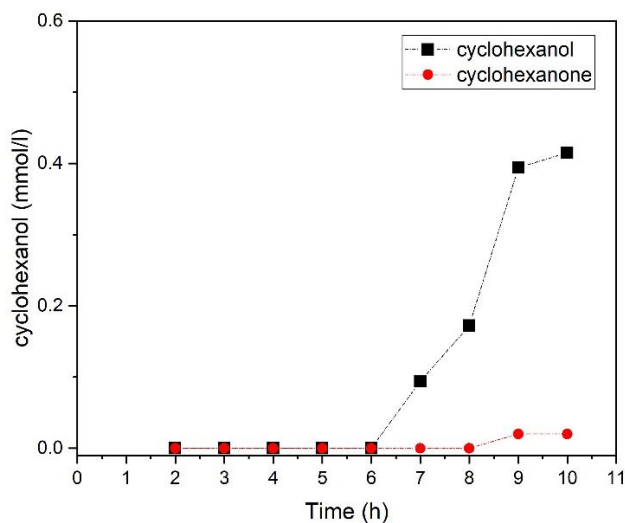
Figure 6-78 $Ag_xAu_{25-x}(SR)_{18}/TiO_2$: concentration of cyclohexanol and cyclohexanone over the reaction time
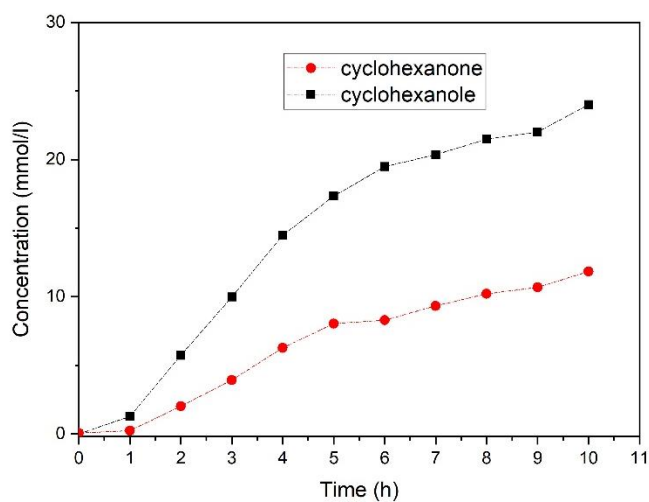
Figure 6-79 $Ag_xAu_{25-x}(SR)_{18}/SiO_2$: concentration of cyclohexanol and cyclohexanone over the reaction time

References

[1] G. Rupprechter, Sum Frequency Generation and Polarization–Modulation Infrared Reflection Absorption Spectroscopy of Functioning Model Catalysts from Ultrahigh Vacuum to Ambient Pressure, in: B.C. Gates, H. Knözinger (Eds.) Advances in Catalysis, Academic Press2007, pp. 133-263.

[2] J. Silvestre-Albero, G. Rupprechter, H.-J. Freund, From Pd nanoparticles to single crystals: 1,3-butadiene hydrogenation on well-defined model catalysts, Chemical Communications, (2006) 80-82.

[3] G. Schmid, The relevance of shape and size of Au55 clusters, Chemical Society Reviews, 37 (2008) 1909-1930.

[4] V. Sudheeshkumar, K.O. Sulaiman, R.W.J. Scott, Activation of atom-precise clusters for catalysis, Nanoscale Advances, 2 (2020) 55-69.

[5] Y. Suchorski, S.M. Kozlov, I. Bespalov, M. Datler, D. Vogel, Z. Budinska, K.M. Neyman, G. Rupprechter, The role of metal/oxide interfaces for long-range metal particle activation during CO oxidation, Nature Materials, 17 (2018) 519-522.

[6] A. Shivhare, S.J. Ambrose, H.X. Zhang, R.W. Purves, R.W.J. Scott, Stable and recyclable Au-25 clusters for the reduction of 4-nitrophenol, Chemical Communications, 49 (2013) 276-278.

[7] H.F. Qian, R.C. Jin, Ambient Synthesis of Au-144(SR)(60) Nanoclusters in Methanol, Chemistry of Materials, 23 (2011) 2209-2217.

[8] M. Brust, M. Walker, D. Bethell, D.J. Schiffrin, R. Whyman, Synthesis of Thiol-Derivatized Gold Nanoparticles in a 2-Phase Liquid-Liquid System, Journal of the Chemical Society-Chemical Communications, (1994) 801-802.

[9] A. Sels, N. Barrabes, S. Knoppe, T. Burgi, Isolation of atomically precise mixed ligand shell PdAu24 clusters, Nanoscale, 8 (2016) 11130-11135.

[10] A. Sels, G. Salassa, S. Pollitt, C. Guglieri, G. Rupprechter, N. Barrabés, T. Bürgi, Structural Investigation of the Ligand Exchange Reaction with Rigid Dithiol on Doped (Pt, Pd) Au25 Clusters, The Journal of Physical Chemistry C, 121 (2017) 10919-10926.

[11] L.X. Yuan, X.P. Qiu, L.Q. Chen, W.T. Zhu, New insight into the discharge process of sulfur cathode by electrochemical impedance spectroscopy, J Power Sources, 189 (2009) 127-132.

[12] N. Barrabés, B. Zhang, T. Bürgi, Racemization of Chiral Pd2Au36(SC2H4Ph)24: Doping Increases the Flexibility of the Cluster Surface, Journal of the American Chemical Society, 136 (2014) 14361-14364.

[13] Y. Negishi, K. Igarashi, K. Munakata, W. Ohgake, K. Nobusada, Palladium doping of magic gold cluster Au38(SC2H4Ph)24: formation of Pd2Au36(SC2H4Ph)24 with higher stability than Au38(SC2H4Ph)24, Chemical Communications, 48 (2012) 660-662.

[14] E. Gottlieb, H. Qian, R. Jin, Atomic-Level Alloying and De-alloying in Doped Gold Nanoparticles, Chem. Eur. J., 19 (2013) 4238 - 4243.

[15] C. Gautier, R. Taras, S. Gladiali, T. Bürgi, Chiral 1,1'-binaphthyl-2,2'-dithiol-stabilized gold clusters: Size separation and optical activity in the UV–vis, Chirality, 20 (2008) 486-493.

[16] W. Li, Q. Ge, X. Ma, Y. Chen, M. Zhu, H. Xu, R. Jin, Mild activation of CeO2-supported gold nanoclusters and insight into the catalytic behavior in CO oxidation, Nanoscale, 8 (2016) 2378-2385.

[17] J.H. Scofield, Hartree-Slater Subshell Photoionization Cross-Sections at 1254 and 1487ev, J Electron Spectrosc, 8 (1976) 129-137.

[18] Y.M. Liu, H. Tsunoyama, T. Akita, S.H. Xie, T. Tsukuda, Aerobic Oxidation of Cyclohexane Catalyzed by Size-Controlled Au Clusters on Hydroxyapatite: Size Effect in the Sub-2 nm Regime, Acs Catalysis, 1 (2011) 2-6.

[19] L.X. Xu, C.H. He, M.Q. Zhu, S. Fang, A highly active Au/Al2O3 catalyst for cyclohexane oxidation using molecular oxygen, Catalysis Letters, 114 (2007) 202-205.

[20] J.L. Campbell, T. Papp, WIDTHS OF THE ATOMIC K–N7 LEVELS, Atomic Data and Nuclear Data Tables, 77 (2001) 1-56.

[21] B. Ravel, M. Newville, ATHENA, ARTEMIS, HEPHAESTUS: data analysis for X-ray absorption spectroscopy using IFEFFIT, Journal of Synchrotron Radiation, 12 (2005) 537-541.

[22] J.J. Rehr, R.C. Albers, Theoretical approaches to x-ray absorption fine structure, Reviews of Modern Physics, 72 (2000) 621-654.

[23] M. Haruta, N. Yamada, T. Kobayashi, S. Iijima, Gold catalysts prepared by coprecipitation for low-temperature oxidation of hydrogen and of carbon monoxide, Journal of Catalysis, 115 (1989) 301-309.

[24] S. Takano, T. Tsukuda, Chapter 2 - Controlled Synthesis: Size Control, in: T. Tsukuda, H. Häkkinen (Eds.) Frontiers of Nanoscience, Elsevier2015, pp. 9-38.

[25] R.R. Nasaruddin, T. Chen, N. Yan, J. Xie, Roles of thiolate ligands in the synthesis, properties and catalytic application of gold nanoclusters, Coordination Chemistry Reviews, 368 (2018) 60-79.

[26] R.C. Jin, C.J. Zeng, M. Zhou, Y.X. Chen, Atomically Precise Colloidal Metal Nanoclusters and Nanoparticles: Fundamentals and Opportunities, Chemical Reviews, 116 (2016) 10346-10413.

[27] Q. Yao, T. Chen, X. Yuan, J. Xie, Toward Total Synthesis of Thiolate-Protected Metal Nanoclusters, Accounts of Chemical Research, 51 (2018) 1338-1348.

[28] Q. Yao, X. Yuan, T. Chen, D.T. Leong, J. Xie, Metal Nanoclusters: Engineering Functional Metal Materials at the Atomic Level (Adv. Mater. 47/2018), Advanced Materials, 30 (2018) 1870358.

[29] Z. Ma, P. Wang, L. Xiong, Y. Pei, Thiolate-protected gold nanoclusters: structural prediction and the understandings of electronic stability from first principles simulations, Wiley Interdisciplinary Reviews: Computational Molecular Science, 7 (2017) e1315.

[30] Y. Negishi, T. Nakazaki, S. Malola, S. Takano, Y. Niihori, W. Kurashige, S. Yamazoe, T. Tsukuda, H. Häkkinen, A Critical Size for Emergence of Nonbulk Electronic and Geometric Structures in Dodecanethiolate-Protected Au Clusters, Journal of the American Chemical Society, 137 (2015) 1206-1212.

[31] J. Zhao, R. Jin, Heterogeneous catalysis by gold and gold-based bimetal nanoclusters, Nano Today, 18 (2018) 86-102.

[32] X.-K. Wan, J.-Q. Wang, Z.-A. Nan, Q.-M. Wang, Ligand effects in catalysis by atomically precise gold nanoclusters, Science Advances, 3 (2017).

[33] G. Li, R. Jin, Atomically Precise Gold Nanoclusters as New Model Catalysts, Accounts of Chemical Research, 46 (2013) 1749-1758.

[34] M. Valden, X. Lai, D.W. Goodman, Onset of Catalytic Activity of Gold Clusters on Titania with the Appearance of Nonmetallic Properties, Science, 281 (1998) 1647-1650.

[35] O. Lopez-Acevedo, K.A. Kacprzak, J. Akola, H. Häkkinen, Quantum size effects in ambient CO oxidation catalysed by ligand-protected gold clusters, Nat Chem, 2 (2010) 329-334.

[36] Y. Zhang, P. Song, T. Chen, X. Liu, T. Chen, Z. Wu, Y. Wang, J. Xie, W. Xu, Unique size-dependent nanocatalysis revealed at the single atomically precise gold cluster level, Proceedings of the National Academy of Sciences, 115 (2018) 10588-10593.

[37] S. Yamazoe, K. Koyasu, T. Tsukuda, Nonscalable Oxidation Catalysis of Gold Clusters, Accounts of Chemical Research, 47 (2014) 816-824.

[38] P. Maity, S.H. Xie, M. Yamauchi, T. Tsukuda, Stabilized gold clusters: from isolation toward controlled synthesis, Nanoscale, 4 (2012) 4027-4037.

[39] R. Zhao, D. Ji, G. Lv, G. Qian, L. Yan, X. Wang, J. Suo, A highly efficient oxidation of cyclohexane over Au/ZSM-5 molecular sieve catalyst with oxygen as oxidant, Chemical Communications, (2004) 904-905.

[40] G. Lü, R. Zhao, G. Qian, Y. Qi, X. Wang, J. Suo, A Highly Efficient Catalyst Au/MCM-41 for Selective Oxidation Cyclohexane Using Oxygen, Catalysis Letters, 97 (2004) 115-118.

[41] L.-X. Xu, C.-H. He, M.-Q. Zhu, S. Fang, A highly active Au/Al2O3 catalyst for cyclohexane oxidation using molecular oxygen, Catalysis Letters, 114 (2007) 202-205.

[42] B.P.C. Hereijgers, B.M. Weckhuysen, Aerobic oxidation of cyclohexane by gold-based catalysts: New mechanistic insight by thorough product analysis, Journal of Catalysis, 270 (2010) 16-25.

[43] P. Wu, P. Bai, Z. Yan, G.X.S. Zhao, Gold nanoparticles supported on mesoporous silica: origin of high activity and role of Au NPs in selective oxidation of cyclohexane, Scientific Reports, 6 (2016) 18817.

[44] S. Yamazoe, T. Yoskamtorn, S. Takano, S. Yadnum, J. Limtrakul, T. Tsukuda, Controlled Synthesis of Carbon-Supported Gold Clusters for Rational Catalyst Design, The Chemical Record, 16 (2016) 2338-2348.

[45] T. Yoskamtorn, S. Yamazoe, R. Takahata, J. Nishigaki, A. Thivasasith, J. Limtrakul, T. Tsukuda, Thiolate-Mediated Selectivity Control in Aerobic Alcohol Oxidation by Porous Carbon-Supported Au-25 Clusters, Acs Catalysis, 4 (2014) 3696-3700.

[46] M.W. Heaven, A. Dass, P.S. White, K.M. Holt, R.W. Murray, Crystal Structure of the Gold Nanoparticle [N(C8H17)4][Au25(SCH2CH2Ph)18], Journal of the American Chemical Society, 130 (2008) 3754-3755.

[47] M. Zhu, C.M. Aikens, F.J. Hollander, G.C. Schatz, R. Jin, Correlating the Crystal Structure of A Thiol-Protected Au25 Cluster and Optical Properties, Journal of the American Chemical Society, 130 (2008) 5883-5885.

[48] O. Lopez-Acevedo, J. Akola, R.L. Whetten, H. Grönbeck, H. Häkkinen, Structure and Bonding in the Ubiquitous Icosahedral Metallic Gold Cluster Au144(SR)60, The Journal of Physical Chemistry C, 113 (2009) 5035-5038.

[49] K.M.Ø. Jensen, P. Juhas, M.A. Tofanelli, C.L. Heinecke, G. Vaughan, C.J. Ackerson, S.J.L. Billinge, Polymorphism in magic-sized Au144(SR)60 clusters, Nature Communications, 7 (2016) 11859.

[50] J. Fang, B. Zhang, Q. Yao, Y. Yang, J. Xie, N. Yan, Recent advances in the synthesis and catalytic applications of ligand-protected, atomically precise metal nanoclusters, Coordination Chemistry Reviews, 322 (2016) 1-29.

[51] B. Zhang, S. Kaziz, H. Li, M.G. Hevia, D. Wodka, C. Mazet, T. Burgi, N. Barrabes, Modulation of Active Sites in Supported Au-38(SC2H4Ph)(24) Cluster Catalysts: Effect of Atmosphere and Support Material, Journal of Physical Chemistry C, 119 (2015) 11193-11199.

[52] J. Fang, J.G. Li, B. Zhang, X. Yuan, H. Asakura, T. Tanaka, K. Teramura, J.P. Xie, N. Yan, The support effect on the size and catalytic activity of thiolated Au-25 nanoclusters as precatalysts, Nanoscale, 7 (2015) 6325-6333.

[53] G. Ma, A. Binder, M. Chi, C. Liu, R. Jin, D.-e. Jiang, J. Fan, S. Dai, Stabilizing gold clusters by heterostructured transition-metal oxide–mesoporous silica supports for enhanced catalytic activities for CO oxidation, Chemical Communications, 48 (2012) 11413-11415.

[54] S. Das, A. Goswami, M. Hesari, J.F. Al-Sharab, E. Mikmeková, F. Maran, T. Asefa, Reductive Deprotection of Monolayer Protected Nanoclusters: An Efficient Route to Supported Ultrasmall Au Nanocatalysts for Selective Oxidation, Small, 10 (2014) 1473-1478.

[55] A. Shivhare, D.M. Chevrier, R.W. Purves, R.W.J. Scott, Following the Thermal Activation of Au-25(SR)(18) Clusters for Catalysis by X-ray Absorption Spectroscopy, Journal of Physical Chemistry C, 117 (2013) 20007-20016.

[56] B. Zhang, O.V. Safonova, S. Pollitt, G. Salassa, A. Sels, R. Kazan, Y. Wang, G. Rupprechter, N. Barrabés, T. Bürgi, On the mechanism of rapid metal exchange between thiolate-protected gold and gold/silver clusters: a time-resolved in situ XAFS study, Physical Chemistry Chemical Physics, 20 (2018) 5312-5318.

[57] H. Murayama, N. Ichikuni, Y. Negishi, T. Nagata, T. Tsukuda, EXAFS study on interfacial structure between Pd cluster and n-octadecanethiolate monolayer: formation of mixed Pd-S interlayer, Chem. Phys. Lett., 376 (2003) 26-32.

[58] S. Yamazoe, W. Kurashige, K. Nobusada, Y. Negishi, T. Tsukuda, Preferential Location of Coinage Metal Dopants (M = Ag or Cu) in [Au25-XMX(SC2H4Ph)(18)](-) (x similar to 1) As Determined by Extended X-ray Absorption Fine Structure and Density Functional Theory Calculations, Journal of Physical Chemistry C, 118 (2014) 25284-25290.

[59] B. Zhang, S. Kaziz, H.H. Li, D. Wodka, S. Malola, O. Safonova, M. Nachtegaal, C. Mazet, I. Dolamic, J. Llorca, E. Kalenius, L.M.L. Daku, H. Hakkinen, T. Burgi, N. Barrabes, Pd2Au36(SR)(24) cluster: structure studies, Nanoscale, 7 (2015) 17012-17019.

[60] S. Yamazoe, S. Takano, W. Kurashige, T. Yokoyama, K. Nitta, Y. Negishi, T. Tsukuda, Hierarchy of bond stiffnesses within icosahedral-based gold clusters protected by thiolates, Nature Communications, 7 (2016) 10414.

[61] P. Zhang, X-ray Spectroscopy of Gold–Thiolate Nanoclusters, The Journal of Physical Chemistry C, 118 (2014) 25291-25299.

[62] P. Glatzel, T.-C. Weng, K. Kvashnina, J. Swarbrick, M. Sikora, E. Gallo, N. Smolentsev, R.A. Mori, Reflections on hard X-ray photon-in/photon-out spectroscopy for electronic structure studies, Journal of Electron Spectroscopy and Related Phenomena, 188 (2013) 17-25.

[63] M. Zhou, C.J. Zeng, Y.X. Chen, S. Zhao, M.Y. Sfeir, M.Z. Zhu, R.C. Jin, Evolution from the plasmon to exciton state in ligand-protected atomically precise gold nanoparticles, Nature Communications, 7 (2016).

[64] S. Malola, L. Lehtovaara, J. Enkovaara, H. Hakkinen, Birth of the Localized Surface Plasmon Resonance in Mono layer-Protected Gold Nanoclusters, Acs Nano, 7 (2013) 10263-10270.

[65] D.P. Anderson, R.H. Adnan, J.F. Alvino, O. Shipper, B. Donoeva, J.Y. Ruzicka, H. Al Qahtani, H.H. Harris, B. Cowie, J.B. Aitken, V.B. Golovko, G.F. Metha, G.G. Andersson, Chemically synthesised atomically precise gold clusters deposited and activated on titania. Part II, Physical Chemistry Chemical Physics, 15 (2013) 14806-14813.

[66] Contributors, in: T. Tsukuda, H. Häkkinen (Eds.) Frontiers of Nanoscience, Elsevier2015, pp. xi-xii.

[67] L.-X. Xu, C.-H. He, M.-Q. Zhu, K.-J. Wu, Y.-L. Lai, Silica-Supported Gold Catalyst Modified by Doping with Titania for Cyclohexane Oxidation, Catalysis Letters, 118 (2007) 248-253.

[68] P.P. Wu, P. Bai, Z.F. Yan, G.X.S. Zhao, Gold nanoparticles supported on mesoporous silica: origin of high activity and role of Au NPs in selective oxidation of cyclohexane, Scientific Reports, 6 (2016).

[69] A.R. Almeida, J.A. Moulijn, G. Mul, In Situ ATR-FTIR Study on the Selective Photo-oxidation of Cyclohexane over Anatase TiO2, The Journal of Physical Chemistry C, 112 (2008) 1552-1561.

[70] A.R. Almeida, R. Berger, J.A. Moulijn, G. Mul, Photo-catalytic oxidation of cyclohexane over TiO2: a novel interpretation of temperature dependent performance, Physical Chemistry Chemical Physics, 13 (2011) 1345-1355.

[71] Tables of molecular vibrational frequencies. Consolidated volume II, Journal of Physical and Chemical Reference Data, 6 (1977) 993-1102.

[72] G. Socrates, Infrared and Raman Characteristic Group Frequencies: Tables and Charts, Wiley2004.

[73] A.N. Mansour, J.W. Cook, D.E. Sayers, Quantitative technique for the determination of the number of unoccupied d-electron states in a platinum catalyst using the L2,3 x-ray absorption edge spectra, The Journal of Physical Chemistry, 88 (1984) 2330-2334.

[74] A. Pantelouris, G. Kueper, J. Hormes, C. Feldmann, M. Jansen, Anionic Gold in Cs3AuO and Rb3AuO Established by X-ray Absorption Spectroscopy, Journal of the American Chemical Society, 117 (1995) 11749-11753.

[75] M.F. Lengke, B. Ravel, M.E. Fleet, G. Wanger, R.A. Gordon, G. Southam, Mechanisms of Gold Bioaccumulation by Filamentous Cyanobacteria from Gold(III)–Chloride Complex, Environmental Science & Technology, 40 (2006) 6304-6309.

[76] P. Zhang, T.K. Sham, Tuning the electronic behavior of Au nanoparticles with capping molecules, Applied Physics Letters, 81 (2002) 736-738.

[77] P. Zhang, T.K. Sham, X-Ray Studies of the Structure and Electronic Behavior of Alkanethiolate-Capped Gold Nanoparticles: The Interplay of Size and Surface Effects, Physical Review Letters, 90 (2003) 245502.

[78] J.A. van Bokhoven, J.T. Miller, d Electron Density and Reactivity of the d Band as a Function of Particle Size in Supported Gold Catalysts, The Journal of Physical Chemistry C, 111 (2007) 9245-9249.

[79] J.A. van Bokhoven, C. Louis, J.T. Miller, M. Tromp, O.V. Safonova, P. Glatzel, Activation of oxygen on gold/alumina catalysts: in situ high-energy-resolution fluorescence and time-resolved X-ray spectroscopy, Angew Chem Int Ed Engl, 45 (2006) 4651-4654.

[80] T. Ishida, T. Murayama, A. Taketoshi, M. Haruta, Importance of Size and Contact Structure of Gold Nanoparticles for the Genesis of Unique Catalytic Processes, Chemical Reviews, 120 (2020) 464-525.

[81] M. Sankar, Q. He, R.V. Engel, M.A. Sainna, A.J. Logsdail, A. Roldan, D.J. Willock, N. Agarwal, C.J. Kiely, G.J. Hutchings, Role of the Support in Gold-Containing Nanoparticles as Heterogeneous Catalysts, Chemical Reviews, 120 (2020) 3890-3938.

[82] L. Liu, A. Corma, Metal Catalysts for Heterogeneous Catalysis: From Single Atoms to Nanoclusters and Nanoparticles, Chemical Reviews, 118 (2018) 4981-5079.

[83] M. Stratakis, H. Garcia, Catalysis by Supported Gold Nanoparticles: Beyond Aerobic Oxidative Processes, Chemical Reviews, 112 (2012) 4469-4506.

[84] T. Tsukuda, H. Häkkinen, Chapter 1 - Introduction, in: T. Tsukuda, H. Häkkinen (Eds.) Frontiers of Nanoscience, Elsevier2015, pp. 1-7.

[85] Y. Du, H. Sheng, D. Astruc, M. Zhu, Atomically Precise Noble Metal Nanoclusters as Efficient Catalysts: A Bridge between Structure and Properties, Chemical Reviews, 120 (2020) 526-622.

[86] Y. Negishi, W. Kurashige, Y. Niihori, T. Iwasa, K. Nobusada, Isolation, structure, and stability of a dodecanethiolate-protected Pd1Au24 cluster, Physical Chemistry Chemical Physics, 12 (2010) 6219-6225.

[87] S. Sharma, S. Yamazoe, T. Ono, W. Kurashige, Y. Niihori, K. Nobusada, T. Tsukuda, Y. Negishi, Tuning the electronic structure of thiolate-protected 25-atom clusters by co-substitution with metals having different preferential sites, Dalton Transactions, 45 (2016) 18064-18068.

[88] S. Yamazoe, W. Kurashige, K. Nobusada, Y. Negishi, T. Tsukuda, Preferential Location of Coinage Metal Dopants (M = Ag or Cu) in [Au25–xMx(SC2H4Ph)18]− (x ∼ 1) As Determined by Extended X-ray Absorption Fine Structure and Density Functional Theory Calculations, The Journal of Physical Chemistry C, 118 (2014) 25284-25290.

[89] M.A. Tofanelli, T.W. Ni, B.D. Phillips, C.J. Ackerson, Crystal Structure of the PdAu24(SR)180 Superatom, Inorganic Chemistry, 55 (2016) 999-1001.

[90] S. Hossain, Y. Niihori, L.V. Nair, B. Kumar, W. Kurashige, Y. Negishi, Alloy Clusters: Precise Synthesis and Mixing Effects, Accounts of Chemical Research, 51 (2018) 3114-3124.

[91] K.R. Krishnadas, A. Ghosh, A. Baksi, I. Chakraborty, G. Natarajan, T. Pradeep, Intercluster Reactions between Au25(SR)18 and Ag44(SR)30, Journal of the American Chemical Society, 138 (2016) 140-148.

[92] K.R. Krishnadas, A. Baksi, A. Ghosh, G. Natarajan, T. Pradeep, Structure-conserving spontaneous transformations between nanoparticles, Nature Communications, 7 (2016) 13447.

[93] K.R. Krishnadas, A. Baksi, A. Ghosh, G. Natarajan, A. Som, T. Pradeep, Interparticle Reactions: An Emerging Direction in Nanomaterials Chemistry, Accounts of Chemical Research, 50 (2017) 1988-1996.

[94] K.R. Krishnadas, D. Ghosh, A. Ghosh, G. Natarajan, T. Pradeep, Structure–Reactivity Correlations in Metal Atom Substitutions of Monolayer-Protected Noble Metal Alloy Clusters, The Journal of Physical Chemistry C, 121 (2017) 23224-23232.

[95] K.R. Krishnadas, A. Baksi, A. Ghosh, G. Natarajan, T. Pradeep, Manifestation of Geometric and Electronic Shell Structures of Metal Clusters in Intercluster Reactions, ACS Nano, 11 (2017) 6015-6023.

[96] K.R. Krishnadas, G. Natarajan, A. Baksi, A. Ghosh, E. Khatun, T. Pradeep, Metal–Ligand Interface in the Chemical Reactions of Ligand-Protected Noble Metal Clusters, Langmuir, 35 (2019) 11243-11254.

[97] A. Baksi, E.K. Schneider, P. Weis, K.R. Krishnadas, D. Ghosh, H. Hahn, T. Pradeep, M.M. Kappes, Nanogymnastics: Visualization of Intercluster Reactions by High-Resolution Trapped Ion Mobility Mass Spectrometry, The Journal of Physical Chemistry C, 123 (2019) 28477-28485.

[98] E. Khatun, P. Chakraborty, B.R. Jacob, G. Paramasivam, M. Bodiuzzaman, W.A. Dar, T. Pradeep, Intercluster Reactions Resulting in Silver-Rich Trimetallic Nanoclusters, Chemistry of Materials, 32 (2020) 611-619.

[99] B. Zhang, G. Salassa, T. Bürgi, Silver migration between Au38(SC2H4Ph)24 and doped AgxAu38−x(SC2H4Ph)24 nanoclusters, Chemical Communications, 52 (2016) 9205-9207.

[100] Y. Niihori, S. Hashimoto, Y. Koyama, S. Hossain, W. Kurashige, Y. Negishi, Dynamic Behavior of Thiolate-Protected Gold–Silver 38-Atom Alloy Clusters in Solution, The Journal of Physical Chemistry C, 123 (2019) 13324-13329.

[101] R. Kazan, U. Müller, T. Bürgi, Doping of thiolate protected gold clusters through reaction with metal surfaces, Nanoscale, 11 (2019) 2938-2945.

[102] Y. Li, M. Chen, S. Wang, M. Zhu, Intramolecular Metal Exchange Reaction Promoted by Thiol Ligands, Nanomaterials, 8 (2018) 1070.

[103] H. Deng, S. Wang, S. Jin, S. Yang, Y. Xu, L. Liu, J. Xiang, D. Hu, M. Zhu, Active metal (cadmium) doping enhanced the stability of inert metal (gold) nanocluster under O2 atmosphere and the catalysis activity of benzyl alcohol oxidation, Gold Bulletin, 48 (2015) 161-167.

[104] K. Kwak, Q. Tang, M. Kim, D.-e. Jiang, D. Lee, Interconversion between Superatomic 6-Electron and 8-Electron Configurations of M@Au24(SR)18 Clusters (M = Pd, Pt), Journal of the American Chemical Society, 137 (2015) 10833-10840.

[105] H. Qian, D.-e. Jiang, G. Li, C. Gayathri, A. Das, R.R. Gil, R. Jin, Monoplatinum Doping of Gold Nanoclusters and Catalytic Application, Journal of the American Chemical Society, 134 (2012) 16159-16162.

[106] W. Kurashige, R. Hayashi, K. Wakamatsu, Y. Kataoka, S. Hossain, A. Iwase, A. Kudo, S. Yamazoe, Y. Negishi, Atomic-Level Understanding of the Effect of Heteroatom Doping of the Cocatalyst on Water-Splitting Activity in AuPd or AuPt Alloy Cluster-Loaded BaLa4Ti4O15, ACS Applied Energy Materials, 2 (2019) 4175-4187.

[107] K. Kwak, W. Choi, Q. Tang, M. Kim, Y. Lee, D.-e. Jiang, D. Lee, A molecule-like PtAu24(SC6H13)18 nanocluster as an electrocatalyst for hydrogen production, Nature Communications, 8 (2017) 14723.

[108] S. Xie, H. Tsunoyama, W. Kurashige, Y. Negishi, T. Tsukuda, Enhancement in Aerobic Alcohol Oxidation Catalysis of Au25 Clusters by Single Pd Atom Doping, ACS Catalysis, 2 (2012) 1519-1523.

[109] B. Kumar, T. Kawawaki, N. Shimizu, Y. Imai, D. Suzuki, S. Hossain, L.V. Nair, Y. Negishi, Gold nanoclusters as electrocatalysts: size, ligands, heteroatom doping, and charge dependences, Nanoscale, (2020).

[110] F. Gao, D.W. Goodman, Pd–Au bimetallic catalysts: understanding alloy effects from planar models and (supported) nanoparticles, Chem. Soc. Rev., 41 (2012) 8009-8020.

[111] M. Chen, D. Kumar, C.-W. Yi, D.W. Goodman, The Promotional Effect of Gold in Catalysis by Palladium-Gold, Science, 310 (2005) 291-293.

[112] T. Balcha, J.R. Strobl, C. Fowler, P. Dash, R.W.J. Scott, Selective Aerobic Oxidation of Crotyl Alcohol Using AuPd Core-Shell Nanoparticles, ACS Catalysis, 1 (2011) 425-436.

[113] K.E. Lee, A. Shivhare, Y. Hu, R.W.J. Scott, Supported bimetallic AuPd clusters using activated Au25 clusters, Catalysis Today, 280 (2017) 259-265.

[114] S. Hayashi, R. Ishida, S. Hasegawa, S. Yamazoe, T. Tsukuda, Doping a Single Palladium Atom into Gold Superatoms Stabilized by PVP: Emergence of Hydrogenation Catalysis, Topics in Catalysis, 61 (2018) 136-141.

[115] A. Shivhare, R.W.J. Scott, Au25 clusters as precursors for the synthesis of AuPd bimetallic nanoparticles with isolated atomic Pd-surface sites, Molecular Catalysis, 457 (2018) 33-40.

[116] A. Shivhare, K.E. Lee, Y. Hu, R.W.J. Scott, Following the Reactivity of Au25(SC8H9)18– Clusters with Pd2+ and Ag+ Ions Using in Situ X-ray Absorption Spectroscopy: A Tale of Two Metals, The Journal of Physical Chemistry C, 119 (2015) 23279-23284.

[117] J. Timoshenko, A. Shivhare, R.W.J. Scott, D. Lu, A.I. Frenkel, Solving local structure around dopants in metal nanoparticles with ab initio modeling of X-ray absorption near edge structure, Physical Chemistry Chemical Physics, 18 (2016) 19621-19630.

[118] M.M. Schubert, S. Hackenberg, A.C. van Veen, M. Muhler, V. Plzak, R.J. Behm, CO Oxidation over Supported Gold Catalysts—"Inert" and "Active" Support Materials and Their Role for the Oxygen Supply during Reaction, Journal of Catalysis, 197 (2001) 113-122.

[119] M.A. Bollinger, M.A. Vannice, A kinetic and DRIFTS study of low-temperature carbon monoxide oxidation over Au—TiO2 catalysts, Applied Catalysis B: Environmental, 8 (1996) 417-443.

[120] X. Nie, C. Zeng, X. Ma, H. Qian, Q. Ge, H. Xu, R. Jin, CeO2-supported Au38(SR)24 nanocluster catalysts for CO oxidation: a comparison of ligand-on and -off catalysts, Nanoscale, 5 (2013) 5912-5918.

[121] X. Nie, H. Qian, Q. Ge, H. Xu, R. Jin, CO Oxidation Catalyzed by Oxide-Supported Au25(SR)18 Nanoclusters and Identification of Perimeter Sites as Active Centers, ACS Nano, 6 (2012) 6014-6022.

[122] J. Good, P.N. Duchesne, P. Zhang, W. Koshut, M. Zhou, R. Jin, On the functional role of the cerium oxide support in the Au38(SR)24/CeO2 catalyst for CO oxidation, Catalysis Today, 280 (2017) 239-245.

[123] Z. Wu, D.-e. Jiang, A.K.P. Mann, D.R. Mullins, Z.-A. Qiao, L.F. Allard, C. Zeng, R. Jin, S.H. Overbury, Thiolate Ligands as a Double-Edged Sword for CO Oxidation on CeO2 Supported Au25(SCH2CH2Ph)18 Nanoclusters, Journal of the American Chemical Society, 136 (2014) 6111-6122.

[124] Y. Li, Y. Chen, S.D. House, S. Zhao, Z. Wahab, J.C. Yang, R. Jin, Interface Engineering of Gold Nanoclusters for CO Oxidation Catalysis, ACS Applied Materials & Interfaces, 10 (2018) 29425-29434.

[125] W. Li, C. Liu, H. Abroshan, Q. Ge, X. Yang, H. Xu, G. Li, Catalytic CO Oxidation Using Bimetallic MxAu25–x Clusters: A Combined Experimental and Computational Study on Doping Effects, The Journal of Physical Chemistry C, 120 (2016) 10261-10267.

[126] F. Gao, Y. Wang, D.W. Goodman, CO Oxidation over AuPd(100) from Ultrahigh Vacuum to Near-Atmospheric Pressures: CO Adsorption-Induced Surface Segregation and Reaction Kinetics, The Journal of Physical Chemistry C, 113 (2009) 14993-15000.

[127] C. García, S. Pollitt, M. van der Linden, V. Truttmann, C. Rameshan, R. Rameshan, E. Pittenauer, G. Allmaier, P. Kregsamer, M. Stöger-Pollach, N. Barrabés, G. Rupprechter, Support effect on the reactivity and stability of Au25(SR)18 and Au144(SR)60 nanoclusters in liquid phase cyclohexane oxidation, Catalysis Today, 336 (2019) 174-185.

[128] S. Pollitt, V. Truttmann, T. Haunold, C. Garcia, W. Olszewski, J. Llorca, N. Barrabes, G. Rupprechter, The Dynamic Structure of Au38(SR)24 Nanoclusters Supported on CeO2 upon Pretreatment and CO Oxidation, ACS Catal., (2020).

[129] G. Tofighi, X. Yu, H. Lichtenberg, D.E. Doronkin, W. Wang, C. Wöll, Y. Wang, J.-D. Grunwaldt, Chemical Nature of Microfluidically Synthesized AuPd Nanoalloys Supported on TiO2, ACS Catalysis, 9 (2019) 5462-5473.

[130] M. Luneau, E. Guan, W. Chen, A.C. Foucher, N. Marcella, T. Shirman, D.M.A. Verbart, J. Aizenberg, M. Aizenberg, E.A. Stach, R.J. Madix, A.I. Frenkel, C.M. Friend, Enhancing catalytic performance of dilute metal alloy nanomaterials, Commun. Chem., 3 (2020) 46.

[131] B. Zhu, G. Thrimurthulu, L. Delannoy, C. Louis, C. Mottet, J. Creuze, B. Legrand, H. Guesmi, Evidence of Pd segregation and stabilization at edges of AuPd nano-clusters in the presence of CO: A combined DFT and DRIFTS study, Journal of Catalysis, 308 (2013) 272-281.

[132] E.K. Gibson, A.M. Beale, C.R.A. Catlow, A. Chutia, D. Gianolio, A. Gould, A. Kroner, K.M.H. Mohammed, M. Perdjon, S.M. Rogers, P.P. Wells, Restructuring of AuPd Nanoparticles Studied by a Combined XAFS/DRIFTS Approach, Chemistry of Materials, 27 (2015) 3714-3720.

[133] A.V. Bukhtiyarov, I.P. Prosvirin, A.A. Saraev, A.Y. Klyushin, A. Knop-Gericke, V.I. Bukhtiyarov, In situ formation of the active sites in Pd–Au bimetallic nanocatalysts for CO oxidation: NAP (near ambient pressure) XPS and MS study, Farraday Discuss., 208 (2018) 255-268.

[134] B. Zhang, A. Sels, G. Salassa, S. Pollitt, V. Truttmann, C. Rameshan, J. Llorca, W. Olszewski, G. Rupprechter, T. Bürgi, N. Barrabés, Ligand Migration from Cluster to Support: A Crucial Factor for Catalysis by Thiolate-protected Gold Clusters, ChemCatChem, 10 (2018) 5372-5376.

[135] S. Hossain, Y. Imai, D. Suzuki, W. Choi, Z. Chen, T. Suzuki, M. Yoshioka, T. Kawawaki, D. Lee, Y. Negishi, Elucidating ligand effects in thiolate-protected metal clusters using Au24Pt(TBBT)18 as a model cluster, Nanoscale, 11 (2019) 22089-22098.

[136] K. Zorn, S. Giorgio, E. Halwax, C.R. Henry, H. Grönbeck, G. Rupprechter, CO Oxidation on Technological Pd–Al2O3 Catalysts: Oxidation State and Activity, J. Phys. Chem. C, 115 (2011) 1103-1111.

[137] D. Vogel, C. Spiel, Y. Suchorski, A. Trinchero, R. Schlögl, H. Grönbeck, G. Rupprechter, Local Catalytic Ignition during CO Oxidation on Low-Index Pt and Pd Surfaces: A Combined PEEM, MS, and DFT Study, Angew. Chem., Int. Ed., 51 (2012) 10041-10044.

[138] X.T. Nie, H.F. Qian, Q.J. Ge, H.Y. Xu, R.C. Jin, CO Oxidation Catalyzed by Oxide-Supported Au-25(SR)(18) Nanoclusters and Identification of Perimeter Sites as Active Centers, Acs Nano, 6 (2012) 6014-6022.

[139] S. Gaur, Z.L. Wu, G.G. Stanley, C. Kumar, J. Spivey, On the deactivation of Au-38 cluster-derived Au/TiO2 catalyst during CO oxidation, Abstracts of Papers of the American Chemical Society, 244 (2012).

[140] S. Gaur, J.T. Miller, D. Stellwagen, A.S. Ido, C.S.S.R. Jumar, J.J. Spivey, Synthesis of thiol-ligated Au38 clusters supported on titania: Effects of heat treatment on CO oxidation catalyst activity, Abstracts of Papers of the American Chemical Society, 242 (2011).

[141] T. Lear, R. Marshall, J.A. Lopez-Sanchez, S.D. Jackson, T.M. Klapötke, M. Bäumer, G. Rupprechter, H.-J. Freund, D. Lennon, The application of infrared spectroscopy to probe the surface morphology of alumina-supported palladium catalysts, J. Chem. Phys., 123 (2005) 174706.

[142] F. Gao, Y. Wang, D.W. Goodman, Reaction Kinetics and Polarization-Modulation Infrared Reflection Absorption Spectroscopy (PM-IRAS) Investigation of CO Oxidation over Supported Pd–Au Alloy Catalysts, The Journal of Physical Chemistry C, 114 (2010) 4036-4043.

[143] M. García-Mota, N. López, Temperature and pressure effects in CO titration of ensembles in PdAu(111) alloys using first principles, Phys. Rev. B, 82 (2010) 075411.

[144] I.V. Yudanov, R. Sahnoun, K.M. Neyman, N. Rösch, J. Hoffmann, S. Schauermann, V. Johánek, H. Unterhalt, G. Rupprechter, J. Libuda, H.-J. Freund, CO Adsorption on Pd

Nanoparticles: Density Functional and Vibrational Spectroscopy Studies, J. Phys. Chem. B, 107 (2003) 255-264.

[145] B. Hammer, J.K. Nørskov, Theoretical surface science and catalysis—calculations and concepts, Advances in Catalysis, Academic Press2000, pp. 71-129.

[146] X. Zhu, Q. Guo, Y. Sun, S. Chen, J.-Q. Wang, M. Wu, W. Fu, Y. Tang, X. Duan, D. Chen, Y. Wan, Optimising surface d charge of AuPd nanoalloy catalysts for enhanced catalytic activity, Nature Communications, 10 (2019) 1428.

[147] P.A.P. Nascente, S.G.C. de Castro, R. Landers, G.G. Kleiman, X-ray photoemission and Auger energy shifts in some gold-palladium alloys, Phys. Rev. B, 43 (1991) 4659-4666.

[148] F. Liu, D. Wechsler, P. Zhang, Alloy-structure-dependent electronic behavior and surface properties of Au–Pd nanoparticles, Chem. Phys. Lett., 461 (2008) 254-259.

[149] Y. Negishi, W. Kurashige, Y. Kobayashi, S. Yamazoe, N. Kojima, M. Seto, T. Tsukuda, Formation of a Pd@Au12 Superatomic Core in Au24Pd1(SC12H25)18 Probed by 197Au Mössbauer and Pd K-Edge EXAFS Spectroscopy, The Journal of Physical Chemistry Letters, 4 (2013) 3579-3583.

[150] A.I. Frenkel, C.W. Hills, R.G. Nuzzo, A View from the Inside: Complexity in the Atomic Scale Ordering of Supported Metal Nanoparticles, J. Phys. Chem. B, 105 (2001) 12689-12703.

[151] E. Bus, J.A. van Bokhoven, Electronic and Geometric Structures of Supported Platinum, Gold, and Platinum–Gold Catalysts, J. Phys. Chem. C, 111 (2007) 9761-9768.

[152] R. Jin, K. Nobusada, Doping and alloying in atomically precise gold nanoparticles, Nano Research, 7 (2014) 285-300.

[153] C. Garcia, S. Pollitt, M. van der Linden, V. Truttmann, C. Rameshan, R. Rameshan, E. Pittenauer, G. Allmaier, P. Kregsamer, M. Stoger-Pollach, N. Barrabes, G. Rupprechter, Support effect on the reactivity and stability of Au-25(SR)(18) and Au-144(SR)(60) nanoclusters in liquid phase cyclohexane oxidation, Catalysis Today, 336 (2019) 174-185.

[154] G. Tofighi, A. Gaur, D.E. Doronkin, H. Lichtenberg, W. Wang, D. Wang, G. Rinke, A. Ewinger, R. Dittmeyer, J.-D. Grunwaldt, Microfluidic Synthesis of Ultrasmall AuPd Nanoparticles with a Homogeneously Mixed Alloy Structure in Fast Continuous Flow for Catalytic Applications, The Journal of Physical Chemistry C, 122 (2018) 1721-1731.

[155] B. Zhang, S. Kaziz, H. Li, D. Wodka, S. Malola, O. Safonova, M. Nachtegaal, C. Mazet, I. Dolamic, J. Llorca, E. Kalenius, L.M. Lawson Daku, H. Hakkinen, T. Bürgi, N. Barrabés, Pd2Au36(SR)24 cluster: structure studies, Nanoscale, 7 (2015) 17012-17019.

[156] A. Shivhare, S.J. Ambrose, H. Zhang, R.W. Purves, R.W.J. Scott, Stable and recyclable Au25 clusters for the reduction of 4-nitrophenol, Chemical Communications, 49 (2013) 276-278.

[157] L. Wang, Y. Zhou, J. Timoshenko, S. Liu, Q. Qiao, K. Kisslinger, M. Cuiffo, Y.-C. Chuang, X. Zuo, Y. Xue, Y. Guo, C. Pan, H. Li, C.-Y. Nam, S. Bliznakov, P. Liu, A.I. Frenkel, Y. Zhu, M.H. Rafailovich, Designing Nanoplatelet Alloy/Nafion Catalytic Interface for Optimization of PEMFCs: Performance, Durability, and CO Resistance, ACS Catal., 9 (2019) 1446-1456.

[158] D.-e. Jiang, S. Dai, From Superatomic Au25(SR)18− to Superatomic M@Au24(SR)18q Core−Shell Clusters, Inorganic Chemistry, 48 (2009) 2720-2722.

[159] M.A. Tafoughalt, M. Samah, Structural properties and relative stability of silver-doped gold clusters AgAun−1 (n=3–13): Density functional calculations, Computational and Theoretical Chemistry, 1033 (2014) 23-30.

[160] R. Du, S. Tang, X. Wu, Y. Xu, R. Chen, T. Liu, Theoretical study of the structures of bimetallic Ag–Au and Cu–Au clusters up to 108 atoms, Royal Society Open Science, 6 (2019) 190342.

[161] P. Lu, X.-Y. Kuang, A.-J. Mao, Z.-H. Wang, Y.-R. Zhao, Structural and electronic properties of silver-doped gold clusters Au nAgv (2≤n≤10; V = 0,±1): Comparison with pure gold clusters, Molecular Physics, 109 (2011) 2057-2068.

[162] R. Juarez-Mosqueda, S. Malola, H. Häkkinen, Stability, electronic structure, and optical properties of protected gold-doped silver Ag29–xAux (x = 0–5) nanoclusters, Physical Chemistry Chemical Physics, 19 (2017) 13868-13874.

[163] D. Mishra, V. Lobodin, C. Zhang, F. Aldeek, E. Lochner, H. Mattoussi, Gold-doped silver nanoclusters with enhanced photophysical properties, Physical Chemistry Chemical Physics, 20 (2018) 12992-13007.

[164] B. Zhang, T. Bürgi, Doping Silver Increases the Au 38 (SR) 24 Cluster Surface Flexibility, The Journal of Physical Chemistry C, 120 (2016).

[165] S. Malola, H. Häkkinen, Chiral Inversion of Thiolate-Protected Gold Nanoclusters via Core Reconstruction without Breaking a Au-S Bond, J Am Chem Soc, 141 (2019) 6006-6012.

[166] Z. Wang, Z. Zhu, C. Zhao, Q. Yao, X. Li, H. Liu, F. Du, X. Yuan, J. Xie, Silver Doping-Induced Luminescence Enhancement and Red-Shift of Gold Nanoclusters with Aggregation-Induced Emission, Chemistry – An Asian Journal, 14 (2019) 765-769.

[167] J. Haeck, N. Veldeman, E. Janssens, M. Andersson, P. Lievens, Carbon Monoxide Adsorption on Silver Doped Gold Clusters, The journal of physical chemistry. A, 115 (2011) 2103-2109.

[168] N.K. Chaki, H. Tsunoyama, Y. Negishi, H. Sakurai, T. Tsukuda, Effect of Ag-Doping on the Catalytic Activity of Polymer-Stabilized Au Clusters in Aerobic Oxidation of Alcohol, The Journal of Physical Chemistry C, 111 (2007) 4885-4888.

[169] Z. Li, X. Yang, C. Liu, J. Wang, G. Li, Effects of doping in 25-atom bimetallic nanocluster catalysts for carbon–carbon coupling reaction of iodoanisole and phenylacetylene, Progress in Natural Science: Materials International, 26 (2016) 477-482.

[170] S. Wang, Y. Song, S. Jin, X. Liu, J. Zhang, Y. Pei, X. Meng, M. Chen, P. Li, M. Zhu, Metal Exchange Method Using Au25 Nanoclusters as Templates for Alloy Nanoclusters with Atomic Precision, J Am Chem Soc, 137 (2015) 4018-4021.

[171] E.B. Guidez, V. Mäkinen, H. Häkkinen, C.M. Aikens, Effects of Silver Doping on the Geometric and Electronic Structure and Optical Absorption Spectra of the Au25–nAgn(SH)18– (n = 1, 2, 4, 6, 8, 10, 12) Bimetallic Nanoclusters, The Journal of Physical Chemistry C, 116 (2012) 20617-20624.

[172] B. Zhang, T. Bürgi, Doping Silver Increases the Au38(SR)24 Cluster Surface Flexibility, The Journal of Physical Chemistry C, 120 (2016) 4660-4666.

[173] Q. Yao, Y. Feng, V. Fung, Y. Yu, D.-E. Jiang, J. Yang, J. Xie, Precise control of alloying sites of bimetallic nanoclusters via surface motif exchange reaction, Nature communications, 8 (2017) 1555-1555.

[174] Y. Negishi, K. Munakata, W. Ohgake, K. Nobusada, Effect of Copper Doping on Electronic Structure, Geometric Structure, and Stability of Thiolate-Protected Au25 Nanoclusters, The Journal of Physical Chemistry Letters, 3 (2012) 2209-2214.

[175] J. Weitkamp, Zeolites and catalysis, Solid State Ionics, 131 (2000) 175-188.

[176] A. Corma, V. Fornés, J.M. Guil, S. Pergher, T.L.M. Maesen, J.G. Buglass, Preparation, characterisation and catalytic activity of ITQ-2, a delaminated zeolite, Micropor Mesopor Mat, 38 (2000) 301-309.

[177] I. López-Hernández, C. García, V. Truttmann, S. Pollitt, N. Barrabés, G. Rupprechter, F. Rey, A.E. Palomares, Evaluation of the silver species nature in Ag-ITQ2 zeolites by the CO oxidation reaction, Catal Today, 345 (2020) 22-26.

Chapter 7

Conclusions

Conclusions

During this thesis, different cluster sizes were synthesized, namely, $Au_{25}(SR)_{18}$ and $Au_{144}(SR)_{60}$, as well as doped clusters (with palladium and silver doping) and characterized by UV-Vis and MALDI-TOF. The resulting clusters were impreganated on different support materials (TiO_2, SiO_2 and zeolites in the case of silver doped clusters). The resulting catalysts were then characterized using DRS and HAADF-STEM, confirming the well-defined size and monodisperse structure characteristic of these type of clusters. The influence of pretreatment has also been discussed in relation to the HAADF-STEM and DRS results. In order to activate the catalyst for the cyclohexane oxidation reaction, a mild pretreatment at 150°C was found to be optimal in order to partially remove the ligands, thereby preventing aggregation. Regarding CO oxidation in gas phase the optimal pretreatment was found to be a combination of oxidation and reduction (hydrogenation), leading to higher catalytic activity (see Chapter 5).

During the first part of this thesis, size and support effect were studied. In terms of size, the use of Au_{144} results in higher TOF values than Au_{25}, particularly in the case of SiO_2 supported catalysts. In contrast, the use of TiO_2 supported catalysts results in higher KA production than SiO_2 supported ones. The support effect was studied in more detail by in-situ ATR. In the case of titanium oxide, a predominant band emerges at 3538 cm^{-1}, which is attributed to hydroperoxide intermediates. This different in the reaction mechanism may play a big role in catalytic activity enhancement, disclosing the active role of the support in the reaction. In this section, HERFD-XAS measurements were done, revealing a pronounced cluster structure modification towards bulk gold during the reaction. Those changes were more dramatic in the case of Au_{144}/TiO_2, in contrast to a high stability in Au_{144}/SiO_2. Of the two different sized clusters, Au_{144} showed higher stability than Au_{25}.

During the second part, the doping effect was investigated. The effect of palladium doping on cyclohexane oxidation is discussed in Chapter 5, highlighting an enhancement in both catalytic activity and selectivity in the case of SiO_2 supported clusters, and no relevant differences being noted for titanium oxide due to the strong support effect. XAFS analysis demonstrated differences in the stability depending on the support.

In the same chapter, titanium supported PdAu$_{24}$ nanoclusters were also tested in the CO oxidation reaction, showing significantly higher activity than monometallic Au$_{25}$ nanoclusters. In order to understand the catalytic activity enhancement here, in-situ DRIFTS studies were performed. An unexpected contribution of Pd-CO vibrations was detected, indicating migration of the Pd dopant from its original position in the center of the cluster core to the surface during pretreatment and CO oxidation reaction. Moreover, the incorporation of more atoms of Pd to the structure led to the preferential incorporation of Pd in the S-(M-S)n protecting staple motifs of the cluster. A combination of oxidative and reductive thermal pretreatment resulted in the formation of isolated Pd surface sites, which may be the active centres during CO oxidation (as indicated by in-situ XAFS measurements).

In the final chapter, silver doped clusters were supported on TiO$_2$, SiO$_2$ and two types of zeolites (aluminosilicate zeolites and silicate zeolites). For the cyclohexane oxidation reaction, the activity decreases in the order TiO$_2$> silicate Zeolites > SiO$_2$ > aluminosilicate zeolites. For both reactions, a lower catalytic activity is observed for the doped system, while a higher selectivity to the desired products is achieved in the cyclohexane oxidation reaction. In the case of CO oxidation, silver doping leads to a decrease in catalytic activity, possibly due to a stability decrease.

It is hoped that this work will help to better understand the application of thiolate protected gold clusters as catalysts. It has been confirmed that size, support and doping affect both catalytic activity and stability, why these parameters must be taken into account when designing new systems. The evolution of the cluster structure under pretreatment and reaction conditions was monitored, and depended on the oxide material employed as support. Furthermore, mobility of doping atoms inside the structure is also observed, resulting in alloy surfaces with single sites, in the case of Pd doping. Thus, detailed studies under reaction conditions are required in order to determine the active surface configuration in nanocluster catalysts for optimized future applications.

Curriculum vitae

Personal Information

Name:	Clara Isabel Garcia Yago
Address:	Südtirolerplatz 9/24 1040 Wien
E-Mail:	claragarciaviena@gmail.com
D.O.B.:	15 April 1987 in Valencia
Nationality:	Spanish
DNI:	44876292A

Education

Nov 2016 – June 2020	**PhD in Material Chemistry** Topic: "Thiolate protected clusters for catalysis"
2010 – 2013	**Master in Environmental Engineering** Polytechnic University of Valencia.
2006 – 2010	**Bachelor of Chemical Engineering, specialization: Analytical Chemistry,** Polytechnic University of Valencia.

Work Experience

Nov. 2016- June 2020	**University & Project assistant** at the Institute of Materials Chemistry (IMC), Technical University of Vienna, Supervisors: Prof. Günther Rupprechter and Dr. Noelia Barrabes.
April 2015- Nov. 2016	**Quality Specialist** in Dr. Peithner KGB (Medical Product Producer)
August 2014- March 2015	**Laboratory Analyst** in Sandoz, Tirol (International Antibiotic Producer)
March- August 2013	**Internship** in the University of Natural Resources and Life, Tulln an der Donau, Vienna, Austria
Feb. – May. 2012	**Internship** in Environmental Research Centre in Valencia, Spain
Sep. 2010 – Sep. 2011	**Student scholarship** in the Chemical and Nuclear Engineering department (Polytechnic University of Valencia)

Publications

- *Support effect on the reactivity and stability of $Au_{25}(SR)_{18}$ and $Au_{144}(SR)_{60}$ nanoclusters in liquid phase cyclohexane oxidation.*
  C.García, S.Pollitt, M. van der Linden, V.Truttmann, Ch.Rameshan, Raffael Rameshan, E.Pittenauer, G.Allmaier, P. Kregsamer, M.Stöger-Pollach, N.Barrabés*, G.Rupprechter,
  Catalysis Today (2018) DOI: https://doi.org/10.1016/j.cattod.2018.12.013

- *Ligand and support effects on the reactivity and stability of $Au_{38}(SR)_{24}$ catalysts in oxidation reactions.*
  Bei Zhang, Annelies Sels, Giovanni Salassa, Clara García, Christoph Rameshan, Jordi Llorca, Klaudia Hradil , Günther Rupprecht, Noelia Barrabés* and Thomas Bürgi*
  Catalysis Communications (2019) DOI: https://doi.org/10.1016/j.catcom.2019.105768

- *Evaluation of the silver species nature in Ag-ITQ2 zeolites by the CO oxidation reaction.*
  López-Hernández, C. García, V. Truttmann, S. Pollitt, N. Barrabés, G. Rupprechter, F. Rey, A.E. Palomares;
  Catalysis Today, 2019, ISSN 0920-5861, DOI: https://doi.org/10.1016/j.cattod.2019.12.001.

- *The Dynamic Structure of $Au_{38}(SR)_{24}$ Nanoclusters Supported on CeO_2 upon Pretreatment and CO Oxidation*
  Stephan Pollitt, Vera Truttmann, Thomas Haunold, Clara Garcia, Wojciech Olszewski[b], Jordi Llorca, Noelia Barrabés*, Günther Rupprechter
  ACS Catal. 2020, 10, XXX, 6144–6148, https://doi.org/10.1021/acscatal.0c01621

- *Dynamics of Pd atoms inside Au nanoclusters under catalytic CO oxidation reaction conditions*
  Clara Garcia, Vera Truttmann, Irene Lopez, Thomas Haunold, Carlo Marini, Christoph Rameshan, Ernst Pittenauer, Peter Kregsamer, Michael Stöger-Pollach, Noelia Barrabés,* Günther Rupprechter. Manuscript has been submitted to The Journal of Physical Chemistry in June 2020.

Teaching and supervising experience

March 2017-June 2017	"Grundlagen der Chemie und Labortechnik" (Basics of chemistry and laboratory)
Sept. 2017-December 2017	„Physikalische Chemie" (Physical chemistry laboratory)
March 2018-June 2018	"Grundlagen der Chemie und Labortechnik" (Basics of chemistry and laboratory)

Sept. 2018-December 2018   „Physikalische Chemie" (Physical chemistry laboratory)

March 2019-June 2019   "Grundlagen der Chemie und Labortechnik" (Basics of chemistry and laboratory)

Sept. 2019-December 2019   „Physikalische Chemie" (Physical chemistry laboratory)

Student supervision:

- Bachelor Students:
    o Lukas Drexel (October 2018)
    o Dominik Wacht (October 2018)
    o Karim Selmi (April 2019)
    o Adrian Ertl (Oct 2019)
- Praktikum (Ag-Sept 2018):
    o Florian Ehrschwendtner

Conferences and academic activities

Selected Talks

- TU Wien Young Scientist Symposium (VSS 2017) (1 June -2 June 2017)
- 7th Annual PhD Workshop "Functional Oxide Surfaces and Interfaces (FOXSKI)", 31 January - 3 February 2018 at Haus im Ennstal (Styria)
- TU Wien young scientist symposium (VSS 2018) (7 June - 8 June 2018)
- 34th Workshop on Novel Materials and Superconductivity, JUFA Schladming, (10 February – 15 February 2019)
- TU Wien Young Scientist Symposium (VSS 2019) (13 June -14 June 2019)
- 14th European Congress on Catalysis, EuropaCat 2019, to be held in Aachen, Germany, (18 – 23 August, 2019)

Selected posters

- 6th Annual PhD Workshop "Functional Oxide Surfaces and Interfaces (FOXSI)", 1 February - 4 February 2017 at Gasthof Stenitzer, 8967 Haus im Ennstal (Styria)

- International "Functional Oxide Surfaces and Interfaces (FOXSI)" Conference 2017, 15 -17 February 2017, Title of the poster: "Interaction of $Au_n(SR)_m$ cluster on different oxides (SiO_2, ZrO_2, TiO_2) and pretreatment effect"

- 5th International Symposium on Monolayer-Protected Clusters 2017, Ascona, Switzerland.

- 17th Austrian Chemistry Days, Salzburg, Austria

- 1th FemChem Scientific Workshop at TU Wien (25th June 2018)

- 6th International Symposium on Monolayer Protected Clusters 2019, 23 - 26 September, in Xiamen University，Xiamen，China

- 35th Workshop on Novel Materials and Superconductivity, JUFA Schladming, (9 February – 14 February 2020)

Beamtimes

- 27 Nov. 2016 - 2 Dec. 2016   SLS beamtime

- 4 April 2017- 11 April 2017   SLS beamtime (Proposal N°20161366)

  Title of the project: Structure-activity study of supported $CoAu_{24}(SC_2H_4Ph)_{18}$ and $Cox(SC_2H_4Ph)_m$ clusters on CeO_2 under CO oxidation by in situ EXAFS studies, Proposer: Dr. Noelia Barrabes (TU Vienna)

- 28 February 2018 – 4 March 2018   Grenoble, CH5496, Beamline ID26

  Title of the project: Structure study of ligand-protected gold clusters measured by HERFD-XANES (gold L-edge). Proposer: Dr. Marte van der Linden

- 19 May 2018 – 5 June 2018   ALBA CLAESS beamline, Spain

  Title of the project: CO Oxidation with Co_xAu_y clusters (proposal 2017092492). Proposer: Dr. Noelia Barrabes (TU Vienna)

- 14 Nov. 2018 – 19 Nov. 2018   ALBA CLAESS beamline, Spain

  Structure determination and stability under thermal treatment of Agn(SR)m cluster depending on the supported material: Ag k-edge and S k-edge operando study (proposal 2018022763). Proposer: Prof. Dr. Fernando Rey (Polytechnic University of Valencia)

- 5 Nov. 2019 – 10 Nov.2019   ALBA CLAESS beamline, Spain

Pd-doped Au$_{24}$(SR)$_{18}$ clusters supported on oxides: in situ *Au L$_3$-edge and S K-edge XAFS study of structure, stability and metal/oxide interaction under oxidative conditions (*proposal 2019023443). *Proposer: Clara Isabel Garcia Yago*

Summerschool

- 2 July 2017 – 7 July 2017   Elitecat 2017, Lyon-Villeurbanne

Awards

- "Best presentation on catalysis", TU Wien Young Scientist Symposium (VSS 2019) (13 June -14 June 2019)